6. ACTIVATION OF THE PEPTIDE BOND FORMATION

6.1 INTRODUCTION

Our living world is constituted by a huge amount of diverse creatures. In any organism one can find nucleic acids, proteins and lipids. The first two groups are made by the combination of basic molecular building blocks; i. e. the linkage of nucleobases, sugar and phosphate gives nucleotides of DNA and RNA, whereas the condensation of amino acids gives proteins. It has been one of the major achievements of modern molecular biology to determine that living organisms share the same molecular building blocks in a molecular logic way.

The synthesis and handling of the needed macromolecules is nowadays carried out by the metabolism occuring in living cells. Metabolysm is a fantastic complicated chain of self-substained biochemical reactions which are carried out in different cellular districts. However, the key questions are: when, where and how this was achieved before the advent of the first cell?

The solar system was formed about 4.5 billion years ago from a swirling cloud of gas and dust. For about 700 million years the planets were pounded by debris as the primordial material aggregated into larger bodies. The early days of our planets have been characterized by heavy meteoritic bombardments of the Earth's surface lasting 1 billion years. On the other hand, the oldest microbe, actually a prokaryotic cyanobacterium-like microorganism was dated to be 3.4 billion year-old and evidences the antiquity of life. Thus, the window in which life emerged is very sharp and is suggested to have occurred 3.8 billion years ago. But how life arose?

One possibility is to consider a mixture of CH_4, NH_3, H_2O, N_2 and H_2 in conditions that resembles to those the primitive Earth; i. e., a strongly reducing atmosphere and providing energy in form of heat and light. This was indeed proved by Miller in the 50s and showed that the products formed were amino acids as well as other organic molecules.[285] This experiment gave rise to the so-called primordial soup theory because it concerns the formation of a prebiotic soup of biomonomers. After Miller's work many variants of his procedure have been tested, in which 17 of the 20 amino acids and all purines and pyrimidines were obtained, but the abiotic synthesis of ribose and nucleosides

was much more difficult.[286-289] However, the primordial soup theory is subjected to two uncertain points. The first one is that recent studies point out that the early Earth atmosphere could never have been strongly reducing. The second point is how polymers – the basis of life itself – could be assembled. Nevertheless, these experiments demonstrated that the first building blocks could have been formed through standard chemical processes.

A second possibility is the impact theory deeply studied by Pizzarello and coworkers. It is hold by the fact that a substantial proportion of meteorites that fall on the Earth (belonging to a class known as carbonaceous chondrites) contain a significant amount of organic carbon and because some of the standard amino acids and nucleic acid bases are present.[290] Therefore, they have been proposed as an important source of raw molecular material when intense bombardments occurred in the first years of Earth's existence. Along the same line, deep-space synthesis proposed by Allamandola et al. suggested that molecules like CO, nitriles, ammonia or formaldehyde get adsorbed on the icy particles belonging to the ultra cold deep-space environments.[291] Ice-covered dust particles are subjected to UV radiation that may sufficiently activate the molecules to become reactive to form ethers, alcohols, amino acids and so on.

The newest suspects are the deep-sea vents, submarine cracks in the Earth's surface commonly found in places that are volcanically active, where superheated water rich in transition metal ions and hydrogen sulphide mixes abruptly with cold sea water.[292, 293] Since these vents are sites of abundant biological activity, the vent theory proposed by Wächtershäuer suggests that Reaction 6.1 could provide the free energy necessary for the reduction of CO_2 to molecules capable of supporting the origin of life (Reaction 6.2).

$$FeS + H_2S \rightarrow FeS_2 + H_2 + energy \qquad \textbf{Reaction 6.1}$$

$$energy + H_2 + CO_2 \rightarrow HCOOH \qquad \textbf{Reaction 6.2}$$

It is clear, then, that building blocks have probably different chances to be synthesized. However, nowadays it is still not known how to join them in a proper and controlled way in order to make active biopolymers. Starting from the monomers, for almost all important biopolymers, a condensation reaction is needed to elongate the polymer chain. For proteins, for instance, a peptide bond is formed by nucleophylic attack and further elimination of one water molecule. This reaction is nearly isoergonic in gas phase and becomes disfavoured in water excess. Because the amount of available building

blocks was small this was always the case. Furthermore, the newly synthesized peptides may be washed away or destroyed by UV light which possesses problems for their elongation. One should then figure out how these key steps were achieved.

An early suggestion came from Desmon Bernal,[294] back in 1949. He advocated the special role of clays as promoters for the condensation of monomer building blocks into biopolymers. Earth's crust is primarily formed from low-melting silicates such as feldspars, quartz, olivines, pyroxenes, amphiboles, garnets and micas. For pyroxenes, for instance, the general formula $XY(Si,Al)_2O_6$ implies the presence of a number of cations (X=Ca, Na, Fe^{2+}, Mg; Y=Cr, Al, Fe^{3+}, Mn) in an otherwise silica-tetrahedra framework. Clays are ubiquitous minerals with regularly layered atomic structures. Because layers in clays are held by relatively weak interactions they can intercalate molecular building blocks. Clay can extract, store and protect from the UV light the monomers, keeping them close together. It can also activate them allowing for an easier polymerization and cations may also capture water molecules deriving from the condensation reactions. Figure 6.1 shows a scheme of this process. This idea of polymerization on the rocks has been further expanded since Bernal's proposal by many researchers.[295-303] It is of particular interest the proposal of Orgel,[295] who suggested that once the size of an oligomer exceeds a certain minimum, adsorption is essentially irreversible.

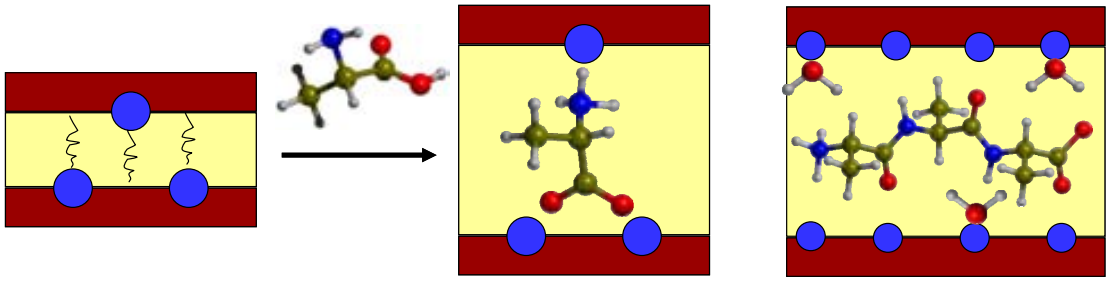

Figure 6.1 Schematic representation of the role played by clays during the condensation process of amino acids.

Apart of clays, metal cation interactions have also been invoked to facilitate the formation of the early peptide bonds.[304-309] In particular, the mechanism for the condensation reaction between two amino acids in aqueous solution, which is called Salt Induced Peptide Formation (SIPF) theory and was proposed by Rode et al,[308] invokes Cu^{2+} to play a major role under conditions that resembles to those of the primitive Earth. Its mechanism is shown in Figure 6.2 and is based on the formation of a monochlorocuprate complex with two amino acids that coordinate the metal cation in the

presence of high concentrations of NaCl. From such a complex the reaction leads to the formation of the peptide bond through an intracomplex condensation between the two amino acids. This process is in principle activated and favoured as a consequence of the coordination of the amino acids to the metal dication. Since the presence of water in excess will inevitably favour the breaking rather than the making of the peptide bond, the Na^+ ions act as the water-removing force.

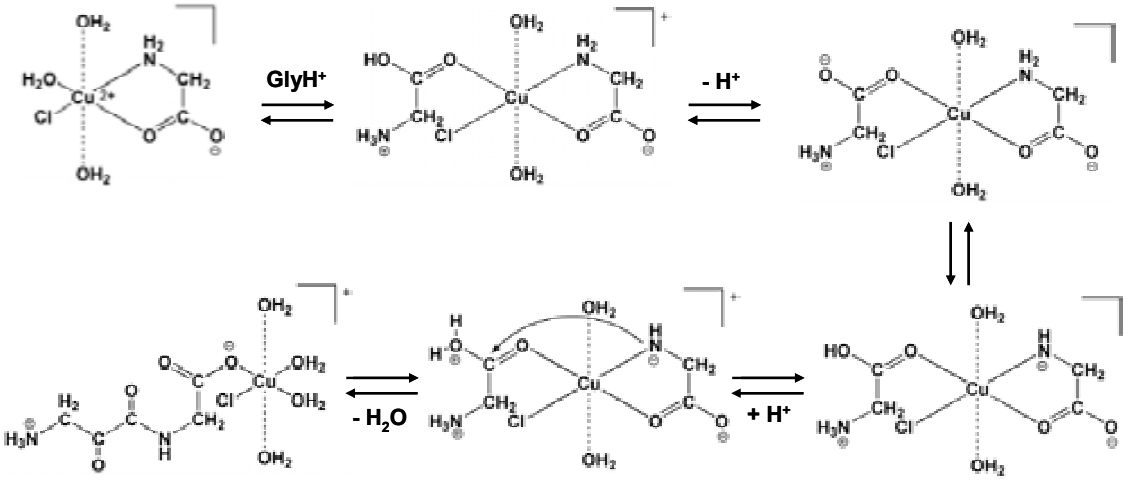

Figure 6.2 Mechanism for the peptide bond formation according to the SIPF reaction.

The SIPF theory has been widely tested in a great variety of experiments,[307, 308, 310-313] but furthermore it has also inspired mechanistic proposals for fragmentations observed in MS/MS experiments. Indeed, an experimental study in gas phase using soft electrospray ionization mass spectrometry techniques showed that Cu^{2+}-(glycine)$_2$ under low energy collision conditions led to the elimination of a water molecule without loss of charge.[145] Based on the spectra and on the SIPF mechanism the authors suggested that an intracomplex peptide bond formation might have occurred.

Therefore, efforts towards understanding whether or not the interaction of metal cations as well as oxide mineral surfaces with early biomolecules is a key step in the formation of the first biopolymers is of great interest in the field of prebiotic chemistry. In this chapter, a detailed theoretical mechanistic analysis of the peptide bond formation reaction including some ways of activation using quantum chemical calculations will be presented. First, the bare reactions in gas phase, i. e. uncatalyzed reactions, for the condensation between two glycine molecules, have been computed. Moreover, the calibration of the theoretical methods employed as well as the validity when using model reactions has also been performed. Secondly, the role of the Cu^{2+} cation as an activator of

the reaction under study both in gas phase and in aqueous solution has been addressed, whose results are compared to the uncatalyzed reactions. Finally, the reaction performed on aluminosilicates has been tested, in which the role of Lewis and Brønsted sites as catalysts of the reaction has been minutely examined.

As aforementioned in the Outlook, this study was carried out in close collaboration with the research group leaded by Dr. Piero Ugliengo of the University of Torino, where I did a short stay of three months during the spring of 2005.

6.2 METHODOLOGY

All calculations were performed using Gaussian03.[252] All structures have been characterized by the analytical calculation of the harmonic frequencies as minima and saddle points. For some intriguing cases IRC calculations have been carried out in order to confirm that the localized transition structures connect the desired reactants and products. Free energy profiles have been derived by using the standard rigid rotor/harmonic oscillator formulae on the corresponding electronic energy values.[253]

The methods and basis set employed for the molecular geometries and the frequency calculations depend on the system treated so that they are described separately as follows:

Gas phase peptide bond formation reactions, section 6.3.1.

Geometry optimizations and harmonic frequency calculations have been performed at the B3LYP[195, 197]/6-31+G(d,p), B3LYP/6-31++G(d,p) and BHLYP[195, 201]/6-31++G(d,p) levels of theory. Single-point energy calculations at the optimized geometries have also been carried out using the B3LYP and CCSD(T)[202] methods with the 6-311++G(2d,2p) and 6-311++G(2df,2pd) standard basis sets, to improve the accuracy in the energetic of the considered reactions. For these single-point calculations the thermal and entropic corrections have been taken from the optimized structures to compute the free energies.

Role of Cu^{2+} on the peptide bond formation, section 6.3.2.

As shown previously, the BHLYP density functional method provides better results than B3LYP compared to the highly correlated CCSD(T) method for Cu^{2+}-containing systems. Therefore, along this section the BHLYP approach has been used for geometry optimizations and frequency calculations. Furthermore, to confirm the reliability of the BHLYP results, for the Cu^{2+}-cationized peptide bond formation in gas phase, B3LYP

optimizations and single point CCSD(T) calculations at these geometries have also been performed and compared.

The Cu^{2+} basis set is derived from (14s9p5d)[203] primitive set of Watchers supplemented with one s, two p and one d diffuse functions[204] as well as on f polarization function, the final contracted basis set being (15s11p6d1f)/[10s7p4d1f]. For C, N, O and H the standard basis set of 6-31++G(d,p) has been used.

Solvent effects have been introduced using the conductor polarized continuum model (CPCM),[314] which is an implementation of the conductor-like screening solvation model (COSMO)[315] in Gaussian03, by performing single-energy calculations on the optimized gas-phase geometries.

Role of aluminosilicates on the peptide bond formation, section 6.3.3.

The level of theory used depends on the cluster considered to model the surface. For isolated Lewis and Brønsted sites, the cluster models adopted are small enough that full optimization of the system using the hybrid B3LYP density functional approach with the 6-31+G(d,p) standard basis set has been possible. The reliability of B3LYP/6-31+G(d,p) to describe the potential energy surface of the considered reactions has been validated[316] by comparing the B3LYP/6-31+G(d,p) results with the CCSD(T)/6-311++G(d,p) ones, resulting that the activation and reaction energies are underestimated by the DFT method by about 3 kcal/mol. In contrast, the clusters adopted to model surfaces that contain both Lewis and Brønsted sites are too large to efficiently explore the potential energy surface at the B3LYP/6-31+G(d,p) level. Therefore, in these cases all structures were optimized using the ONIOM2[214-217] strategy combining the B3LYP/6-31+G(d,p) method for the high-level zone with the MNDO[317] Hamiltonian for the real system. Once a stationary point was located, the energy was re-evaluated by performing single point calculations at the B3LYP/6-31+G(d,p) level. The adopted B3LYP/6-31+G(d,p)//ONIOM2[B3LYP/6-31+G(d,p):MNDO] combination was proved to be a good compromise between accuracy and speed of calculation for silica when studying reactivity.[318] Moreover, in order to further confirm the accuracy of the ONIOM2 geometries, full B3LYP/6-31+G(d,p) optimization were also performed for some selected structures.

Because the adopted methodology does not take into account dispersive forces due to fluctuating istantaneous dipoles, a rather simple strategy has been adopted here, to at least partially take them into account for the processes occuring on the aluminosilicates

derived cluster. The DFT+Dispersion method recently proposed by Grimme has been adopted,[319] which has been proved to be very effective for a number of cases where dispersive interactions are expected to be relevant.[319, 320] The dispersive correction (D) was added to the B3LYP/6-31+G(d,p)//ONIOM2[B3LYP/6-31+G(d,p):MNDO] energy in a posteriori fashion, by implementing the Grimme routine in the MOLDRAW program.[321]

6.3 RESULTS AND DISCUSSION

The peptide bond formation between two α-amino acids implies the formation of the OC-NH bond followed by the release of a water molecule. This process can occur via two different routes: i) a concerted reaction (Figure 6.3a) and ii) a stepwise mechanism (Figure 6.3b). Both cases involve a nucleophilic attack of the nitrogen atom of the NH_2 group belonging to one amino acid to the carbon atom of the COOH group belonging to the second amino acid. The difference between the two mechanisms arises in the path followed when losing the water molecule. In the concerted reaction, simultaneously to the N-C bond formation, a proton transfer takes place from the NH_2 group of the first amino acid to the OH group of the second amino acid in such a way that a water molecule is detached. In contrast, in the stepwise mechanism the proton transfer occurs from the NH_2 group to the CO group, forming thus a metastable diolic intermediate. A second step involving the release of a water molecule from this intermediate gives the final product with the peptide bond formed.

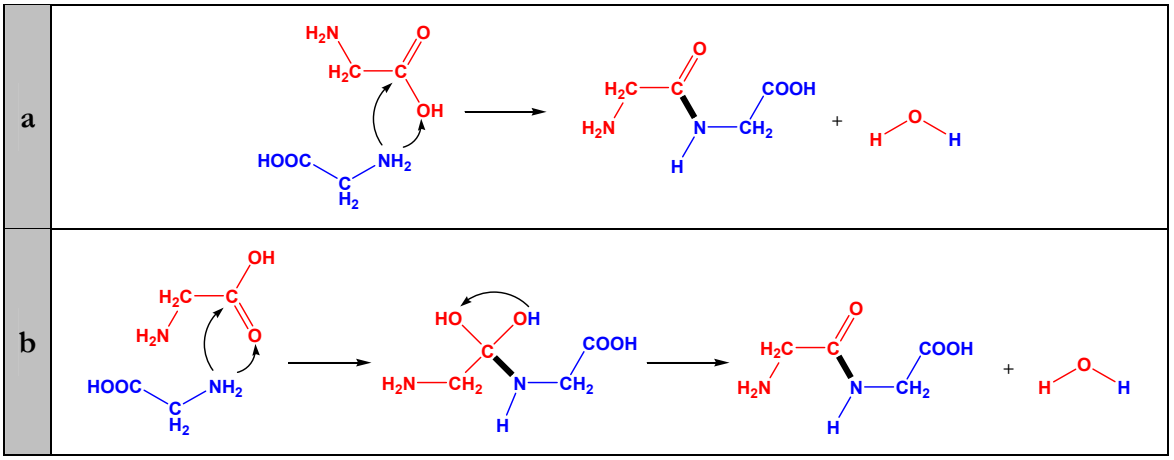

Figure 6.3 Schematic representation of the peptide bond formation following a concerted (a) and stepwise (b) mechanism.

6.3.1 GAS PHASE REACTIONS

6.3.1.1 Condensation between two glycine molecules

The B3LYP-free energy profiles as well as the geometries of the stationary points found both for the concerted and stepwise mechanisms are represented in Figure 6.4.

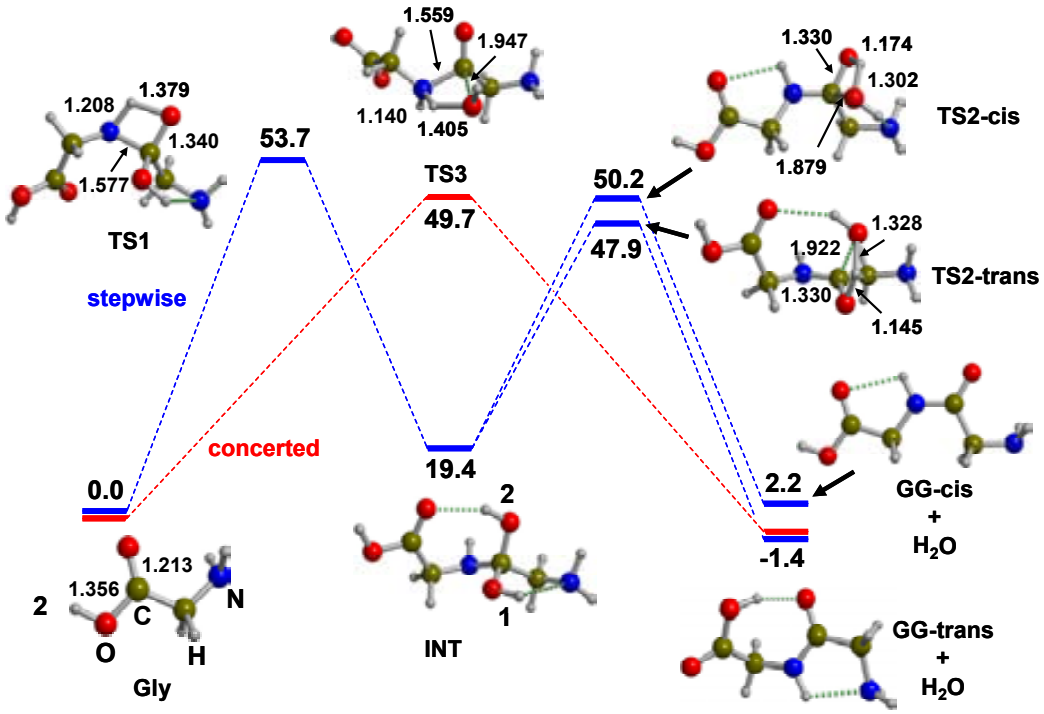

Figure 6.4 Relative free-energy profile, in kcal/mol, for the B3LYP-optimized structures (bond lengths in Å) of the concerted (in red) and stepwise (in blue) gas phase peptide bond formation. Relative free energies with respect to the two separated glycine molecules.

TS1 and **TS3** are very similar, the main difference being the atom that receives the proton, which, as aforementioned, for the concerted mechanism is the oxygen hydroxyl while for the stepwise mechanism is the oxygen carbonyl. Both transition structures are characterized by a fourth-membered ring that involves the proton transfer. However, whereas in **TS3** the C-OH bond is practically broken to release the water molecule, in **TS1** the C-O bond distance has increased slightly, a fact that indicates a partial loss of the double bond character of the carbonyl group. **TS3** yields directly *trans*-glycylglycine (**GG-trans**) as the final product, while in the stepwise mechanism, two possible transition structures from **INT** have been found as the second step. Indeed, two proton transfers can take place to detach water: H1 from O1 to O2, or H2 from O2 to O1 (see **INT** of Figure 6.4). Following the former possibility **TS2-trans** is reached, whose product is the **GG-trans** structure. Contrary, when the second path is followed the final product obtained is

the *cis*-glycylglycine (**GG-cis**) structure through **TS2-cis**. Similarly to **TS3**, both transitions structures present a fourth-membered ring as a consequence of the proton transfer process. Although **TS2-trans** and **TS2-cis** do not directly connect with the **GG-trans** and **GG-cis** isomers shown in Figure 6.4, respectively, these final products have been considered in the profile because they have been recently described as the most stable isomers for *trans*- and *cis*-glycylglycine, respectively.[263]

Focusing on the activation free energies, one can observe that for the stepwise mechanism the highest energy barrier corresponds to the first step, **TS1**, around 54 kcal/mol, the two other barriers being slightly lower, 48 and 50 kcal/mol for **TS2-trans** and **TS2-cis**, respectively. The energy difference between these two barriers is associated to the different stability given by the two final products. On the other hand, the activation free energy of the concerted mechanism is around 50 kcal/mol; that is 4 kcal/mol lower than **TS1**. Therefore, although both mechanisms are quite close in energy, the concerted mechanism is favoured respect to the stepwise one. Finally, it is noteworthy that the reaction free energy of formation of **GG-trans** is slightly negative while for the formation of **GG-cis** is slightly positive (-1.4 and 2.2 kcal/mol, respectively). Such values indicate that gas phase reactions are almost isoergonic.

6.3.1.2 Calibration of the method and assessment of model reactions

Since the gas phase reactions are understood as the uncatalyzed processes, the aim of the present study is to find agents that show catalytic activity in the reaction. However, it is first necessary to consolidate two key points: i) the theoretical method, and ii) model reactions. The first premise implies an assessment of both the functional and the basis set to be employed when studying the catalytic routes for this process. The second one concerns to the possibility of using simpler reaction models in order to avoid excessively expensive calculations, especially when considering potential catalytic agents that will increase the computational cost, such as aluminosilicate surfaces.

The condensation of two glycine molecules represents the true peptide bond formation. However, two model reactions using simpler molecules can be used to analyze the fundamental aspects of this reaction. These are the reaction of formic acid with ammonia to give formamide and water ($HCOOH + NH_3 \rightarrow HC(O)NH_2 + H_2O$), and the reaction between glycine and ammonia to give 2-aminoacetamide and water ($H_2NCH_2COOH + NH_3 \rightarrow H_2NCH_2C(O)NH_2 + H_2O$). It is noticeable that, since rigorously the peptide bond formation proceeds between the amino group of one amino

acid and the α-carboxyl group of another, for such model reactions the result is the formation of an amide bond.

The three reactions (HCOOH + NH_3, Gly +NH_3 and Gly + Gly) have been tested using the B3LYP and BHLYP density functionals with a great variety of basis sets, whose results have been compared to those obtained at the CCSD(T) level. The study has only been performed for the concerted mechanism because it concerns only one step and presents the lowest energy barrier. The geometry of the transition structures for these reactions are shown in Figure 6.5, and the activation free energies ($\Delta G_{298}^{\neq}$) and the reaction free energies ($\Delta_r G_{298}$) are summarized in Table 6.1.

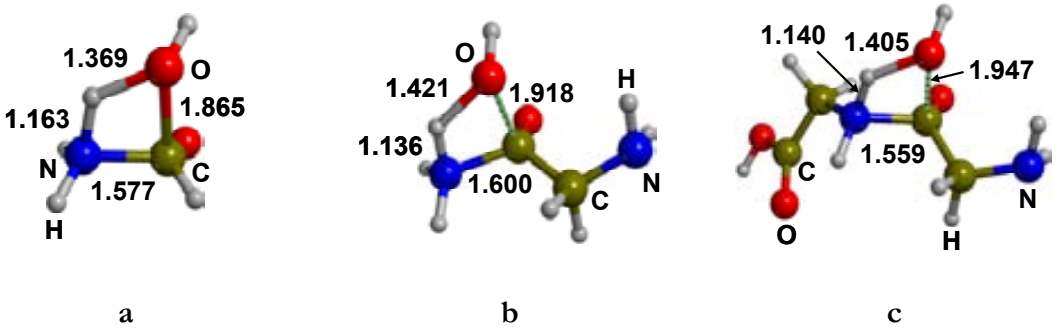

a **b** **c**

Figure 6.5 Optimized transition structures of the model reactions: a) HCOOH + NH_3 at B3LYP/6-31+G(d,p) level, b) Gly + NH_3 at B3LYP/6-31+G(d,p) level, and c) Gly + Gly at B3LYP/6-31++G(d,p) level. Bond distances in Å.

Table 6.1 Activation free energy barrier ($\Delta G_{298}^{\neq}$) and reaction free energy ($\Delta_r G_{298}$) for the considered reactions at different levels of calculation, in kcal/mol. For single-point energy calculations, extended basis set and CCSD(T), the thermal and entropic corrections have been taken from the the optimized structures (opt). All values are computed with respect to the free reactants.

	$\Delta G_{298}^{\neq}$			$\Delta_r G_{298}$		
	opt	extended	CCSD(T)	opt	extended	CCSD(T)
HCOOH + NH_3	50.7[a] 56.6[h]	52.7[b]	54.9[d]	-1.7[a] -1.8[h]	-1.6[b]	-1.0[d]
Gly + NH_3	52.0[a] 58.0[h]	54.5[c]	53.6[d]	-1.1[a] -1.3[h]	-0.7[c]	-0.6[d]
Gly + Gly	51.1[e] 55.4[h]	49.3[f]	47.7[g]	-1.4[e] -1.1[h]	-1.7[f]	-4.3[g]

[a] B3LYP/6-31+G(d,p)

[b] B3LYP/6-311++G(2d,2p)//B3LYP/6-31+G(d,p)

[c] B3LYP/6-311++G(2df,2pd)//B3LYP/6-31+G(d,p)

[d] CCSD(T)/6-311++G(2d,2p)//B3LYP/6-31+G(d,p)

[e] B3LYP/6-31++G(d,p)

[f] B3LYP/6-311++G(2df,2pd)//B3LYP/6-31++G(d,p)

[g] CCSD(T)/6-311++G(2d,2p)//B3LYP/6-31++G(d,p)

[h] BHLYP/6-31++G(d,p)

Focusing on the energy barriers, the B3LYP values show that the basis set dependence is relatively small, within differences around 2.5 kcal/mol at the most. Additionally, CCSD(T) data reveal that B3LYP method is providing reasonable accurate values, whereas those obtained with BHLYP are 4 – 6 kcal/mol larger with respect to the B3LYP values. Nevertheless, all methods provide values of reaction energies around -1 kcal/mol.

On the other hand, focusing on the modelling of the reaction, it is interestingly to point out that, using the B3LYP method, the calculated activation and reaction free energies are close enough, regardless of the model used, with small differences of 3 and 1 kcal/mol at the most, respectively.

From these data it appears that the B3LYP with standard basis set level of theory as well as to model the reaction using simpler molecules is adequate for treating the mechanism of the peptide bond formation, a relevant fact when larger and more realistic systems than the gas phase reactions will be treated. However, the reaction in presence of Cu^{2+} cations (vide-infra) both B3LYP and BHLYP functionals will be tested and compared to CCSD(T) results in order to establish the proper method.

6.3.2 ROLE OF Cu^{2+} ON THE PEPTIDE BOND FORMATION

As commented in the introduction, the SIPF theory suggests that Cu^{2+} cation is crucial during the condensation between two amino acids.[308] Additionally, in an experimental gas phase work it was observed the elimination of water from the Cu^{2+}-(glycine)$_2$ ion parent without loss of charge.[145] Based on the SIPF theory, the authors suggested that loss of water resulted from an intracondensation reaction leading to the formation of the peptide bond between the two coordinating glycine molecules.

This section addresses to a computational exploration of the role of Cu^{2+} cation during the peptide bond formation using the BHLYP functional. First, inspired on the available experimental data, the results obtained for the gas phase system will be presented.

Once the intrinsic reactivity of Cu^{2+}-(glycine)$_2$ have been analyzed, i. e., without complicating factors such as solvation, the peptide bond formation between two glycines coordinated to a hydrated Cu^{2+} cation and also in the presence of water molecules will be examined in order to explore the reactivity in aqueous solution.

6.3.2.1 Gas phase system

Collisionally activated dissociations of doubly charged Cu^{2+}-(glycine)$_2$ complexes, generated in ESI-MS experiments, led to the formation of a product ion [Cu^{2+}(glycine)$_2$–H_2O] in which a water molecule was lost without charge reduction, which suggested the occurrence of an intracomplex condensation reaction between the two glycines of the ion.[145] In order to analyze whether or not the observed product ion resulted from the peptide bond formation, an exhaustive exploration of the PES was performed and the reaction and activation free energies for this process were determined.

Before tackling the gas phase reactivity, the structure of the complex generated in the source must be firstly elucidated by analyzing the different modes of coordination. Four possible isomers have been considered, which are represented in Figure 6.6.

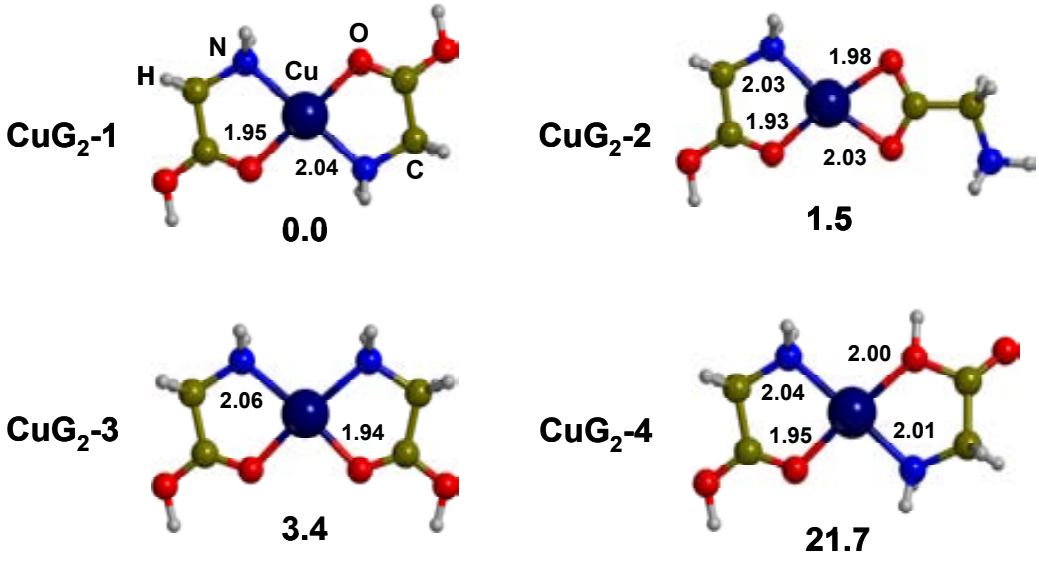

Figure 6.6 BHLYP-optimized geometries for the Cu^{2+}-(glycine)$_2$ isomers. Relative free energies in kcal/mol. Distances in Å.

In the lowest energy isomer (**CuG_2-1**) the glycine ligands are in *trans* disposition and coordinate to the metal cation through the carbonyl oxygen and the nitrogen amino. The *cis* isomer (**CuG_2-3**) is found to lie 3.4 kcal/mol above. As described in the literature and commented in chapters 4 and 5, the zwitterionic forms of amino acids are stable in the gas

phase when interacting with metal cations.[102, 112, 113, 256] Thus, we have also considered an isomer derived from the interaction of the metal cation with the COO^- group belonging to one zwitterionic glycine (**CuG_2-2)**, which has been found to lie 1.5 kcal/mol above **CuG_2-1**. This result indicates that the charge of the metal is significantly screened as a consequence of the interaction with the other glycine ligand and so, the interaction of the zwitterionic form with Cu^{2+} becomes less stable than that of its neutral form, in agreement with observation in chapters 4 and 5 as well as in previous works,[322] which show that additional coordination to the metal cation, either by water molecules or by interacting with side chains, reduces the stability of the zwitterionic form. Since this structure is less stable than **CuG_2-1** the interaction of two zwitterionic glycines would be even more unstable that **CuG_2-2** and it has not been considered. Finally, **CuG_2-4** in which Cu^{2+} is coordinated by the NH_2 and the OH groups of one glycine, is 21.7 kcal/mol high in energy respect to **CuG_2-1**. It should be mentioned that, despite the oxidative character of Cu^{2+} in coordinatively unsaturated complexes, as described in chapter 4 and in the literature,[284, 323, 324] the spin density at the metal cation in these systems is always around 0.80, in agreement with what is usually found in four coordinated square planar systems, as exposed in chapter 5.

The most stable form of Cu^{2+}-$(glycine)_2$, **CuG_2-1**, has been taken as the starting complex for the peptide bond formation in the gas phase. As shown in Figure 6.7, the free energy barrier of this process (97.2 kcal/mol) is much larger than that obtained for the uncatalyzed case (55.4 kcal/mol), whereas the final products Cu^{2+}-(glycylglycine) (**CuGG**) + H_2O is 65.6 kcal/mol above **CuG_2-1**. This process exhibits a surprisingly high activation energy, which can be reasonably understood by examining the transition structure. In order to allow the nucleophilic attack of the amine nitrogen, the NH_2 group needs first to decoordinate from the metal cation, which induces instability of **TS1-CuG_2** with respect to **CuG_2-1**. Moreover, the transfer of one H atom from the attacking NH_2 to OH implies the formation of a highly tensioned four member ring. The loss of coordination, from square planar in the reactant to trigonal in the product, is also responsible for the high value obtained for the reaction free energy (65.6 kcal/mol). For this process in gas phase, calculations at the B3LYP and single points at the CCSD(T) level have also been performed. Results showed that reaction energies are very similar with all methods, largest differences being about 3 kcal/mol. For the energy barriers, differences are somewhat larger, BHLYP values being about 5-6 kcal/mol larger than with B3LYP, whereas CCSD(T) values lie in between. Overall, these results indicate that the loss of water from

low-collision activated dissociation of Cu^{2+}-(glycine)$_2$ does not arise from an intracomplex condensation reaction.

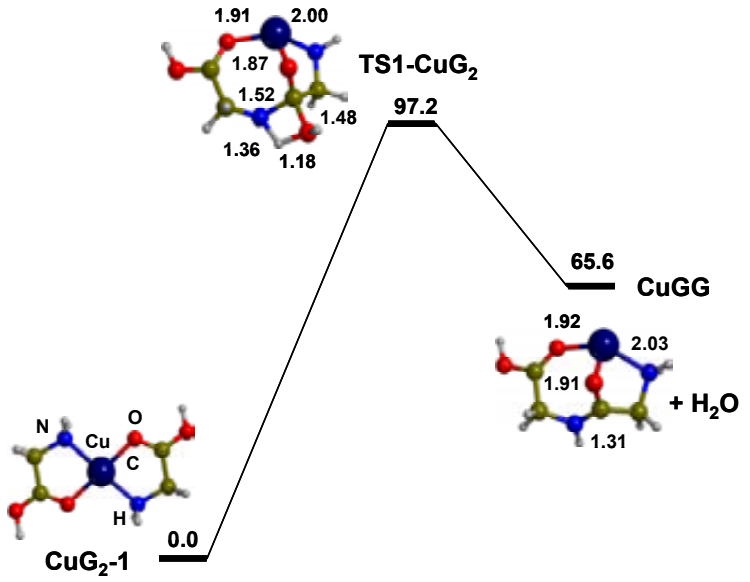

Figure 6.7 Free energy profile, in kcal/mol, for the BHLYP optimized structures (bond lengths in Å) relative to the peptide bond formation reaction in the gas phase. Relative free energies refer to the CuG_2-1 reference sate.

The question is thus, which mechanism enables the loss of water in low collisionally conditions? The elimination of water from transition metal-amino acid systems, as commented in section 4.3.3, is generally observed and it has been traditionally invoked to occur via insertion of the metal cation into the backbone bonds of the amino acids.[56, 68, 76, 125, 126, 129] Because of that, these mechanisms have been theoretically explored and the results reported in Figure 6.8.

All attempts to find a path involving the insertion of Cu^{2+} into the C-C bond for the elimination of water failed. In fact, when simulating the insertion of the metal cation by enlarging the C-C bond, the final products corresponded to the loss of $^{+}H_2N{=}CH_2$ ion, which was also observed in the experimental CAD spectra.[145] Instead, a Cu^{2+} insertion into the C-OH bond from **CuG_2-4** (see path A of Figure 6.8), yields the formation of a water molecule through **TS2-CuG_2** with an overall energy barrier of 64.2 kcal/mol. In addition to the metal bond insertion, this process also involves a hydrogen transfer from the CH_2 to the OH, converting glycine in H_2O + NH_2-CH=C=O. Such a transfer is not surprising since the C-OH cleavage is highly heterolytic, the OH acquiring an important negative charge and the NH_2CH_2CO fragment a positive charge that increases the CH acidity. The direct cleavage of water from **I1-CuG_2** leads to the **Cu(G_2-W)1** product ion (66.4 kcal/mol

above **CuG_2-1**), in which the amino-ketene coordinates Cu^{2+} through the N and C atoms. This pathway presents an overall energy barrier that is 33.0 kcal/mol lower than that computed for the peptide bond formation (see Figure 6.7), indicating, thus, that at least another more favourable process leading to the loss of water exists in the collision cell. The loss of water leading to **Cu(G_2-W)1** can also be produced from the most stable isomer **CuG_2-1** through a mechanism that involves a 1,3-hydrogen transfer from CH_2 to the OH group (see path B of Figure 6.8). However, the activation energy associated to this path is 86.5 kcal/mol, around 20 kcal/mol higher than the path A and thus, it would not take place.

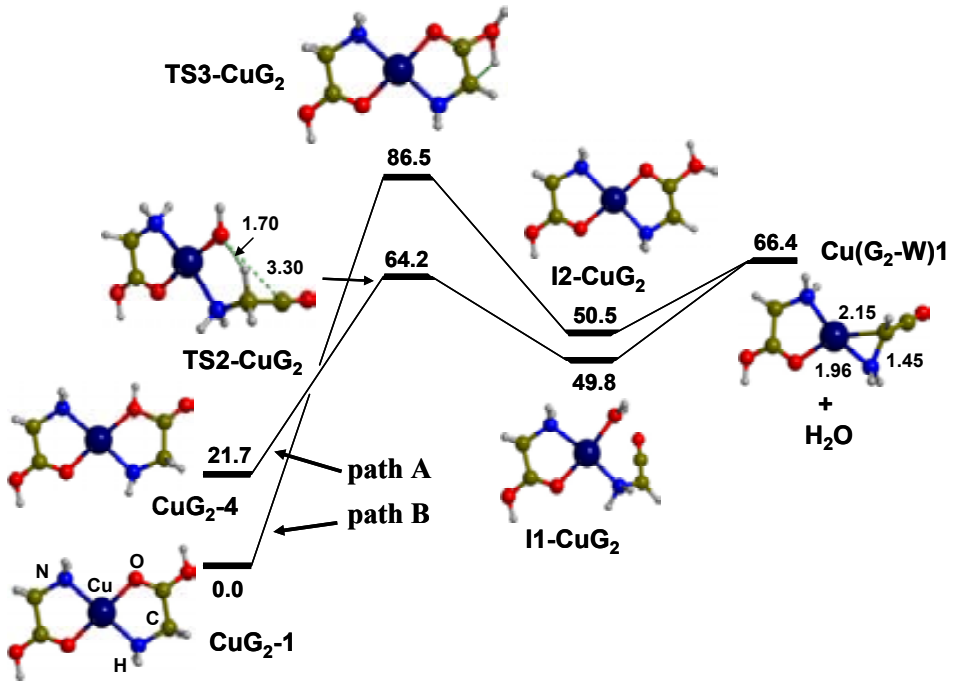

Figure 6.8 Free energy profile, in kcal/mol, for the BHLYP optimized structures (bond lengths in Å) relative to the elimination of water in the gas phase: path A starting from CuG_2-4; path B starting from CuG_2-1. Relative free energies refer to the CuG_2-1 reference sate.

Although other more favourable mechanisms rather than the intracomplex condensation reaction, explain the loss of water observed in the MS/MS experiments, these mechanisms still present too high energy barriers. In fact, the CAD spectra show that the loss of water takes place through a practically barrierless process. Thus, in order to explain the experimental findings by means of computational methods, other mechanisms should be accounted for.

One important thing observed in the experiments is the presence of background water (BW) in the collision cell, in such a way that the Cu^{2+}-$(glycine)_2(H_2O)$ complex was

formed. The presence of low amount of water can affect the intrinsic gas phase reactivity and so that another mechanism for the elimination of H_2O in presence of one discrete water representing the conditions of the collision cell has also been considered.

Figure 6.9 shows the free energy profile for this elimination after forming the Cu^{2+}-(glycine)$_2$(H_2O) adduct (**[CuG$_2$]$_{bw}$**), in which the water is in the apical position of the complex. As a first step, this water molecule decoordinates from the metal centre and acts as assistant in the proton transfer from NH_2 to the OH group. This transfer takes place through a barrier of 53.7 kcal/mol above **CuG$_2$-1** + H_2O and leads to the formation of the intermediate **[I1-CuG$_2$]$_{bw}$**, in which the H_3O^+ hydronium ion is formed. Because direct cleavage of water cannot proceed from **[I1-CuG$_2$]$_{bw}$**, a C-C bond breaking takes place through the **[TS2-CuG$_2$]$_{bw}$** structure, which has an energy 66.9 kcal/mol higher than **CuG$_2$-1**. Finally, direct elimination of two water molecules from **[I2-CuG$_2$]$_{bw}$** occurs, giving rise to the **Cu(G$_2$-W)2** product, which presents a square planar coordination in which the metal cation interacts with glycine in a bidentate manner, with CO (through the O atom) and with $NH{=}CH_2$ (through the N atom). This **Cu(G$_2$-W)2** + H_2O asymptote lies 46.7 kcal/mol above **CuG$_2$-1**. A slightly more stable isomer of the final copper complex **Cu(G$_2$-W)3,** in which the CO coordinates through the C atom, has also been found.

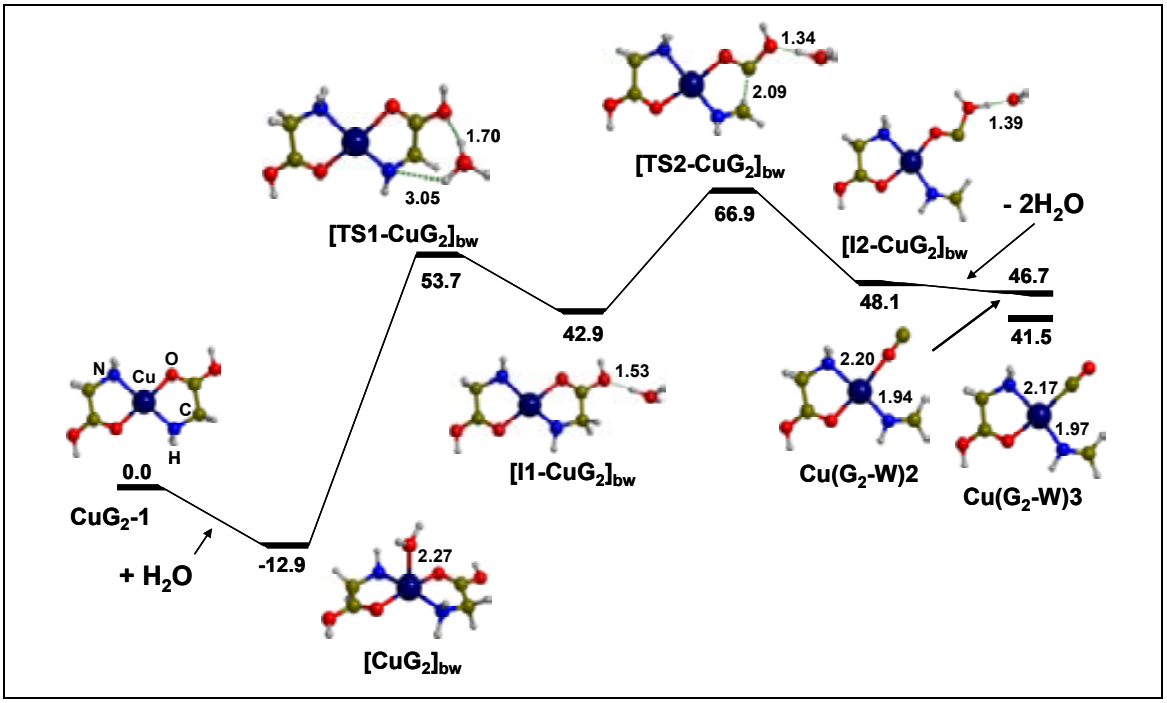

Figure 6.9 Free energy profile, in kcal/mol, for the BHLYP optimized structures (bond lengths in Å) relative to the elimination of water in the gas phase in presence of one water molecule from the background. Relative free energies refer to the CuG$_2$-1 + H_2O reference sate.

Although this mechanism leads to a much more stable product (**Cu(G_2-W)3**), compared to those shown in Figure 6.7, **CuGG**, and Figure 6.8, (**Cu(G_2-W)1**), the overall energy barrier (66.9 kcal/mol) is very similar to that obtained for path A in Figure 6.8 (66.4 kcal/mol) and thus, still would not explain the formation of [Cu^{2+}(Glycine)$_2$ –H_2O] at low collisionally activation energies. Accordingly, the loss of water from Cu^{2+}-(glycine)$_2$ is rather a mystery and other explanations for the experimental observations should probably be considered (see next section).

6.3.2.2 Reaction in aqueous solution

It is well known that solvation can largely affect the reactivity of any process, particularly when metal cations are involved, because water molecules can participate in the coordination sphere of the cation. In the present section the peptide bond formation is analyzed by including discrete water molecules as well as the continuous CPCM solvation model.[314]

The starting complex is the Cu^{2+}-(glycine)$_2$(H_2O)$_2$ system, for which four isomers have been localized. Optimized structures are reported in Figure 6.10. The most stable one is **CuG_2W_2-1**, whose glycine ligands are in the equatorial plane and in *trans* disposition, the apical metal-ligand distances being 0.4 Å larger than the equatorial ones, due to the Jahn Teller distortion. This structure is in agreement with a X-ray absorption spectroscopy study for the bis(glycinato)copper(II) complex in aqueous solution,[325] the differences in the Cu^{2+}-ligand bond distances being around 0.05 Å at the most. The remaining three isomers **CuG_2W_2-2**, **CuG_2W_2-3** and **CuG_2W_2-4** lie 2.4, 5.2 and 6.1 kcal/mol above **CuG_2W_2-1**. The glycine ligands of these isomers are not disposed in a coplanar fashion and they differ basically in the relative position of the donor groups: CO in *trans* and NH_2 in *cis* disposition (**CuG_2W_2-2**), CO in *cis* and NH_2 in *trans* disposition (**CuG_2W_2-3**) and both CO and NH_2 in *cis* disposition (**CuG_2W_2-4**).

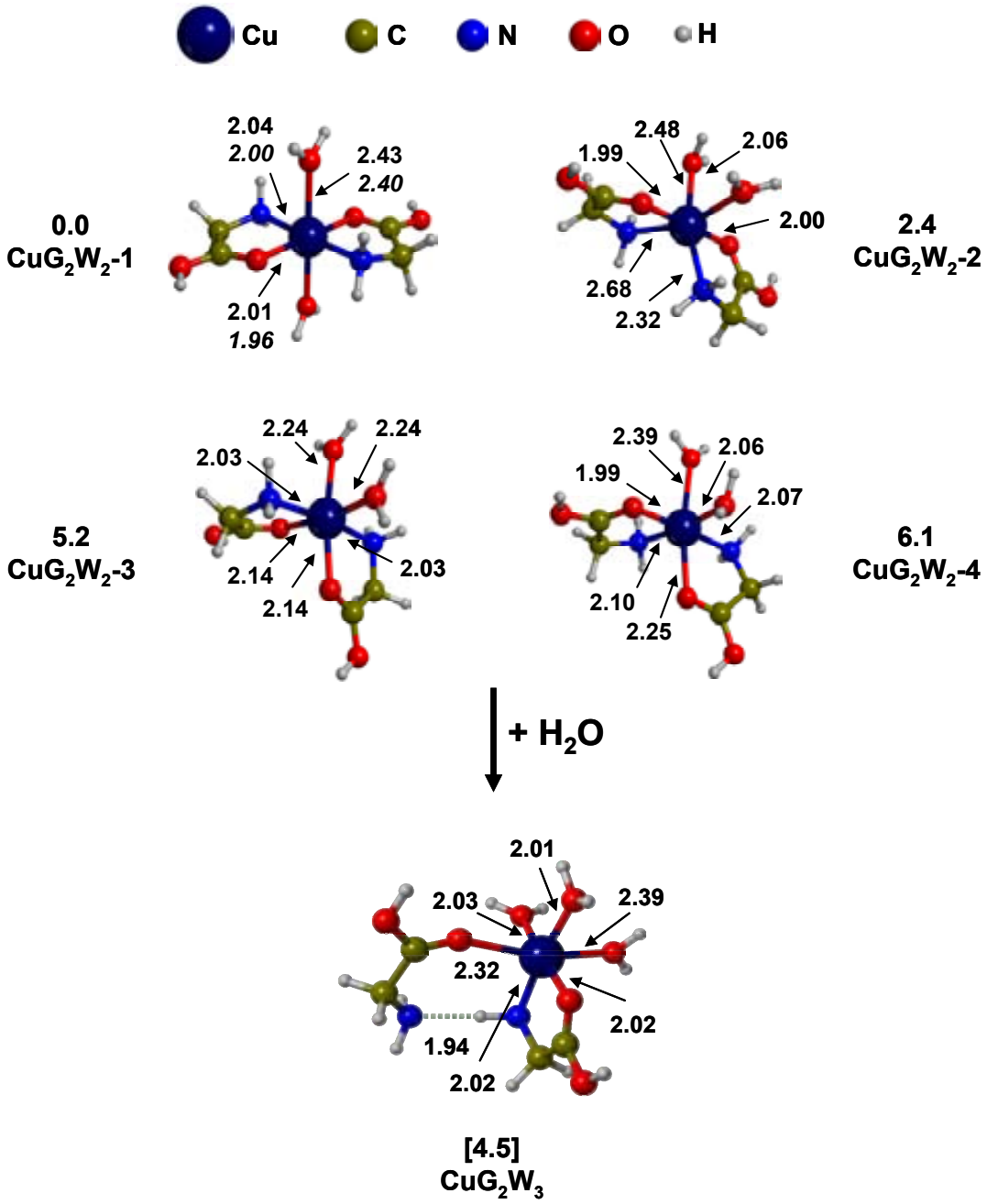

Figure 6.10 BHLYP-optimized geometries (bond lengths in Å) of the structures obtained for the Cu^{2+}-(glycine)$_2$(H_2O)$_2$ complex. Italics bond distances for CuG_2W_2-1 corresponds to experimental values of the bis(glycinato)copper(II) complex. Bare energy values refers to the free relative energies of the Cu^{2+}-(glycine)$_2$(H_2O)$_2$ complexes. The value in brackets is the reaction free energy CuG_2W_2-1 + H_2O → CuG_2W_3, in kcal/mol.

The nucleophilic attack of the NH_2 group of one glycine to the other one implies changes on the coordination sphere of the metal. As mentioned, in gas phase such changes led to a loss of coordination that gave rise to a high energy barrier. Nevertheless, in aqueous solution the vacancy originated upon decoordination of the NH_2 can be occupied

by a water molecule arising from the solvent. According to that, **CuG_2W_3** has been found as the pre-reactant complex for the peptide bond formation. As shown in Figure 6.10, the NH_2 group of one glycine in **CuG_2W_3** is not interacting with the metal whereas three water molecules are coordinated to Cu^{2+}. The free energy of the **CuG_2W_2-1** + H_2O → **CuG_2W_3** reaction is 4.5 kcal/mol.

Figure 6.11 shows the energy barriers and reaction energies for the different peptide bond formation processes considered and Figure 6.12 summarizes the geometries of the stationary points involved.

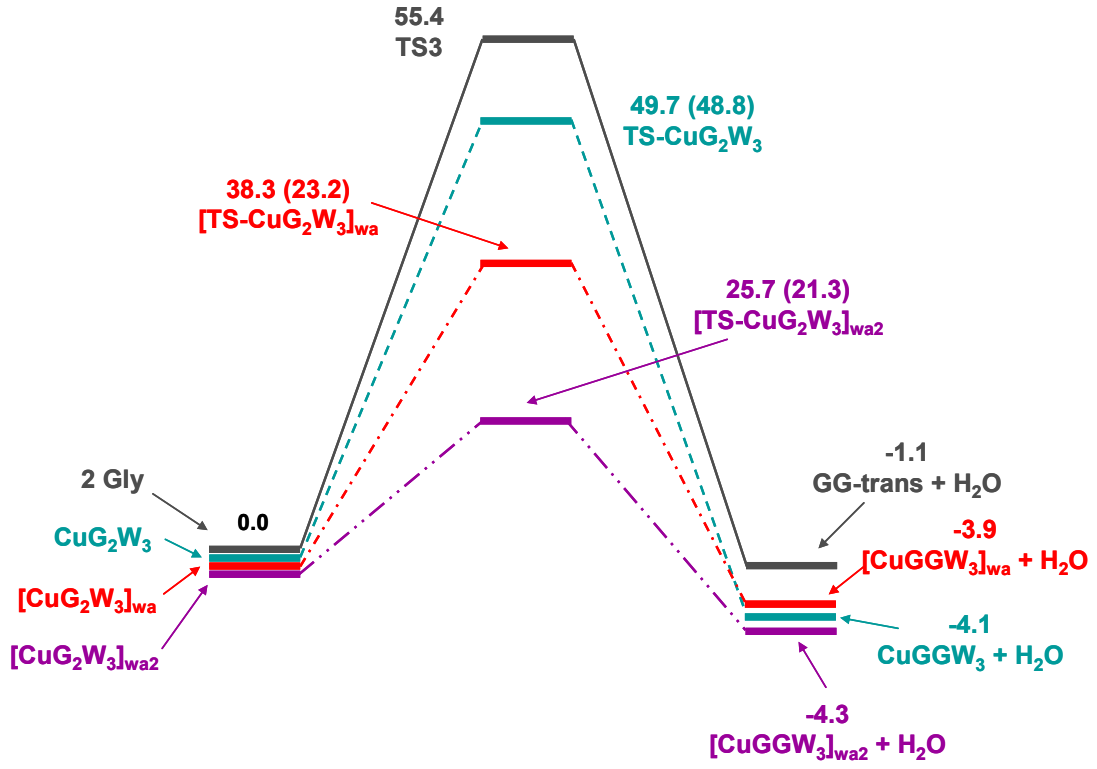

Figure 6.11 BHLYP-free energy profile, in kcal/mol, relative to the peptide bond formation for: two glycine molecules (solid grey line), intracomplex condensation starting from CuG_2W_3 (dashed green lines), water-assisted intracomplex condensation starting from $[CuG_2W_3]_{wa}$ (dashed-pointed red lines), and double water-assisted intracomplex condensation starting from $[CuG_2W_3]_{wa2}$ (dashed-double-pointed purple lines). In parenthesis the values computed using the CPCM solvation model.

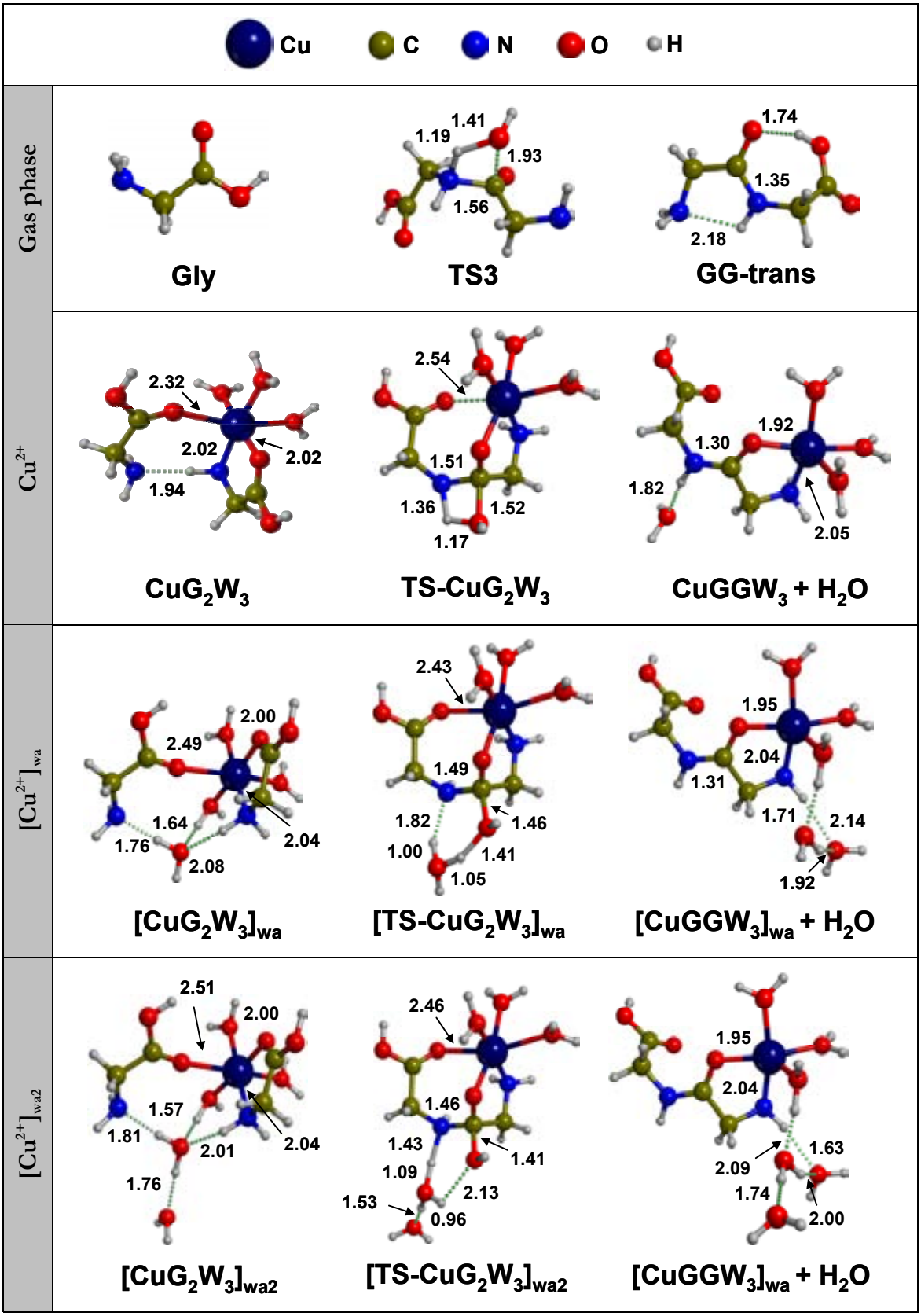

Figure 6.12 BHLYP-optimized geometries relative to the reactions involved in Figure 6.11. Bond distances in Å.

As previously mentioned, the condensation between two neutral glycines in gas phase has an activation energy of 55.4 kcal/mol (**TS3**). On the other hand, the peptide bond formation starting from the $\mathbf{CuG_2W_3}$ complex and occurring via $\mathbf{TS\text{-}CuG_2W_3}$ is associated to an energy barrier of 49.7 kcal/mol, which implies a decrease of around 6 kcal/mol compared to the uncatalyzed reaction. Thus, the reaction is slightly activated. This activation also manifests itself in the geometry of the transition structure, since the N-C distance of the forming bond in $\mathbf{TS\text{-}CuG_2W_3}$ is shorter (1.51 Å) than in the uncatalyzed reaction (1.56 Å) and the H of the NH_2 is much more transferred to the OH group in $\mathbf{TS\text{-}CuG_2W_3}$ (H···O distance is 1.17 Å) than in **TS3** (H···O distance is 1.41 Å). Despite that, the decrease in the energy barrier is not as large as one would expect from the enhancement of the electrophilic character of the carbon atom by the interaction of the CO with the metal cation. This is mainly due to two factors: i) the intracomplex nucleophilic attack implies a lengthening of the Cu-O distance of the attacking glycine from 2.32 Å in $\mathbf{CuG_2W_3}$ to 2.54 Å in $\mathbf{TS\text{-}CuG_2W_3}$ and so, there is a loss of stabilizing interaction and ii) the transition structure presents a highly tensioned four member ring associated to the formation of the forming C-N bond and the transfer of the H atom to OH.

In $\mathbf{TS\text{-}CuG_2W_3}$ the waters are coordinated to Cu^{2+}, just exerting a screening effect on the metal cation. They are simple spectators that do not take part in the reaction. However, it is well known that protic solvents can act as potential proton-transfer helpers.[326-328] Accordingly, reactions in which a water molecule assists the hydrogen transfer from NH_2 to OH groups have also been explored. The water-assisted reaction starting from $\mathbf{[CuG_2W_3]_{wa}}$ and proceeding through $\mathbf{[TS\text{-}CuG_2W_3]_{wa}}$ results in an activation energy of 38.3 kcal/mol, which means a significant decrease (around 11 kcal/mol) on the energy barrier with respect to $\mathbf{TS\text{-}CuG_2W_3}$. This is mainly due to the fact that the presence of the added water allows for a smaller distortion of the $\mathbf{CuG_2W_3}$ complex upon producing the nucleophilic attack, i.e. the Cu-OC distance of the attacking glycine is now 2.43 Å instead of 2.54 Å, and also to the fact that the water molecule act as a proton transport catalyst, the proton from NH_2 being transferred to the assistant water molecule in $\mathbf{[TS\text{-}CuG_2W_3]_{wa}}$ That is, the water assistant molecule becomes an hydronium ion in the transition structure. Because such ions are largely stabilized by the interaction with water molecules[329] it has also considered the water-assisted reaction with additional water molecule that is hydrogen bonded to the helper one. The process occurs now through $\mathbf{[TS\text{-}CuG_2W_3]_{wa2}}$ with an activation barrier of 25.8 kcal/mol with respect to $\mathbf{[CuG_2W_3]_{wa}}$. In addition, if the effects of the dielectric medium are accounted for with the continuum

CPCM solvation model, the energy barrier is reduced to 21.3 kcal/mol. It is quite remarkable that the introduction of solvent effects in $\mathbf{[CuG_2W_3]_{wa}}$ leads to an energy barrier of 23.3 kcal/mol, similarly to the 21.3 kcal/mol value obtained for $\mathbf{[CuG_2W_3]_{wa2}}$; that is, the continuum model seems to capture well the large influence of the second water molecule.

Finally, the values obtained for the reaction free energies indicate that the presence of Cu^{2+} cation favours the reaction compared to gas phase system (the reaction free energy is -4.0 kcal/mol for Cu^{2+} complexes versus -1.0 kcal/mol for gas phase system). This is probably due to the fact that in the final product, N-glycylglycine coordinates Cu^{2+} in a bidentate manner through the amino group and the carbonyl oxygen of the amide bond. The interaction of the metal cation with the amide carbonyl oxygen stabilizes the $-(H)^{+}N=C-(O^{-})-$ resonant form of the peptide bond, which leads to a shorter CO-Cu^{2+} distance (as observed in chapter 5),[117] compared to that of CO(carboxylic)-Cu^{2+} in the reactants, as well as to a strengthening of the peptide bond. Note that the distance corresponding to the peptide bond in the Cu^{2+} complexes is 1.30-1.31 Å, whereas in N-glycylglycine in gas phase this value is 1.35 Å. These facts stabilize the final complex, making the peptide bond formation a thermodynamically more favorable process.

Overall, these results suggest that simultaneous presence of both the Cu^{2+} metal cation and water molecules provides the situation that exhibits the lowest activation barrier to form the peptide bond between two glycine molecules in aqueous solution, as a consequence of the synergy between these two factors. That is, Cu^{2+} strongly coordinates glycine molecules whereas water molecules efficiently catalyze the condensation reaction. Moreover, the peptide product becomes thermodynamically more stable in the presence of Cu^{2+} cations.

6.3.2.3 Gas phase versus solution reactions

The present calculations suggest that the elimination of water experimentally observed in gas phase does not result from an intracomplex peptide bond formation due to the high energy barrier (97 kcal/mol) and reaction free energy (66 kcal/mol) computed for this process. These high values are associated to the loss of coordination of the metal cation in the transition structure and in the product. Other mechanisms leading to the loss of water and to more stable products have been found to present lower energy values. The most favourable process found, however, has an energy barrier of 66 kcal/mol, much larger than what one would expect considering the low-collisionally spectra.

On the other hand, it has been found that the important coordination changes observed in the gas phase and that lead to so high energy barriers are largely attenuated when considering hydrated cations. Moreover, results show that solvent molecules can act as proton transport catalysts while simultaneously avoiding significant distortions in the coordination sphere. Among the reactions tested, the less energy-demanding one, with a free energy barrier of 21 kcal/mol, occurs via an intracomplex water-assisted condensation with the particularity that a second water molecule from the medium interacts through a hydrogen bond with the assistant one, a fact that induces high stability to the transition structure due to the formation of a $H_5O_2^+$ specie. Thus, the condensation between two glycine molecules can readily occur in the presence of Cu^{2+} cations and water molecules. According to this result, the peptide bond formation may have occurred in the ion source, previously to generating the ions in gas phase, since Cu^{2+} cations and glycine molecules are mixed in an aqueous solution and submitted to a high voltage. In fact, it has been described in literature that intracomplex rearrangements can take place during the solvent evaporation.[66] This means that the condensation would occur in the ion source rather than in the collision cell and the peak observed at m/z = 106.5 would correspond to the Cu^{2+}-(glycylglycine)(H_2O) complex and not to Cu^{2+}-$(glycine)_2$ so that, the elimination of water observed in the collision cell would arise from Cu^{2+}-(glycylglycine)(H_2O); i. e., from the present results, the most plausible explanation for the experimental observations is that the peptide bond formation has already occurred at the ion source, the ions being generated with somewhat excess of energy. However, the computed reaction free energy for Cu^{2+}-(glycylglycine)(H_2O) → Cu^{2+}-(glycylglycine) + H_2O is about 40 kcal/mol. Although this value is smaller than the lowest energy barrier (47 kcal/mol) obtained for the formation of Cu^{2+}(glycine)(CO)($NHCH_2$) in the presence of water background molecules, it still appears to be too high considering the experimental conditions and thus, new experiments to confirm the loss of water from Cu^{2+}-$(glycine)_2$ complex would be desirable.

6.3.3 ROLE OF ALUMINOSILICATES ON THE PEPTIDE BOND FORMATION

As it was shown, the formation of the peptide bond following a concerted mechanism involves two simultaneous processes: i) the nucleophilic attack of the NH_2 group to the carbon atom of the COOH group, and ii) a hydrogen transfer from the NH_2 to the OH groups. It means that agents that favour these two processes should be good catalysts for the condensation reaction. The key is, however, to find these catalysts.

On one hand, the interaction of the CO group of glycine with a Lewis acid implies a charge distribution that results with a decreasing of the electronic charge on the carbon atom, so the COOH group becomes more prone to be attacked by a nucleophilic group than without interacting with the Lewis acid. On the other hand, Brønsted acids can assist the hydrogen transfer process, a fact that infers stability to the transition state and reduce the energy barrier. According to these two statements, it seems clear that the interplay of Lewis and Brønsted catalysts should reduce significantly the activation barrier.

In this sense, it has been found in the previous section that the condensation between two glycine molecules starting from the Cu^{2+}-$(glycine)_2(H_2O)_2$ complex and hydrogen-assisted by two water molecules was associated to a considerably lower barrier than the uncatalyzed reaction. In that case Cu^{2+} acted as the Lewis catalyst while water as the Brønsted one. This interplay between Lewis and Brønsted catalysts can also be applied in the context of the possible role played by the surfaces of oxidic mineral materials in the delicate step of synthesising the first polypeptides, as was suggested by Bernal.[294] Earth's crust is primarily formed form low-melting silicates among which aluminosilicates (including zeolites and some clays) are usually rich in both Brønsted and Lewis sites that might have played the role of catalysts for the early peptide bond formation in the prebiotic chemistry.

Accordingly, the peptide bond formation has been studied using different model clusters of aluminosilicates and the B3LYP functional. First, the reaction will be tackled on an isolated Lewis site, previously exploring the possible adducts formed between the surface and glycine molecule. The same procedure will be followed when considering the reaction on an isolated Brønsted site. Then, the peptide bond formation using models that envisage the interplay between Lewis/Brønsted pair will be analyzed. Finally, the possible role that mineral surfaces could have played in prebiotic conditions in the polimerization of peptides will be also discussed.

Because a full characterization of the PES of the process is desired, reactions on an aluminosilicate surface in a periodic way would be too demanding. Thus, we have resorted to the cluster approach instead. Additionally, here the condensation reaction does not envisage two glycine molecules because it implies too large conformational flexibility, considering that a full glycylglycine molecule sports a large number of different conformations which should, at least in principle, be characterised. To simplify, NH_3 has

been used to play the role of the second glycine. As shown previously, the energetics of this model reaction is close to the values of the real reaction involving two glycine molecules.

6.3.3.1 Lewis site

The surface Lewis site is represented by a 3-coordinatively unsaturated aluminium ($Al(III)_{cus}$) arising from one single framework all-silica $H_8Si_8O_{12}$ cluster belonging to the hydridosilasesquioxanes family. This "cage-like" model, envisaging six fused rings with four Si atoms, has been already adopted in the past to successfully simulate isolated hydroxyl groups at the silica surface[330, 331] and offer the advantage of being quite rigid, which greatly reduces the optimization steps needed to characterize the whole potential energy surface compared to open cluster models. Considering that the mineral surface is usually hydrated, an extra water molecule is coordinated to the Al atom to mimic the presence of water in the reaction medium (see **ZL-H_2O** in Figure 6.13).

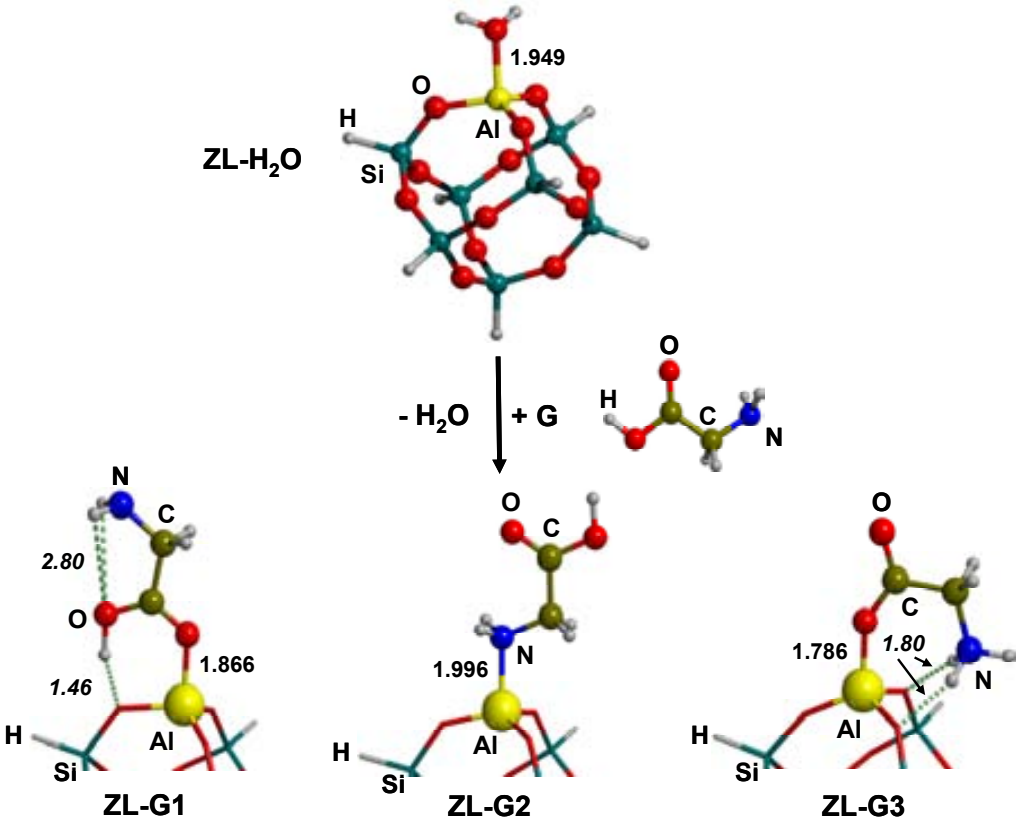

Figure 6.13 B3LYP/6-31+G(d,p) optimized geometries of the cluster adopted to model the isolated Lewis site (ZL-H_2O) and of the different isomers found when glycine interacts with the Lewis site (ZL-G1, ZL-G2 and ZL-G3). Bond distances in Å.

The very first step is the displacement of the water molecule adsorbed on the Lewis site by the amino acid itself. Figure 6.13 shows the possible adducts formed between

glycine and the Lewis site. As summarized in Table 6.2, all of them are more stable than water coordinated to the Lewis site. The most stable structure, **ZL-G1**, shows a direct Al-O bond with the carbonyl oxygen while the OH group is involved in a strong hydrogen bond with an oxygen atom of the aluminosilicate surface. **ZL-G2** has the NH_2 group interacting with Al, while maintaining the ground state conformation of glycine, and only lies 1 kcal/mol higher in energy than **ZL-G1**. **ZL-G3** corresponds to the interaction of the zwitterionic form of glycine with the Al of the surface through one of the carboxylate oxygens. This structure lies 1.4 kcal/mol higher in energy than the ground state structure but if free energies are considered at 298 K, it becomes 4.7 kcal/mol less stable than **ZL-G1** structure. That is, entropic effects seem to disfavour the zwitterionic form, probably due to the additional rather strong hydrogen bonds formed between the NH_3^+ moiety with the surface. It is worth noting that, for all considered structures, the Al atom adopts a tetrahedral coordination when interacting with glycine and that any attempt to obtain a minimum structure with a bidentate coordination through the C=O and NH_2 groups, as found for many metal cations interacting with amino acids, failed and collapsed to **ZL-G1**.

Table 6.2 Electronic energy (ΔE_{displ}) and free energy ($\Delta_{displ}G_{298}$) of the water displacement reactions, ZL-H_2O + G → ZL-G + H_2O. ΔE_{rel} and $\Delta_{rel}G_{298}$ are the corresponding relative energies with respect to the most stable structure computed for ZL site. Data in kcal/mol.

Isomers	ΔE_{displ}	$\Delta_{displ}G_{298}$	ΔE_{rel}	$\Delta_{rel}G_{298}$
ZL-G1	-11.9	-10.1	0.0	0.0
ZL-G2	-10.8	-9.2	1.1	0.9
ZL-G3	-10.5	-5.4	1.4	4.7

Figure 6.14 shows the B3LYP/6-31+G(d,p) free energy profiles and the optimized geometries of the concerted reactions for the different isomers above described. The relative free energies of the different stationary points have been computed taking **ZL-G1** + NH_3 as asymptote. Table 6.3 summarizes the energy barriers and the reaction energies for the computed processes.

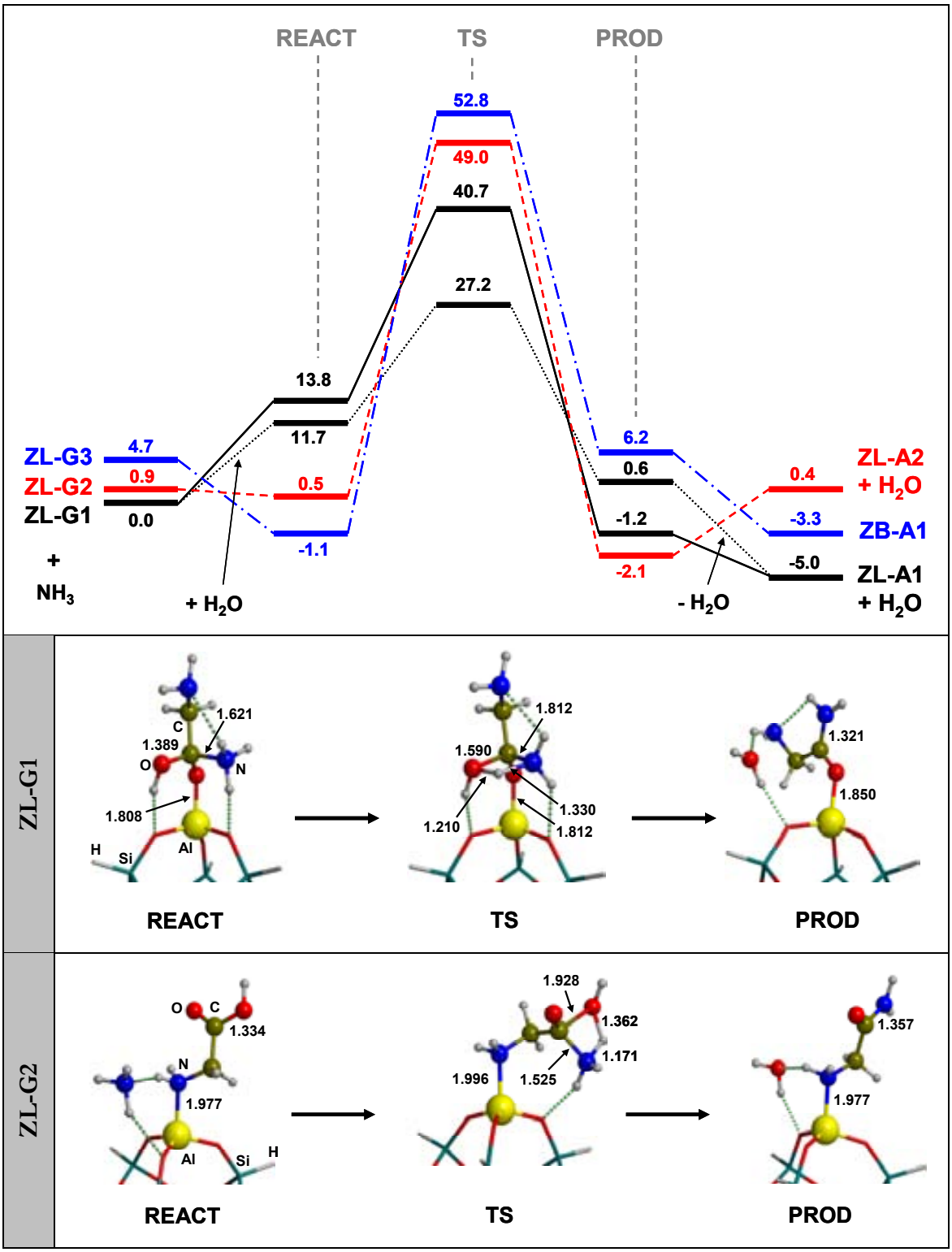
REACT
TS
PROD
52.8
49.0
40.7
27.2
13.8
11.7
0.5
-1.1
4.7
0.9
0.0
6.2
0.6
-1.2
-2.1
0.4
-3.3
-5.0
ZL-G3
ZL-G2
ZL-G1
+
NH3
+ H2O
- H2O
ZL-A2
+ H2O
ZB-A1
ZL-A1
+ H2O
ZL-G1
1.621
C
1.389
O
N
1.808
H
Si
Al
1.812
1.590
1.330
1.812
1.210
1.321
1.850
REACT
TS
PROD
ZL-G2
O
C
1.334
N
1.977
Al
Si
H
1.928
1.362
1.171
1.996
1.525
1.357
1.977
REACT
TS
PROD

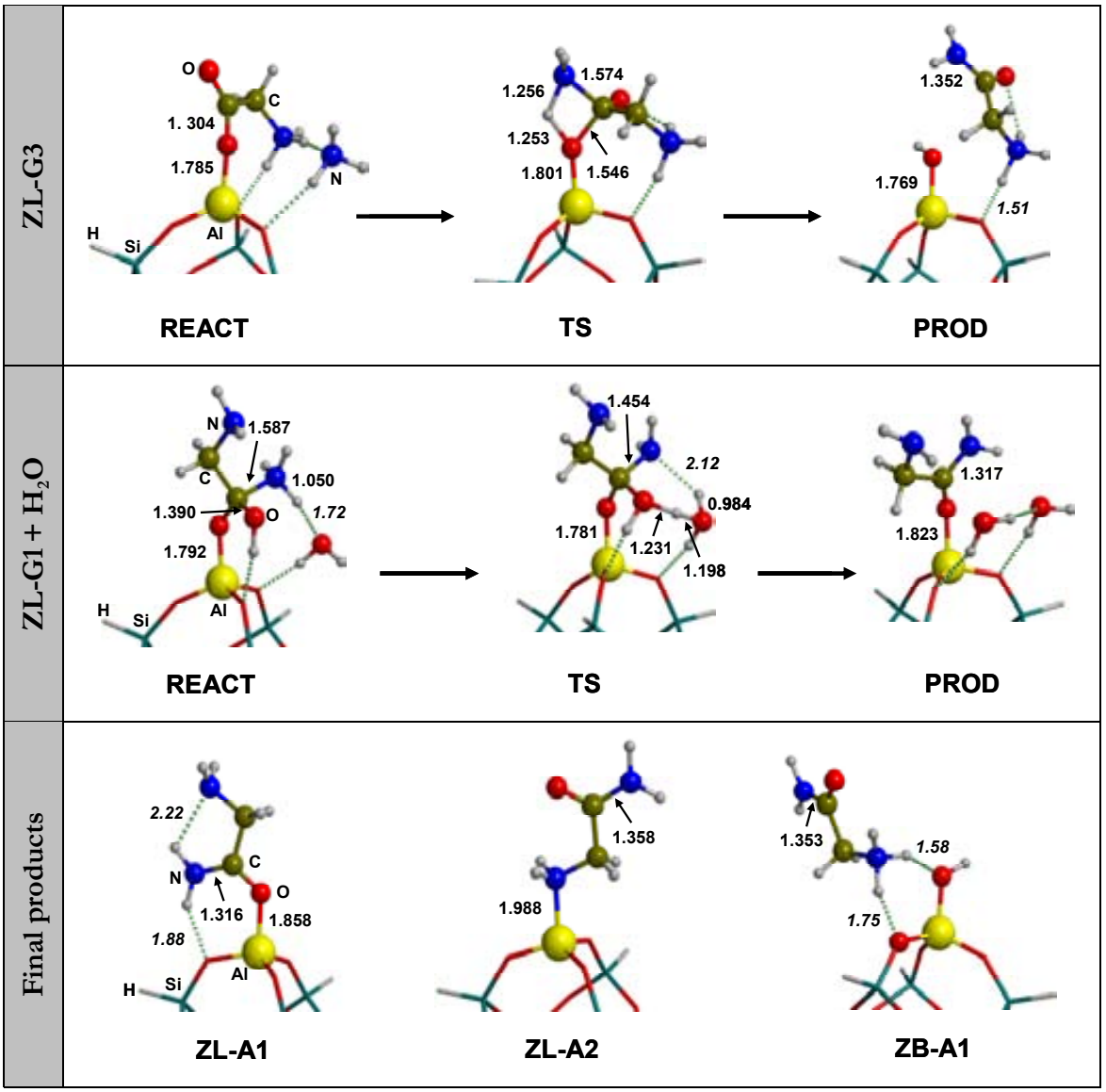

Figure 6.14 Relative free energy profiles, in kcal/mol, and B3LYP/6-31+G(d,p)-optimized geometries (bond distances in Å) for the concerted peptide bond formation processes on an isolated Lewis site taking the different isomers found as the reactive species: solid-black lines referred to ZL-G1 pre-reactant complex; dash-red lines referred to ZL-G2 pre-reactant complex; dash point-blue lines referred to ZL-G3 pre-reactant complex; point-black lines referred to ZL-G1 pre-reactant complex with an additional water molecule acting as proton solvent assistant. Relative free energies refer to ZL-G1 + NH_3 reference state.

Table 6.3 Activation free ($\Delta G^{\neq}_{298}$) energies and reaction free ($\Delta_r G_{298}$) energies of the considered processes. The subscripts *w* and *s* refer to water assisted and stepwise mechanisms, respectively. $\Delta G^{\neq}_{298}$ and $\Delta_{rel} G_{298}$ refer to the corresponding reactions whereas $\Delta G^{\neq}_{298}$ (G1) and $\Delta_r G_{298}$(G1) are respect to the lowest energy asymptote. Data in kcal/mol.

Reactions	$\Delta G^{\neq}_{298}$	$\Delta G^{\neq}_{298}$ (G1)	$\Delta_r G_{298}$	$\Delta_r G_{298}$ (G1)
ZL-G1 + NH_3 → **ZL-A1** + W	40.7	40.7	-5.0	-5.0
ZL-G2 + NH_3 → **ZL-A2** + W	48.5	49.0	-0.5	+0.4
ZL-G3 + NH_3 → **ZB-A1**	53.9	52.8	-8.0	-3.3
[**ZL-G1** + NH_3 + W → **ZL-A1** + 2 W]$_w$	27.2	27.2	-5.0	-5.0
[**ZL-G1** + NH_3 → **ZB-A2**]$_s$	40.8	40.8	+1.0	+1.0

Focusing on the energy barriers, results indicate that glycine is only activated by the mineral support via **ZL-G1** complex, with the energy barrier lowered around 11 kcal/mol compared to the gas phase reaction. In contrast, when the reaction takes place via **ZL-G2** and **ZL-G3** complexes, the Lewis site do not show any catalytic activity, the computed barriers being very similar to that of the gas phase reaction. It is noteworthy that the reactant structure of the reaction via **ZL-G1** complex presents the NH_3 already bonded to the carboxyl carbon atom, the C-N distance being 1.621 Å. This is explained considering that the Al-glycine interaction strongly activates the C=O bond, which is elongated by 0.05 Å, allowing the formation of a bond between the C atom and the incoming NH_3 molecule.

In all these reactions, the displaced water molecule from **ZL-H_2O** complex is a simple spectator that does not participate in the process. However, it has been demonstrated the potentiality of water molecules to act as proton-transfer helpers. Because of that, we have explored the possibility that a water molecule assists the proton transfer from the NH_3 molecule to the hydroxyl oxygen via **ZL-G1** complex. As shown in Figure 6.14 (**ZL-G1** + H_2O), the free energy barrier is significantly lower than that of the non-assisted mechanism (27.2 versus 40.7 kcal/mol, respectively), which indicates the potential catalytic effect on this reaction when the Lewis site and a water of molecule act in a synergic way.

The stepwise reaction has also been considered via **ZL-G1** (Figure 6.15). The results obtained show that the barrier of the first step (40.8 kcal/mol), which is the highest

one, is very similar to that of the concerted reaction (40.7 kcal/mol). Therefore, the surface Lewis sites of aluminosilicates catalyzes the peptide bond formation indistinctly if it proceeds via either concerted or stepwise mechanism. It should be mentioned that the second step does not follow the same way as the gas phase process. Indeed, in this case a proton transfer from the OH group of the diolic intermediate to the surface oxygen takes place and simultaneously the C-OH(Al) bond is broken, the resultant products being the 2-aminoacetamide molecule and the alumino-silicate surface with a Brønsted site.

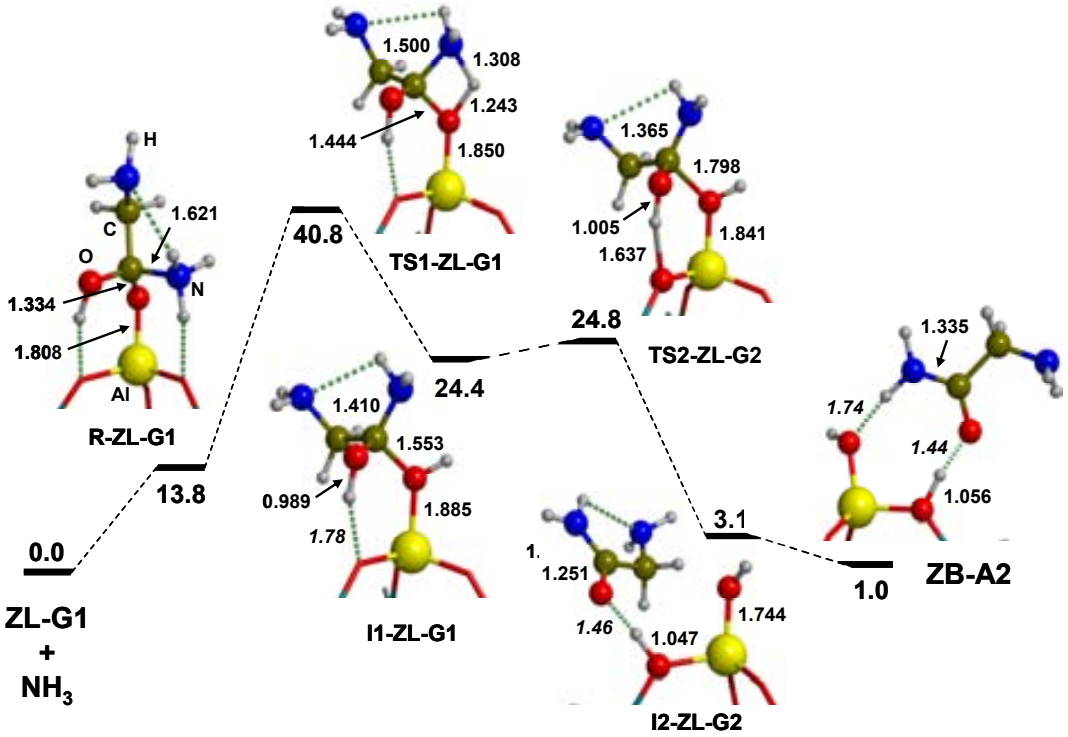

Figure 6.15 Relative free energy profile, in kcal/mol, for the stepwise peptide bond formation process on an isolated Lewis site taking the ZL-G1 structure as the reactive specie. Relative free energies refer to ZL-G1 + NH_3 reference state. Bond distances in Å.

6.3.3.2 Brønsted site

Brønsted sites are usually well characterized in the interior of zeolites and its acidic nature is due to the Si(OH)Al moiety, in which the proton compensates the unbalanced charge generated upon Si/Al substitution. To maximize the internal structural coherence between the cluster models mimicking Lewis and Brønsted sites, the very same cage-like silica cluster topology adopted for the Lewis site has been used to mimic the Brønsted as well. The Brønsted site is generated from the Lewis one by binding one proton of the Al-coordinated water to the nearby framework oxygen. The resulting structure, with one adsorbed extra water molecule to simulate hydration, is shown in Figure 6.16.

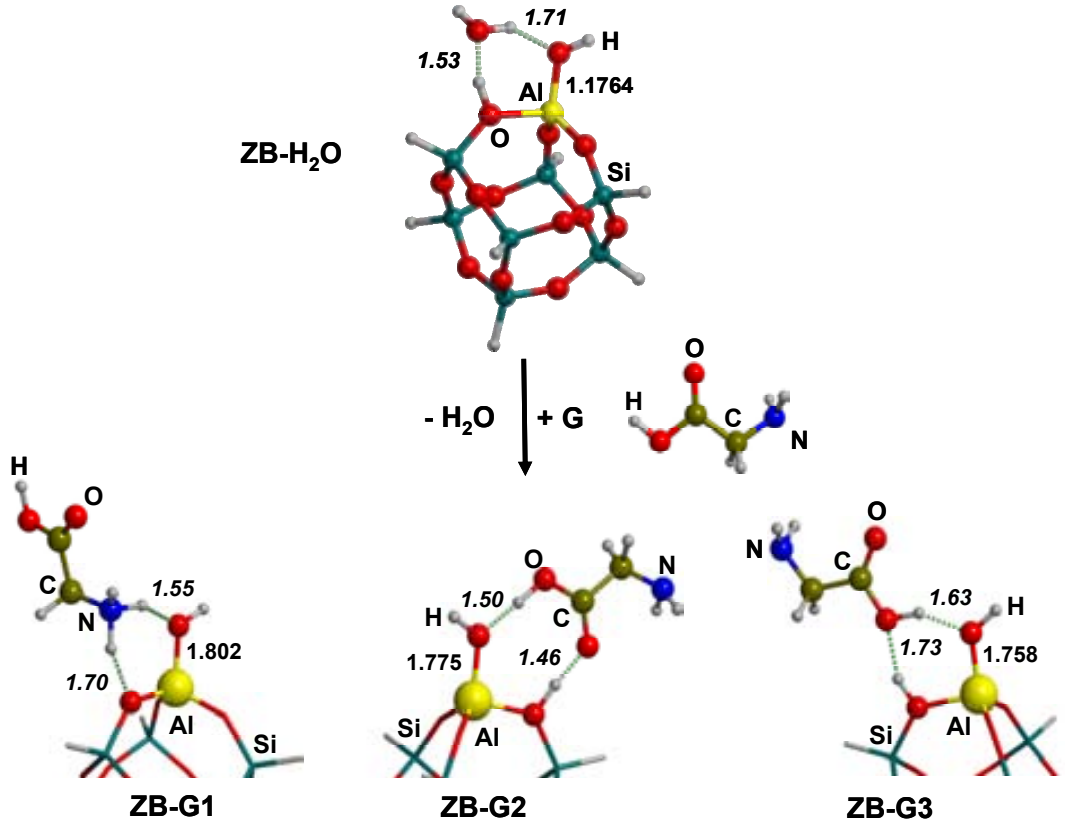

Figure 6.16 B3LYP/6-31+G(d,p) optimized geometries of the cluster adopted to model the isolated Brønsted site (ZB-H_2O) and of the different isomers found when glycine interacts with the Brønsted site (ZB-G1, ZB-G2 and ZB-G3). Bond distances in Å.

Using a similar procedure to the Lewis case, we first considered the water displacement reactions. The optimized structures are shown in Figure 6.16 whereas the relative stabilities and reaction energies are given in Table 6.4. It can be observed that glycine can easily substitute the water interacting with the Brønsted site for **ZB-G1** and **ZB-G2**, but not for the latter adduct (**ZB-G3**) for which the displacement is disfavoured. In the most stable adduct, **ZB-G1**, the adsorption of glycine is accompanied by a spontaneous proton transfer from the acidic site of the surface to the NH_2 of glycine; i. e. the protonated -NH_3^+ group interacts with the negatively charged surface via two strong hydrogen bonds. This behaviour was to be expected considering that the proton affinity of glycine is larger than that of ammonia, for which adsorption on acidic zeolites takes place through the formation of an ion-pair. **ZB-G2** structure shows two hydrogen bonds: one between the C=O group of glycine and the Brønsted site and another one between the carboxylic OH group and the surface terminal OH. Finally, adsorption via the carboxylic OH group as in the **ZB-G3** structure results in a complex that is about 10 kcal/mol higher in free energy than **ZB-G1** (see Table 6.4 and Figure 6.16).

Table 6.4 Electronic energy (ΔE_{displ}) and free energy ($\Delta_{displ}G_{298}$) of the water displacement reactions, ZB-H_2O + G → ZB-G + H_2O. ΔE_{rel} and $\Delta_{rel}G_{298}$ are the corresponding relative energies with respect to the most stable structure computed for ZB site. Data in kcal/mol.

Isomers	ΔE_{displ}	$\Delta_{displ}G_{298}$	ΔE_{rel}	$\Delta_{rel}G_{298}$
ZB-G1	-4.3	-5.4	0.0	0.0
ZB-G2	-3.5	-4.4	0.8	1.0
ZB-G3	7.8	4.3	12.1	9.7

The free energy profiles and the B3LYP/6-31+G(d,p)-optimized geometries of the concerted reaction for the different isomers interacting with the Brønsted site are shown in Figure 6.17. The reported energy values have been computed with respect to the **ZB-G1** + NH_3 asymptote. Energy barriers and reaction energies are given in Table 6.5.

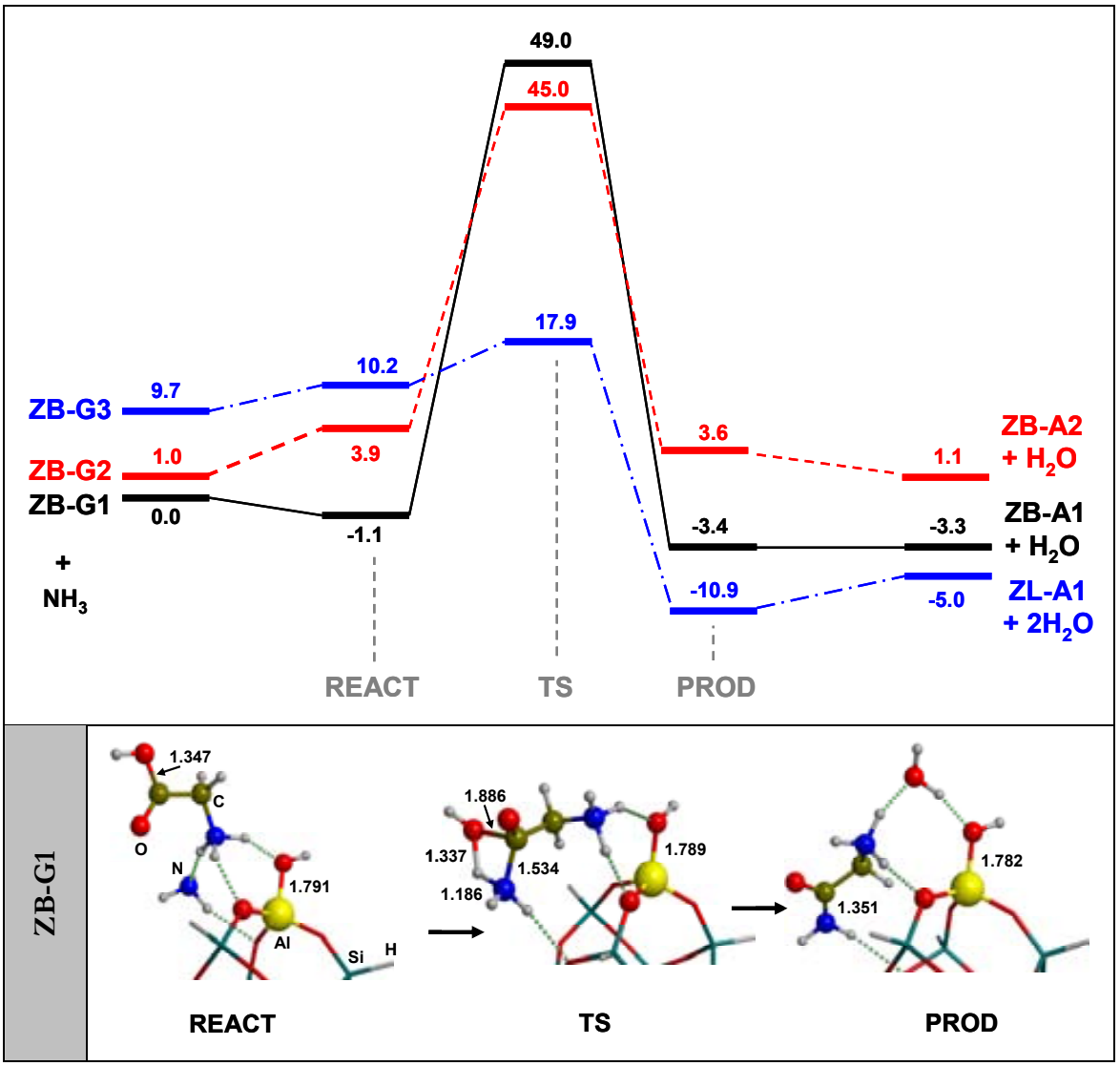

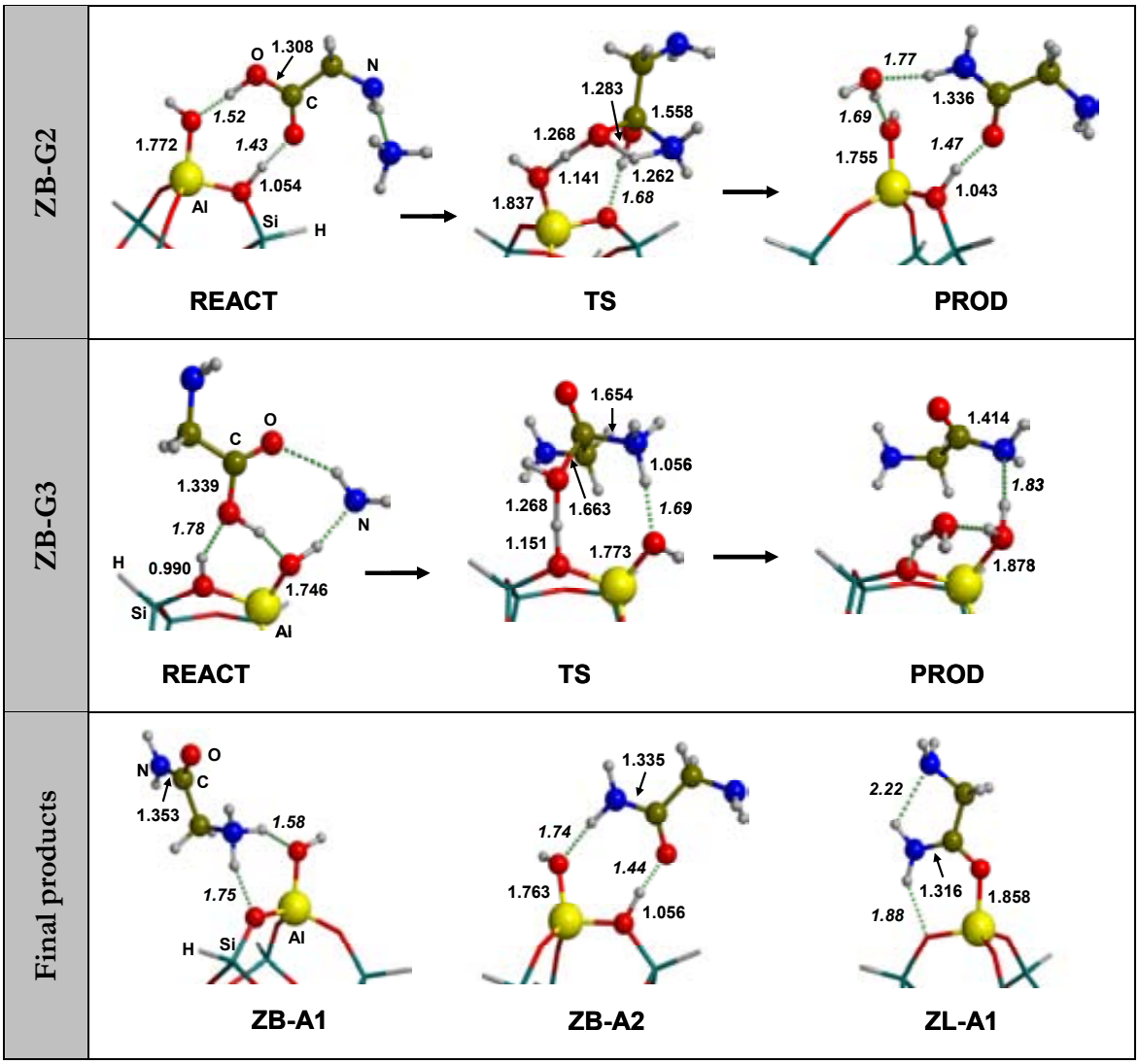

Figure 6.17 Relative free energy profiles, in kcal/mol, for the concerted peptide bond formation processes on an isolated Brønsted site taking the different isomers found as the reactive species: black-solid lines referred to ZB-G1 pre-reactant complex; dash-red lines referred to ZB-G2 pre-reactant complex; dash point-blue lines referred to ZB-G3 pre-reactant complex. Relative free energies refer to ZB-G1 + NH_3 reference state. Bond distances in Å.

Table 6.5 Activation free ($\Delta G^{\neq}_{298}$) energies and reaction free ($\Delta_r G_{298}$) energies of the considered processes. $\Delta G^{\neq}_{298}$ and $\Delta_r G_{298}$ refer to the corresponding reactions whereas $\Delta G^{\neq}_{298}$ (G1) and $\Delta_r G_{298}$(G1) are respect to the lowest energy asymptote. Data in kcal/mol.

Reactions	$\Delta G^{\neq}_{298}$	$\Delta G^{\neq}_{298}$ (G1)	$\Delta_r G_{298}$	$\Delta_r G_{298}$(G1)
ZB-G1 + NH_3 → **ZB-A1** + W	49.0	49.0	-3.3	-3.3
ZB-G2 + NH_3 → **ZB-A2** + W	44.0	45.0	+0.1	+1.1
ZB-G3 + NH_3 → **ZL-A1** + 2 W	8.2	17.9	-14.7	-5.0

First, it is observed that for the two most stable adducts the free activation energies are relatively close to that of the uncatalyzed reaction. This means that neither protonation to the amino group nor the interaction with the carbonyl one induce significant changes on the nucleophilic addition of NH_3 to the COOH group to form the peptide HN-CO bond. However, if one moves from the most stable pre-reactant complex to the least stable one, which has an energy cost of 10 kcal/mol, a very favourable reaction path is found, the transition structure being located as low as 18 kcal/mol respect to the asymptote. This transition structure is characterized by an eighth-membered ring in which the HN-CO bond is formed as a result of a double proton transfer: one from the Brønsted site to the OH group of glycine and the other one from NH_3 to the aluminol group. Moreover, during the reaction the Brønsted site is transformed into a Lewis one, the released water molecule being coordinated to the Al atom.

6.3.3.3 Lewis/Brønsted interplay using an edingtonite framework

In view that both Lewis and Brønsted sites may play an important role as catalysts for the peptide bond formation reaction, now a third more intriguing possibility, the interplay between Lewis and Brønsted sites, will be addressed.

The results obtained in the previously examined cases have to be considered with some caution, because: i) the Lewis and Brønsted sites are completely isolated from the mineral framework to which they belong; ii) because of the relatively small size and topolgy of the adopted clusters, geometrical changes within the clusters during the reactions are relatively small. Point ii) is important because the energetic cost of the geometrical reorganization of the active site during the catalytic process will increase the reaction barrier. For the above reasons, the free energy barriers obtained for the separated clusters

(ZL and ZB) have to be considered as somehow underestimated. In order to overcome the above points a silica-based cluster cut out from the edingtonite framework along the (001) direction, in which two silicon atoms were replaced by aluminium atoms, has been taken as surface model. In this cluster, one of the aluminium atoms, $Al(III)_{cus}$, is tricoordinated and acts as a Lewis centre, whereas the negative charge generated by the other Al atom is neutralized by adding a proton on one of the nearby oxygens which leads to a Brønsted site, (see Figure 6.18). In virtue of the much stronger interaction energy of water on Lewis than on Brønsted sites (-20 and -6.3 kcal/mol for H_2O adsorbed on Lewis or Brønsted sites, respectively), only the former has been solvated by one water molecule. Due to the size of such a cluster model calculations have been carried out by using the ONIOM2 approach described previously in the computational details section.

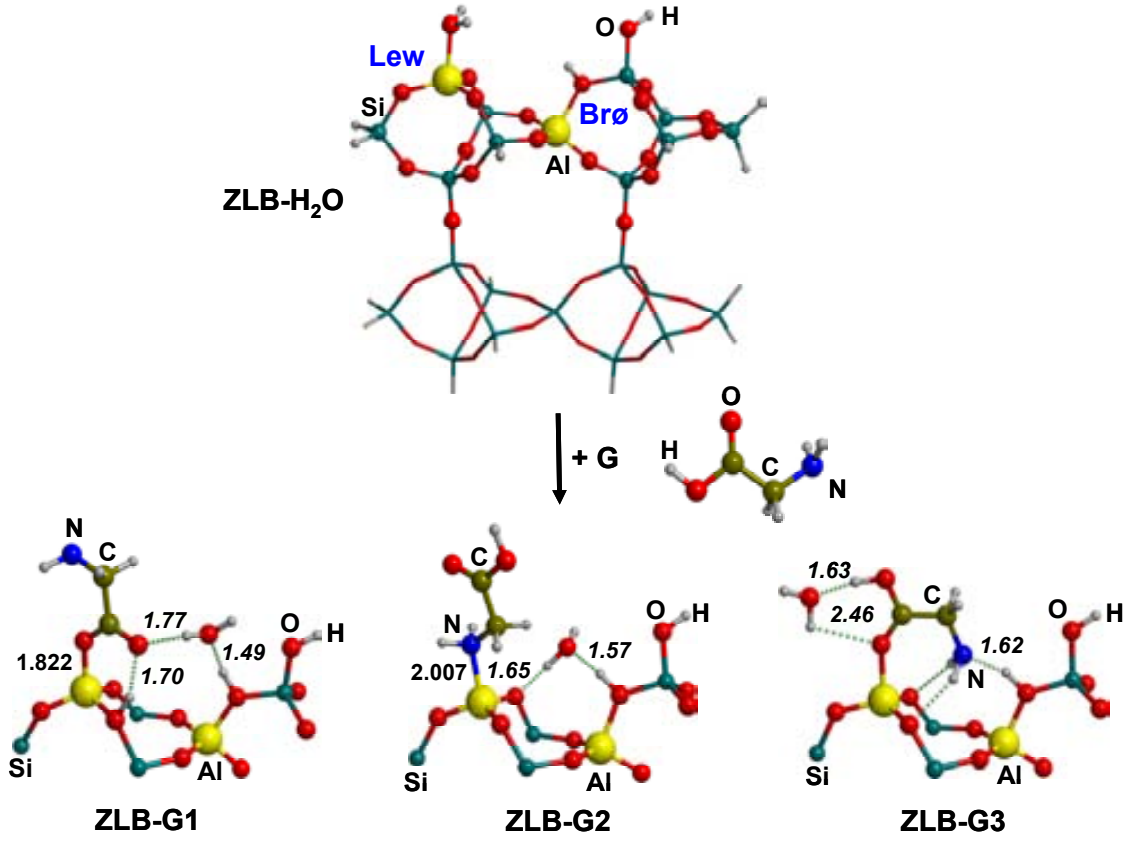

Figure 6.18 ONIOM2 optimized geometries of the cluster adopted to model the presence of the both Lewis and Brønsted sites on an aluminosilicate surface (ZLB-H_2O) and the isomers found when glycine interacts with the surface (ZLB-G1, ZLB-G2 and ZLB-G3). The region treated at high level of theory with ONIOM2 method is shown in balls. Distances in Å.

As done for the previous cases, first the adsorption of glycine on the model surface after displacing the water molecule it has been examined. Since the previous sections have

shown that the adsorption energy of glycine is stronger when it interacts with the Lewis site rather than with the Brønsted one (see Table 6.2 and Table 6.4), we have carefully examined the possible isomers that can be formed when glycine interacts with the Lewis site. The exploration of the whole range of conformers was not performed but three possible candidates close in energy were obtained, whose structures are represented in Figure 6.18: i) **ZLB-G1**, in which the carbonyl oxygen atom interacts with the Lewis site, the carboxylic proton is transferred to a nearby oxygen of the surface and the water molecule is displaced to interact with the Brønsted site, ii) **ZLB-G2**, in which the nitrogen amine interacts with the Lewis site and the water molecule is anew displaced to the Brønsted site; and iii) **ZLB-G3**, where, similar to **ZLB-G1**, the carbonyl oxygen atom interacts with the Lewis site but the amine group is hydrogen bonded by the proton of the Brønsted site and the water molecule is now displaced to interact with the carboxyl group of glycine. Table 6.6 summarizes the reaction energies associated to the glycine adsorption ZLB + G → ZLB-G process and also the relative energies of the isomers found with different levels of theory. It is interesting to remark that results obtained with single-point B3LYP calculations at the ONIOM2 geometries are in excellent agreement with those obtained from full geometry optimizations at the B3LYP level, which confirms the validity of using the above-described methods to compute the energy barriers and reaction energies with the less computationally cost. Because of the **ZLB-G1** is the ground state isomer, such a structure has been taken as the pre-reactant complex to react with NH_3.

Table 6.6 Electronic energy (ΔE_{displ}) and free energy ($\Delta_{displ} G_{298}$) of the water displacement reactions, ZLB-H_2O + G → ZLB-G + H_2O, according to the method employed. ΔE_{rel} and $\Delta_{rel} G_{298}$ are the corresponding relative energies with respect to the most stable structure computed for ZLB site. In kcal/mol.

Isomers	ΔE_{displ}/B1 ($\Delta_{displ} G_{298}$/B1)	ΔE_{displ}/B2	ΔE_{rel}/B1 ($\Delta_{displ} G_{298}$/B1)	ΔE_{rel}/B2
ZLB-G1	-33.9 (-21.0)	-34.0	0.0 (0.0)	0.0
ZLB-G2	-31.6 (-17.5)	-31.7	2.3 (3.5)	2.4
ZLB-G3	-28.3 (-14.4)	-28.4	5.6 (6.6)	5.6

B1: B3LYP/6-31+G(d,p)//ONIOM2[B3LYP/6-31+G(d,p):MNDO]; B2: B3LYP/6-31+G(d,p). The $\Delta_{disp}G_{298}$/B1 and $\Delta_{rel}G_{298}$/B1 values were computed using the B1 electronic energy and the ONIOM2 thermal and entropic corrections.

The free energy profile of the reaction for the **ZLB-G1** isomer is shown in Figure 6.19. The reported energy values have been computed with respect to the **ZLB-G1** + NH_3 asymptote.

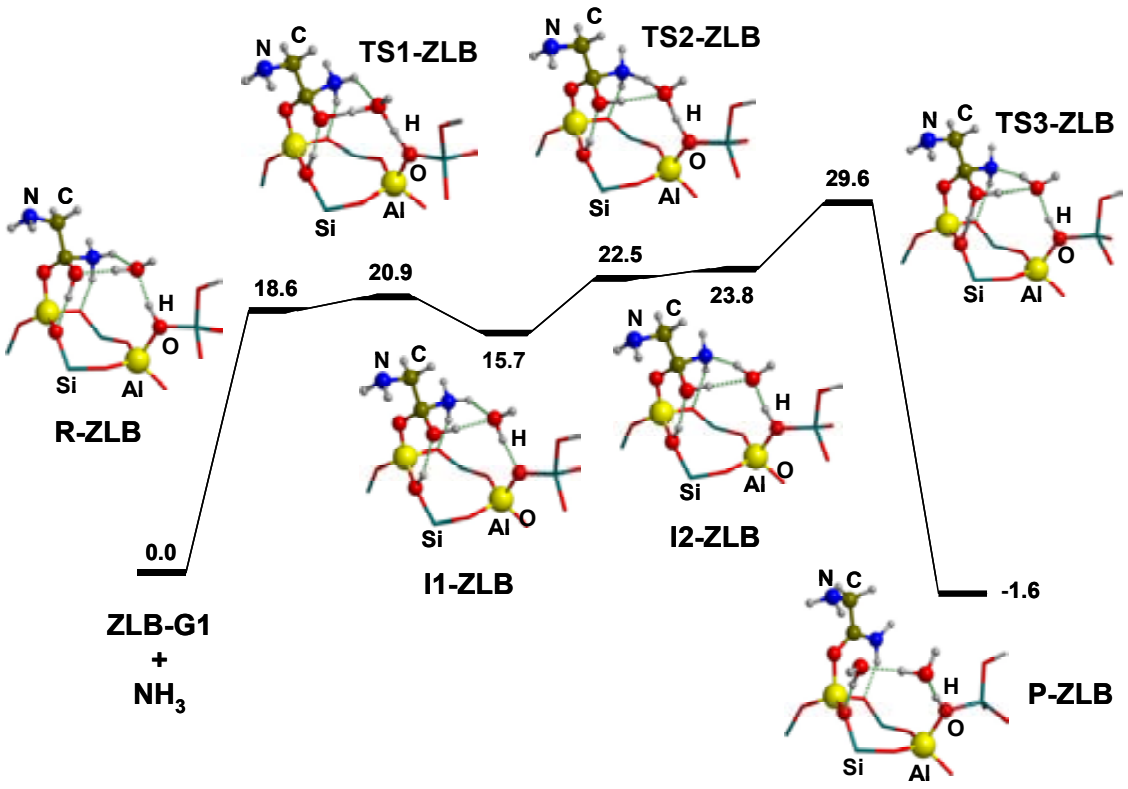

Figure 6.19 Free energy profile, in kcal/mol, of the peptide bond formation reaction taking ZLB-G1 as the pre-reactant complex. Computed at B3LYP/6-31+G(d,p)//B3LYP/6-31+G(d,p):MNDO level including the ONIOM2 thermal and entropic corrections.

The interaction of the ammonia molecule with **ZLB-G1** leads to the formation of the **R-ZLB** complex in which the NH_3 is bound to the carboxyl carbon of glycine and the proton previously transferred to the surface is recovered by the hydroxyl group of glycine. Similar structures were located when considering only the presence of single Lewis sites (**ZL-G1**), and its formation is associated to a clear activation of the carboxyl carbon atom of glycine due to the strong acidity of the Lewis site. **R-ZLB** can be understood as the starting point to effectuate the condensation reaction between glycine and ammonia which, in addition, can be assisted by the water molecule that is hydrogen bonded with the Brønsted site. The exploration of the PES shows that the peptide bond formation proceeds

via a stepwise process involving three main steps. In the first one (**R-ZLB → TS1-ZLB → I1-ZLB**), three simultaneous proton transfer take place: i) from the Brønsted site to the water molecule; ii) from the water molecule to the hydroxyl group of glycine; and iii) from the hydroxyl group of glycine to an oxygen of the surface. That is, in the resultant structure (**I2-ZLB**) the Brønsted site has jumped next to the Lewis site. The second step (**I1-ZLB → TS2-ZLB → I2-ZLB**) occurs via two simultaneous proton transfers: i) from the NH_3 molecule to the water molecule; and ii) from the water molecule to the oxygen of the initial Brønsted site. In **I2-ZLB** the NH-CO bond has already been formed. However, in order to complete the reaction, it is necessary to release a water molecule from the initial glycine. This is effectuated in the third step (**I2-ZLB → TS3-ZLB → P-ZLB**), where the proton of the Brønsted site next to the Lewis one is transferred to the hydroxyl oxygen of glycine, which induces the cleavage of the C-OH bond and the release of water necessary to finish the process. Although the topology of the potential energy surface indicates the presence of two intermediates **I1-ZLB** and **I2-ZLB**, the latter one is not relevant since the inclusion of thermal and entropic effects at 298K makes this structure lie above **TS2-ZLB**.

According to the profile, it is noticeable that the most demanding energy step is the formation of the **R-ZLB** structure, which is around 19 kcal/mol less stable than the reactants per separate. Analysis of the entropic and enthalpic terms show that this difference mainly arise from the entropic term, which is around 18 kcal/mol at 298 K. This fact indicates that the NH_3 needs to be very well orientated towards the carboxyl carbon atom in order to form the **R-ZLB** complex. This instability is kept along the entire reaction path, the global free activation energy of the process resulting around 30 kcal/mol, which is the energy difference between the asymptote and the **TS3-ZLB** points. Despite the entropic cost due to the formation of the **R-ZLB** complex, the global free energy barrier is still significantly lower than that in gas phase. However, the barrier is not as low as one could expect considering the activation observed in the isolated Lewis in presence of water and Brønsted model sites (27 and 18 kcal/mol, respectively). In view of that, the edingtonite surface is not adequate to proper activate the process so that another aluminosilicate surface containing Lewis and Brønsted sites should be considered.

6.3.3.4 Lewis/Brønsted interplay using a sanidine feldspar framework

Feldspar minerals are common aluminosilicates present in nature that possess certain loading of Lewis and Brønsted sites along its surface. Following a suggestion of Smith[332] about the catalytic role of feldspars as the most abundant minerals in the Earth

crust, such as anortite and sanidine (the most common feldspars constituents), we have also used these minerals as catalysts for the peptide bond formation. These materials envisage a silica-based framework in which Ca or K are present as a charge balancing cations for the Al substitution. The watering of the surfaces of these materials, together with fluctuating thermal conditions, will allow for the exchange of some of the cations by protons, resulting in surfaces rich in Lewis and Brønsted sites, as happens for the preparation of acidic zeolites used as cracking catalysts. **SF** of Figure 6.20 is a cartoon of a possible H-exchanged sanidine feldspar surface: terminal silanols (Si-OH), Brønsted sites and Lewis sites with a coordinated water, are all present as active surface sites. This surface has been modelled by the cluster **SF-H_2O** of Figure 6.20 and treated with ONIOM2 method due to its large size. As it can be seen, Lewis and Brønsted sites can also be rather proximal in space, so that their interplay in the adsorption and catalysis may be an important issue.

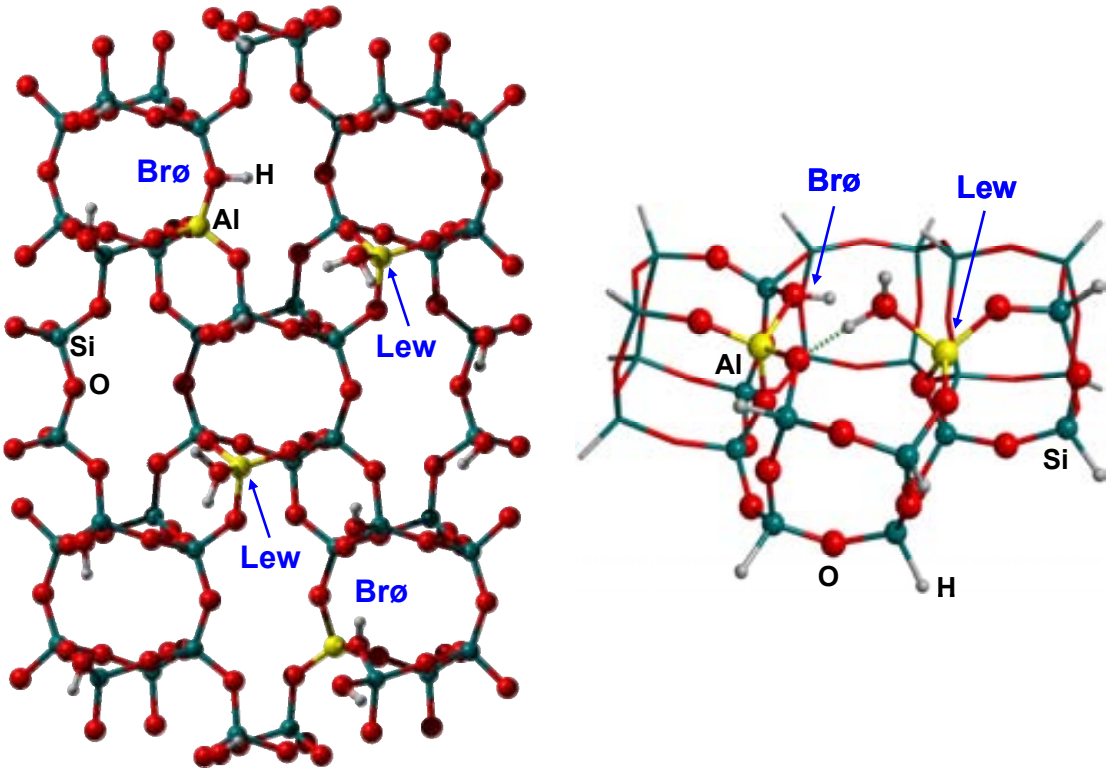

SF **SF-H_2O**

Figure 6.20 Left: top view of the sanidine feldspar (SF) surface containing Lewis and Bronsted sites. Right: Cluster adopted to model the feldspar surface with a water molecule bound to the Lewis site (SF-H_2O). The region treated at high level of theory with ONIOM2 method is shown in balls.

The **SF-H_2O** adduct shows that water bridges, via a rather short hydrogen bond, a second framework oxygen directly bound to the aluminium atom of the Brønsted site. As done for the previous cases, the water displacement process by glycine has first been considered. Since data of the previous sections has showed that glycine adsorbs more tightly on Lewis than on Brønsted sites, only interaction with the former has been considered, to save computer time. Figure 6.21 shows the possible adducts formed bwteen glycine and SF. Table 6.7 summarizes the reaction energies associated to the water displacement by glycine **SF-H_2O** + G → **SF-G** + H_2O and also the corresponding relative energies of the surface/adducts. The corrections to the DFT energy due to dispersive interactions have been estimated for the SF cluster and the corresponding values are reported in parenthesis.

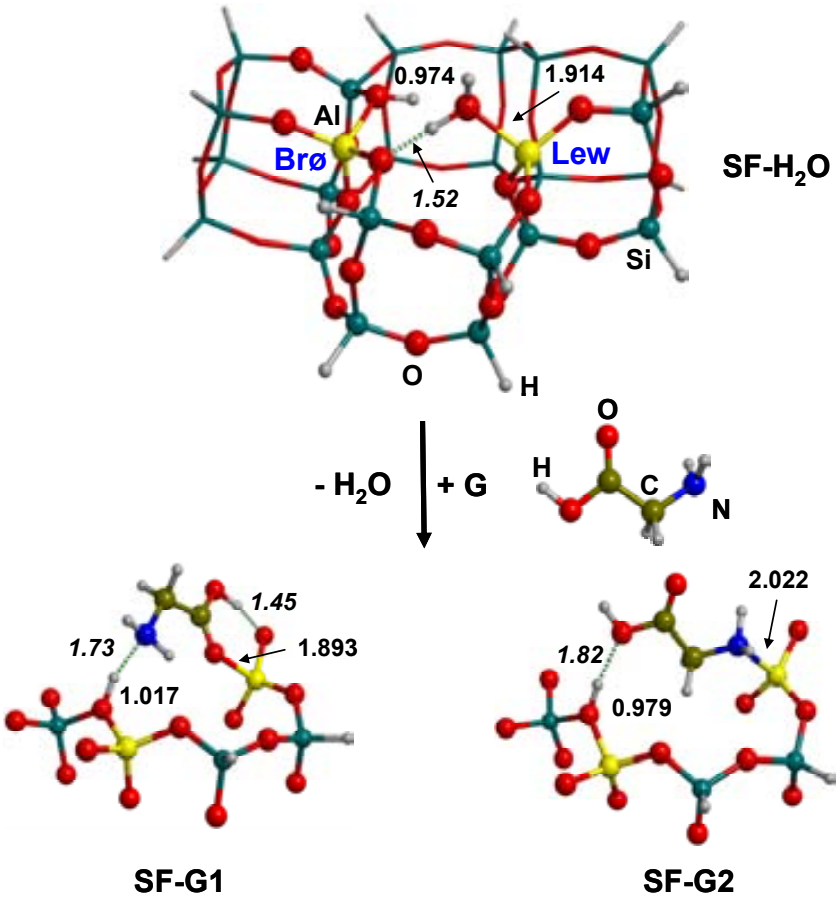

Figure 6.21 ONIOM2[B3LYP/6-31+G(d,p):MNDO] optimized geometries of the SF-H2O and the structures found when adsorbed water is replaced by glycine (SF-G1 and SF-G2). For the sake of clarity only a subportion of the high level zone is shown for SF-G1 and SF-G2. Bond distances in Å.

Table 6.7 Electronic energy (ΔE_{displ}) and free energy ($\Delta_{displ}G_{298}$) of the water displacement reactions, SF-H_2O + G → SF-G + H_2O. ΔE_{rel} and ΔG_{rel} are the corresponding relative energies with respect to the most stable structure computed for the SF site. ΔE computed at the B1=B3LYP/6-31+G(d,p)//ONIOM2[B3LYP/6-31+G(d,p):MNDO] level; ΔG_{298} computed using the B1 electronic energy and the ONIOM2 thermal and entropic corrections. Numbers in parenthesis at B1+D (dispersion included). In kcal/mol.

Isomers	ΔE_{displ}	$\Delta_{displ}G_{298}$	ΔE_{rel}	$\Delta_{rel}G_{298}$
SF-G1	-12.6	-9.4	0.0	0.0
	(-15.9)	(-12.7)	(0.0)	(0.0)
SF-G2	-8.2	-5.3	4.4	4.1
	(-11.7)	(-8.8)	(4.2)	(3.9)

SF-G1, the most stable isomer, envisages the glycine carbonyl oxygen bound to the surface $Al(III)_{cus}$ atom, the carboxylic proton making an hydrogen bond to a surface basic oxygen and the NH_2 group accepting a hydrogen bond from the surface Brønsted OH group. **SF-G2** structure is slightly more unstable than the **SF-G1** one: the glycine NH_2 now bonds to the surface $Al(III)_{cus}$ atom and the OH group accepts a hydrogen bond from the surface Brønsted OH group. As expected, dispersive contribution is much more relevant for the **SF-G1** and **SF-G2** adducts than for the **SF-H_2O** one, due to larger molecular size of glycine compared to water; the relative **SF-G1**/**SF-G2** stability is, however, almost unchanged by the dispersive correction, due to the close similarity of the two adducts.

In principle, both **SF-G1** and **SF-G2** should undergo the reaction with NH_3 to mimick the peptide bond activation by the surface active sites. However, the previous results for the separated ZL and ZB cases showed that the Brønsted site was the most active catalyst (free barrier energy of about 18 kcal/mol), and in particular, when considering the **ZB-G3** adduct as a starting configuration, in which glycine is adsorbed through the Brønsted acidic site via its carboxylic group (see Figure 6.16 and Figure 6.17). For that reason, and also to diminish the computational burden, the **SF-G2** has been selected as the best candidate for the peptide bond activation in virtue of its similarity with the **ZB-G3** one (compare Figure 6.16 and Figure 6.21, **ZB-G3** and **SF-G2**, respectively). The relative **SF-G2** population of $\approx 10^{-3}$ at equilibrium (computed using B1+D data of

Table 6.7) compared to the most stable **SF-G1** adduct is high enough to provide sufficient amount of **SF-G2** on a geological time scale.

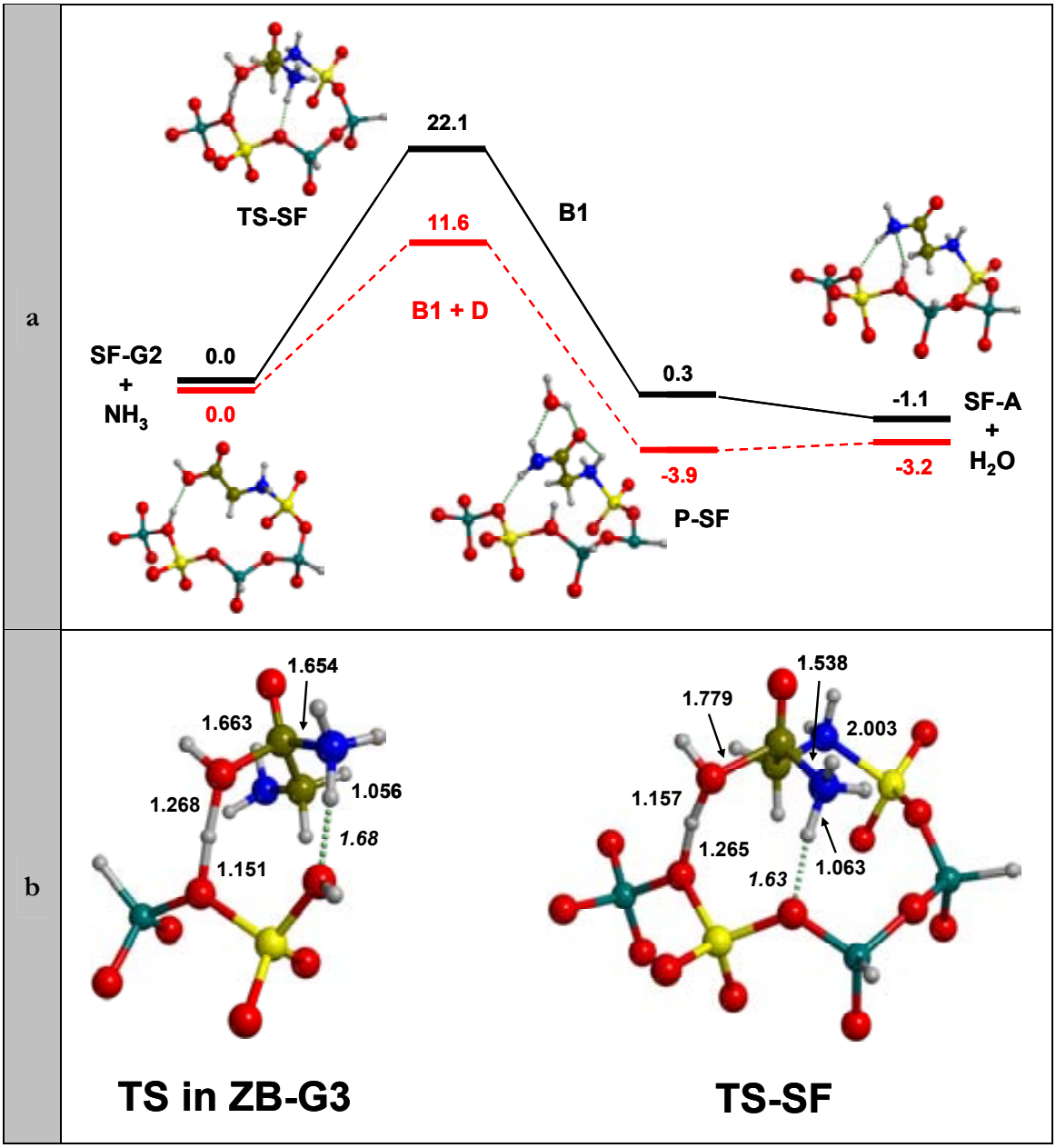

Figure 6.22 a): free energy profiles, in kcal/mol, of the peptide bond formation reaction taking SF-G2 as the pre-reactant complex. Values reported in black color computed at B1=B3LYP/6-31+G(d,p)//ONIOM2[B3LYP/6-31+G(d,p):MNDO] level including the ONIOM2 thermal and entropic corrections. The free energy profile reported in red color (B1+D) includes the dispersive correction to the B1 free energies. b): detailed view of the transition states activated complexes for the isolated Brønsted (TS in ZB-G3) and for the Lewis/Brønsted (TS-SF) cases. Distances in Å.

Figure 6.22 shows the PES for the reaction of NH_3 with the **SF-G2** structure: the transition state activated complex reveals a structure which is very close to the one predicted for the smallest ZB cluster, whereas the final **SF-A** product remains attached to

the mineral surface via a strong bond with the Lewis site and two hydrogen bonds with the regenerated Brønsted site (albeit with the acidic proton displaced on a different AlO_4 oxygen). In Figure 6.22b the geometries of the two activated complexes are compared: for the more realistic SF cluster the acidic proton of the Brønsted site is more elongated than for the ZB case (1.26 Å vs 1.15 Å) whereas the hydrogen bond from the incoming NH_3 with the surface oxygen is shorter for the SF than for the ZB cluster (1.63 Å vs 1.68 Å). The new CN bond is shorter for the SF than for the ZB (1.54 Å vs 1.65 Å) and, consequently the CO bond is longer for the former than for the latter (1.78 Å vs 1.66 Å) showing that the SF activated complex resembles more to the final products than the ZB one. All this effects reveal a higher acidic nature of the larger SF cluster than for the simplest ZB one. The B1 barrier with respect to the **SF-G2** complex is only 22.1 kcal/mol, which becomes 26 kcal/mol when reference to the most stable **SF-G1** complex is made, showing a relevant activation due to the mineral surface compared to the gas phase reaction. Role of dispersion on the PES has also been studied: Figure 7a shows a dramatic reduction of the kinetic barrier, which is now as low as 12 kcal/mol with respect to **SF-G2** (16 kcal/mol with respect to SF-G1), resulting in a speedup of the peptide bond formation of about 27 orders of magnitude compared to the gas phase barrier (including dispersion) of 47.8 kcal/mol. In the SF case, the dispersive correction is about 11 kcal/mol for the activated complex. The inclusion of dispersive effects has also been carried out for the ZB activated complex (derived from the **ZB-G3** adduct, see Figure 6.17), resulting in a reduction of the kinetic barrier by 7 kcal/mol, bringing the final barrier to 11 kcal/mol, very close to computed for the SF case. It is reassuring that, despite the relatively large energetic cost of the geometrical reorganization for the SF cluster (estimated to be 8.7 kcal/mol), the final barrier is close to that computed for the ZB model, in which this extra cost was negligible (estimated to be 1.6 kcal/mol). Dispersive interactions are also important in stabilizing the final ZLB-A product: the B1 value of –1.1 kcal/mol becomes –3.2 kcal/mol when B1+D is adopted, to be compared to the –1.7 kcal/mol value of the gas-phase process.

In conclusion, the Brønsted/Lewis interplay allows firstly capturing the glycine from the aqueous solution, securing it to the mineral surface via a strong interaction with the Lewis site via the NH_2 group, while the COOH moiety becomes activated towards nucleophylic attack by interacting with the nearby Brønsted site. When the reaction with NH_3 is considered, the kinetic barrier for the peptide bond formation is dramatically reduced and the product remains attached to the mineral surface because of the largest

dispersive contribution of the surface compared to the gas phase process. These results evidence the influence of Lewis and Brønsted sites present in aluminosilicates surfaces for the peptide bond formation, suggesting the capability of such supports to be good catalysts in the prebiotic stages.

6.3.3.5 Oligomerization of peptides on surfaces

The present results have shown that peptide bond formation process could have been kinetically and thermodynamically favoured by aluminosilicate surfaces in a primitive Earth conditions. However, the obvious question is if the above-exposed catalyzed reactions could have a cyclic behaviour in order to elongate the peptide chain; that is, if aluminosilicates could have played an important role on the prebiotic peptide oligomerization. The fact that the product 2-aminoacetamide anchored to the mineral surface via its strong interaction with the Lewis site is always more stable than the reactant in such a way that the original catalytic site is not restored is an important point. A question, however, remains: because dispersive interactions between the attached adsorbate and the mineral surfaces are so relevant, should one expect an even more important stabilization when the full reaction involving glycine instead of the simplest NH_3 molecule is studied? Because we cannot afford to study the whole PES for the full reaction, only the product resulting from the condensation of two glycine molecules (**SF-GG**) has been optimized Figure 6.23a. compares the free energy of reaction for the model reaction releasing **SF-A** and water as a product and for the full reaction envisaging two glycine molecules giving rise to **SF-GG** and water as products.

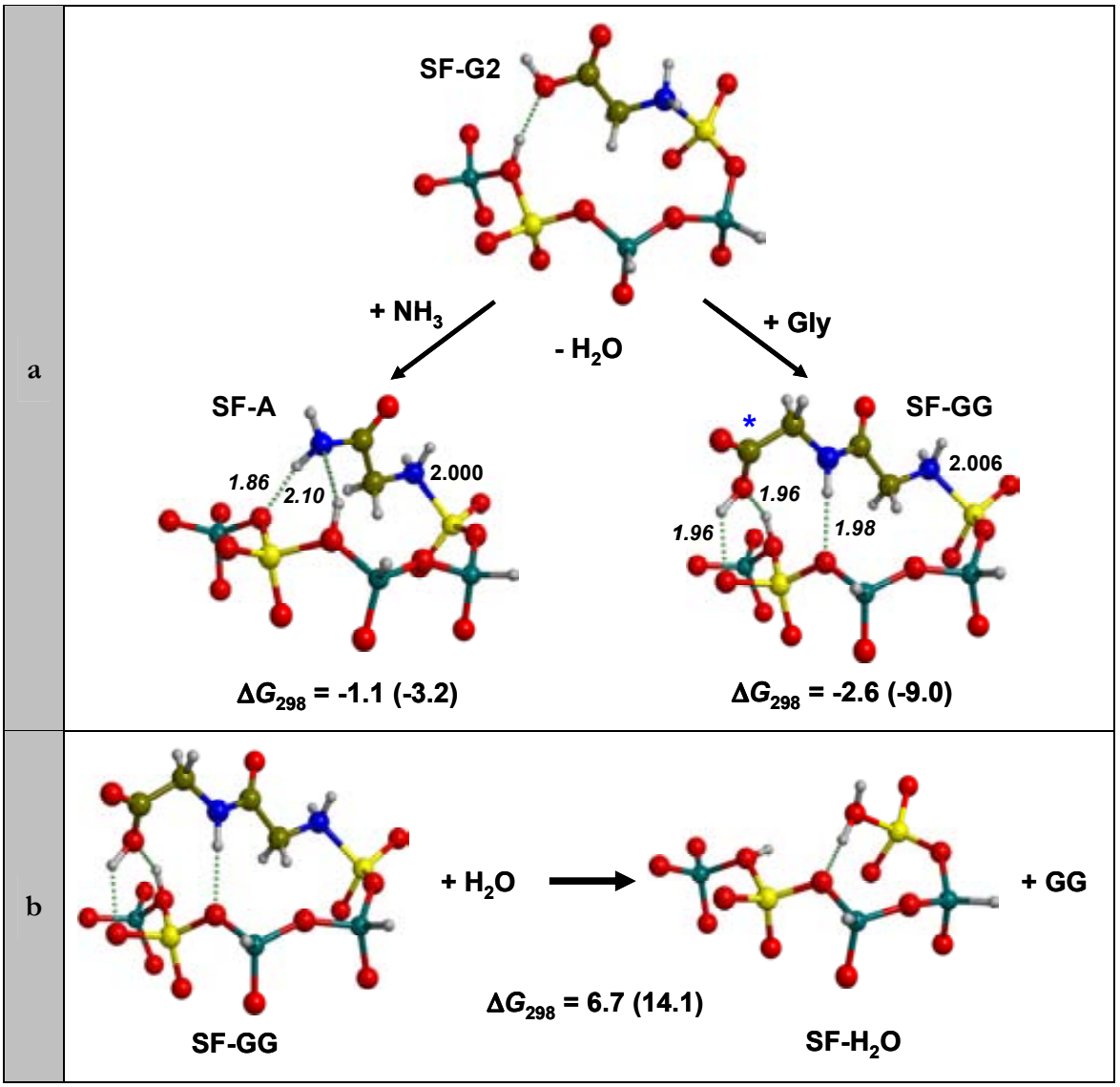

Figure 6.23 a) Free energy of formation of SF-A and SF-GG products. Bond distances in Å. The asterisk indicates the site of the nucleophylic attack by an incoming glycine molecule. b) Water displacement process considering SF-GG as a reactant. Bare numbers at B1=B3LYP/6-31+G(d,p)//ONIOM2[B3LYP/6-31+G(d,p):MNDO] level including the ONIOM2 thermal and entropic corrections, numbers in parenthesis at B1+D (dispersion included). Data in kcal/mol.

Interestingly, whereas the B1 stabilization of the **SF-GG** product is almost doubled compared to **SF-A** product (from –1.1 to –2.6 kcal/mol), taking dispersion into account at the B1+D level greatly stabilizes the **SF-GG** product (from –3.2 to –9.0 kcal/mol). This means that the condensation reaction will thermodynamically favour the corresponding product, because of the rather large dispersive interactions with the mineral surface, a fact which is at variance with what would happen in solution. Therefore, the **SF-GG** product will stay attached to the mineral surface and, as Figure 6.23a shows, can also undergo toward a second nucleophylic attack by means of an incoming glycine molecule, as

indicated by the asterisk. This carbonylic carbon atom is activated by the rather strong hydrogen bond formed by the OH group with the surface Brønsted site. In this way the chain can be elongated, and if the surface presents enough acidic sites, this process can be iterated. To allow for the elongation process in a very diluite environment (as it would probably be the case in the prebiotic world), the population of the **SF-GG** complex should be high enough to allow for numerous reactive encounters with glycine molecules in solution. Figure 6.23b shows the displacement reaction in which glycylglycine is exchanged by water: the reaction is strongly endoergonic, the standard ΔG_{298} of reaction being 6.7 kcal/mol at B1 level and 14.1 kcal/mol at B1+D level, respectively. This means that the **SF-GG** product will stay available for long time for further polymerization, even in presence of a water excess, in agreement with the suggestion put forward by Orgel[295] about polymerization on the rocks, in which the interaction of the polypeptide with the surface becomes more and more important with the chain lengthening due to favorable dispersive and electrostatic interaction, opening the possibility that the polypeptide coating the surface will act as a further template.

7. CONCLUSIONS

It is said that a molecule is activated when, owing to an external agent, it possesses different reactivity than in its normal state. This work addresses the activation of small biomolecules, in particular, the activation of amino acids and peptides by the interaction of $Cu^{+/2+}$ cations and aluminosilicates. Because nowadays generating metal-ligand systems in the gas phase and studying the reactivity induced by the metal cation is feasible by means of mass spectrometry techniques, the work is mainly focused on the context of the metal ion gas phase chemistry. Nevertheless, the activation of biomolecules by the interaction of mineral surfaces has also been addressed since its direct implications in heterogeneous catalysis as well as in novel applications such as bionanotechnology. The present section summarizes the main results obtained along this thesis.

Coordination of $Cu^{+/2+}$ to aromatic amino acids (AA_{arom})

The most stable structure of Cu^{+}-AA_{arom} for AA_{arom} = Phe, Tyr and Trp corresponds to a tridentate N/O/ring with the metal interacting with the π system of the side chain (similar to Cu^{+}-Glycine plus the lateral chain). In contrast, the ground-state structure of the Cu^{+}-His complex does not present cation-π interactions because the metal prefers to interact with the NH_2 and the Nδ of imidazole.

The most stable isomer for Cu^{2+}-Phe, -Tyr and -Trp is bidentate with the oxygen of the carbonyl and the amine nitrogen interacting with the metal cation. This is a consequence of the oxidation induced by Cu^{2+} to the aromatic side chain in such a way that a repulsive electrostatic interaction is generated between the aromatic ring and the metal cation. For Cu^{2+}-His, the ground state structure does not present oxidation of the amino acid, the coordination to Cu^{2+} being tridentate with the oxygen of the carbonyl group, the nitrogen amine and the Nδ imidazole.

The computed binding energies for Cu^{+}-AA_{arom} systems follow the order Cu^{+}-His > Cu^{+}-Trp > Cu^{+}-Tyr > Cu^{+}-Phe, whereas for Cu^{2+}-AA_{arom} the order is Cu^{2+}-Trp >Cu^{2+}-His > Cu^{2+}-Tyr > Cu^{2+}-Phe. While for Cu^{+} systems the obtained order is in very good agreement with the relative cation affinities determined experimentally, for the Cu^{2+} ones the sequence is related to the ionization energy of the ligands for the cases of Phe, Tyr and Trp.

Finally, infrared spectra of the low-lying structures of Cu^+-Phe and Cu^+-His have been simulated, in which the important changes observed among the different isomers can be very useful for structural determination.

Experimental and theoretical exploration of the Cu^+-AA_{arom} complexes reactivity

The ESI-MS experiments of a mixture of copper sulphate with the four aromatic amino acids yield the formation of several Cu^+ complexes, the most important one corresponding to Cu^+-AA_{arom}.

The collision-induced decomposition of Cu^+-AA_{arom} at different collision energies shows that the most important fragmentation is the loss of CH_2O_2 as found for Cu^+-glycine. Other fragmentations corresponding to the loss of $CuC_2O_2NH_4$, CuCOOH, $C_2O_2NH_3$, CO_2NH_3 and H_2O, the formation of Cu^+-NH_3, and the dissociation of the complexes into Cu^+ and respective amino acid are observed in the spectra.

The exploration of the potential energy surface for Cu^+-Phe using the B3LYP functional shows that the most of the observed eliminations are produced from insertion of the metal cation into the backbone C-C bond of Phe (losses of CH_2O_2, CuCOOH and CO_2NH_3) or into the C-R bond (losses of $CuC_2O_2NH_4$ and $C_2O_2NH_3$). For Cu^+-His, loss of CO_2NH_3 presents similar intensity with the loss of CH_2O_2, probably due to the different structure of the ground-state isomer for this system with respect to the others.

Coordination of $Cu^{+/2+}$ to poliglycines

The preferred metal coordination environment for the Cu^+-poliglycine systems does not depend on the peptide chain, following basically a linear dicoordination geometry. This is due to the *sd*σ hybridization that allows the system to efficiently reduce the Pauli repulsion.

In contrast, for Cu^{2+}-poligylicine systems the coordination number of the metal increases with the peptide chain: Cu^{2+}-GG is tricoordinated and Cu^{2+}-GGG and Cu^{2+}-GGGG are tetracoordinated. Additionally, it is found that Cu^{2+} induces less oxidation to poliglycines as the length of the peptide chain increases, a fact that can be explained as an effect of the coordination environment.

Finally, the binding energies for each system show that they increase in longer peptide chains. However, it can be discerned that in longer $(glycyl)_n$glycyl peptides (n > 3) the tendency probably will be to have similar binding energies.

Peptide bond formation catalyzed by Cu^{2+} cations and aluminosilicate surfaces

The catalytic role of Cu^{2+} cations in the peptide bond formation has been examined at the BHLYP level since the SIPF theory as well a mass spectrometry experiments suggested this metal cation to be a crucial activator for this process. Results rule out that an intracomplex condensation starting from Cu^{2+}-$(glycine)_2$ occurrs since it possesses a very high free energy barrier (97 kcal/mol) and reaction free energy (66 kcal/mol), due to the loss of metal ccordination during the reaction. Other mechanisms yielding the elimination of water have been found to present lower activation energies, especially when water molecules are involved as one would expect considering the presence of background water in the collision cell (the most stable path found resulting with an energy barrier of 47 kcal/mol).

The Cu^{2+}-cationized reaction has also been studied in aqueous solution using discrete water molecules and the CPCM continuous method. The synergy between the interaction of glycine molecules with Cu^{2+} and the presence of water molecules acting as proton-transfer helpers significantly lowers the activation barrier to 21 kcal/mol.

Finally, the catalytic role of aluminosilicate surfaces on the polymerization of amino acids early propsed by D. Bernal has computationally been addressed. The Lewis site alone reduces the barrier to 41 kcal/mol, whereas the activation by the Brønsted site dramatically reduces the barrier to 18 kcal/mol. Nevertheless, formation of the prereactant complex in this latter case will rarely occur, since water will easily displace the glycine molecule interacting with the Brønsted site. However, if a realistic feldspar surface with close Brønsted and Lewis sites is considered, the proper prereactant complex is highly stabilized by a simultaneous interaction with the Lewis and the Brønsted sites, in such a way that Lewis site strongly attaches the glycine molecule to the surface whereas the Brønsted site efficiently catalyzes the condensation reaction, showing that the interplay between Lewis/Brønsted sites is an important issue. The free energy barriers computed for the realistic feldspar surface model is 26 kcal/mol. However, role of dispersive interactions on the free energy barrier and the stabilization of the final product, not accounted for by the

B3LYP functional, have been estimated and shown to be substantial, the energy barrier decreasing to 16 kcal/mol.

Methodological aspects

The popular B3LYP method may fail when describing Cu^{2+}-ligand systems due to its tendency to overstabilise delocalized situations and as a consequence of a bad description of its 2nd ionization energy. Results for the low-lying electronic states of Cu^{2+}-H2O and for the relative energies of the Cu^{2+}-His isomers have shown that the BHLYP hybrid density functional (with more percentage of exact exchange than B3LYP) properly describes these situations and can be used as an alternative method for these open-shell systems.

It has been proved that dispersive interactions, accounted for with the Grimme post-DFT corrections, are very important to proper describe the interaction and reactivity of large biomolecules with oxide mineral surfaces.

8. BIBLIOGRAPHY

[1] E. de Hoffmann, J. Charette, V. Stroobant, *Mass Spectrometry: Principles and Applications*, John Wiley & Sons Ltd, Chichester, **1996**.

[2] M. L. Gross, R. Caprioli, Editors-in-chief, *The Encyclopedia of Mass spectrometry*, Elsevier, Oxford, **2003-2005**.

[3] S. Niu, M. B. Hall, *Chem. Rev.* **2000**, *100*, 353.

[4] P. E. M. Siegbahn, M. R. A. Blomberg, *Chem. Rev.* **2000**, *100*, 421.

[5] M. Torrent, M. Solà, G. Frenking, *Chem. Rev.* **2000**, *1000*, 439.

[6] H. Sommer, H. A. Thomas, J. A. Hipple, *Phys. Rev.* **1949**, *76*, 1877.

[7] M. D. Comisarov, A. G. Marshall, *Chem. Phys. Lett.* **1974**, *25*, 282.

[8] F. W. McLafferty, T. A. Bryce, *Chem. Commun.* **1967**, 1215.

[9] K. R. Jenning, *Int. J. Mass Spectrom. Ion Phys.* **1968**, *1*, 227.

[10] K. Eller, H. Schwarz, *Chem. Rev.* **1991**, *91*, 1121.

[11] G. Hornung, D. Schroeder, H. Schwarz, *J. Am. Chem. Soc.* **1995**, *117*, 8192.

[12] K. Seemeyer, D. Schroeder, M. Kempf, O. Lettau, J. Mueller, H. Schwarz, *Organometallics* **1995**, *14*, 4465.

[13] R. H. Hertwig, K. Seemeyer, H. Schwarz, W. Koch, *Chem. Eur. J.* **1997**, *3*, 1315.

[14] S. W. Buckner, R. M. Pope, *Int. J. Mass Spectrom.* **1999**, *182/183*, 197.

[15] J. Loos, D. Schroder, W. Zummack, H. Schwarz, *Int. J. Mass Spectrom.* **2002**, *217*, 169.

[16] S. LeCaer, H. Mestdagh, D. Schroeder, W. Zummack, H. Schwarz, *Int. J. Mass Spectrom.* **2006**, *255-256*, 239.

[17] M. C. Holthausen, A. Fiedler, H. Schwarz, W. Koch, *Angew. Chem. Int. Ed. Engl.* **1995**, *34*, 2282.

[18] D. Schröder, H. Schwarz, *Angew. Chem. Int. Ed. Engl.* **1995**, *34*, 1973.

[19] M. C. Holthausen, W. Koch, *J. Am. Chem. Soc.* **1996**, *118*, 9932.

[20] M. Barber, R. S. Bordoli, R. D. Sedgwick, A. N. Tyler, *J. Chem. Soc., Chem. Commun.* **1981**, *15*, 325.

[21] H. D. Beckey, *Principles of Field Ionization and Field Desorption in Mass Spectrometry*, Pergamon Press, Oxford, **1977**.

[22] R. D. McFarlane, T. F. Torgesson, *Science* **1976**, *191*, 970.

[23] R. D. McFarlane, *J. Am. Chem. Soc.* **1982**, *104*, 2948.

[24] M. Barber, R. S. Bordoli, G. Elliott, D. Fujimoto, J. E. Scott, *J. Chem. Soc., Chem. Commun.* **1982**, *16*, 936.

[25] J. B. Fenn, M. Mann, C. K. Meng, S. F. Wong, C. M. Whitehouse, *Science* **1989**, *246*, 64.

[26] M. Karas, D. Bachmann, U. Bahr, F. Hillenkamp, *Int. J. Mass Spectrom. Ion Processes* **1987**, *78*, 53.

[27] B. Spengler, D. Kirsch, R. Kaufmann, *Rapid. Comm. Mass Spectrom.* **1991**, *5*, 198.

[28] A. L. Lehninger, *Principles of Biochemistry*, Worth Publishers, Inc., **2000**.

[29] P. C. Wilkins, R. G. Wilkins, *Inorganic Chemistry in Biology*, Oxford University Press, **1997**.

[30] A. Sigel, H. Sigel, *Probing of proteins by metal ions and their low-molecular-wieght complexes. [In: Metal ions in biological systems.; Vol. 38]*, Marcel Dekker, Inc., New York, **2001**.

[31] V. C. Wasinger, S. J. Cordwell, A. Cerpa-Poljak, J. X. Yan, A. A. Gooley, M. R. Wilkins, M. W. Duncan, R. Harris, K. L. Williams, I. Humphery-Smith, *Electrophoresis* **1995**, *16*, 1090.

[32] W. J. Henzel, C. Watanabe, J. T. Stults, *J. Am. Soc. Mass Spectrom.* **2003**, *14*, 931.

[33] P. R. Graves, T. A. J. Haystead, *Microbiol. Mol. Biol. Rev.* **2002**, *66*, 39.

[34] I. K. Chu, X. Guo, T.-C. Lau, K. W. M. Siu, *Anal. Chem.* **1999**, *71*, 2364.

[35] I. K. Chu, D. M. Cox, X. Guo, I. Kireeva, T.-C. Lau, J. C. McDermott, K. W. M. Siu, *Anal. Chem.* **2002**, *74*, 2072.

[36] C. L. Gatlin, R. D. Rao, F. Turecek, T. Vaisar, *Anal. Chem.* **1996**, *68*, 263.

[37] S. J. Shields, B. K. Bluhm, D. H. Russell, *J. Am. Soc. Mass Spectrom.* **2000**, *11*, 626.

[38] K. Pierloot, J. O. A. De Kerpel, U. Ryde, M. H. M. Olsson, B. O. Roos, *J. Am. Chem. Soc.* **1998**, *120*, 13156.

[39] M. R. A. Blomberg, P. E. M. Siegbahn, G. T. Babcock, *J. Am. Chem. Soc.* **1998**, *120*, 8812.

[40] J. P. Collman, L. Fu, *Acc. Chem. Res.* **1999**, *32*, 455.

[41] P. Hu, C. Sorensen, M. L. Gross, *J. Am. Soc. Mass Spectrom.* **1995**, *6*, 1079.

[42] L.-J. Ming, J. D. Epperson, *J. Inorg. Biochem.* **2002**, *91*, 46.

[43] A. Gnjec, A. Fonte Justin, C. Atwood, N. Martins Ralph, *Front. Biosci.* **2002**, *7*, d1016.

[44] S. Hippeli, E. F. Elstner, *FEBS Lett.* **1999**, *443*, 1.

[45] C. Metcalfe, J. A. Thomas, *Chem. Soc. Rev.* **2003**, *32*, 215.

[46] E. A. Lewis, W. B. Tolman, *Chem. Rev.* **2004**, *104*, 1047.

[47] T. Prigge Sean, A. Eipper Betty, E. Mains Richard, L. M. Amzel, *Science* **2004**, *304*, 864.

[48] I. Tocheva Elitza, I. Rosell Federico, A. G. Mauk, E. P. Murphy Michael, *Science* **2004**, *304*, 867.

[49] W. Aboelella Nermeen, M. Reynolds Anne, B. Tolman William, *Science* **2004**, *304*, 836.

[50] M. Alcamí, O. Mó, M. Yáñez, *Mass Spectrom. Rev.* **2001**, *20*, 195.

[51] B. Amekraz, J. Tortajada, J. P. Morizur, A. I. Gonzalez, O. Mó, M. Yáñez, I. Leito, P. C. Maria, J. F. Gal, *New J. Chem.* **1996**, *20*, 1011.

[52] A. Luna, B. Amekraz, J. P. Morizur, J. Tortajada, O. Mó, M. Yáñez, *J. Phys. Chem. A* **1997**, *101*, 5931.

[53] A. Luna, B. Amekraz, J. Tortajada, J. P. Morizur, M. Alcamí, O. Mó, M. Yáñez, *J. Am. Chem. Soc.* **1998**, *120*, 5411.

[54] A. Luna, B. Amekraz, J. P. Morizur, J. Tortajada, O. Mó, M. Yáñez, *J. Phys. Chem. A* **2000**, *104*, 3132.

[55] A. Luna, S. Gevrey, J. Tortajada, *J. Phys. Chem. B* **2000**, *104*, 110.

[56] L. Rodríguez-Santiago, M. Sodupe, J. Tortajada, *J. Phys. Chem. A* **2001**, *105*, 5340.

[57] L. Boutreau, E. Leon, L. Rodríguez-Santiago, P. Toulhoat, O. Mó, J. Tortajada, *J. Phys. Chem. A* **2002**, *106*, 10563.

[58] L. Boutreau, P. Toulhoat, J. Tortajada, A. Luna, O. Mó, M. Yáñez, *J. Phys. Chem. A* **2002**, *106*, 9359.

[59] L. Rodríguez-Santiago, J. Tortajada, *Int. J. Mass Spectrom.* **2002**, *219*, 429.

[60] A. Luna, M. Alcami, O. Mó, M. Yáñez, J. Tortajada, *Int. J. Mass Spectrom.* **2002**, *217*, 119.

[61] L. Boutreau, J. Tortajada, A. Luna, M. Alcamí, O. Mó, M. Yáñez, *Int. J. Quant. Chem.* **2002**, *86*, 138.

[62] M. Alcamí, A. Luna, O. Mó, M. Yáñez, L. Boutreau, J. Tortajada, *J. Phys. Chem. A* **2002**, *106*, 2641.

[63] L. Rodríguez-Santiago, M. Noguera, M. Sodupe, J. Y. Salpin, J. Tortajada, *J. Phys. Chem. A* **2003**, *107*, 9865.

[64] T. N. Parac, G. M. Ullmann, N. M. Kostic, *J. Am. Chem. Soc.* **1999**, *121*, 3127.

[65] I. K. Chu, C. F. Rodriquez, T.-C. Lau, A. C. Hopkinson, K. W. M. Siu, *J. Phys. Chem. B* **2000**, *104*, 3393.

[66] F. Rogalewicz, Y. Hoppilliard, G. Ohanessian, *Int. J. Mass Spectrom.* **2000**, *201*, 307.

[67] I. K. Chu, T. Shoeib, X. Guo, C. F. Rodriquez, A. C. Hopkinson, K. W. M. Siu, T. C. Lau, *J. Am. Soc. Mass Spectrom.* **2001**, *12*, 163.

[68] E. R. Talaty, B. A. Perera, A. L. Gallardo, J. M. Barr, M. J. Van Stipdonk, *J. Phys. Chem. A* **2001**, *105*, 8059.

[69] F. Rogalewicz, Y. Hoppilliard, G. Ohanessian, *Int. J. Mass Spectrom.* **2001**, *206*, 45.

[70] T. Shoeib, A. C. Hopkinson, K. W. M. Siu, *J. Phys. Chem. B* **2001**, *105*, 12399.

[71] Y. Hoppilliard, F. Rogalewicz, G. Ohanessian, *Int. J. Mass Spectrom.* **2001**, *204*, 267.

[72] T. Shoeib, A. Cunje, A. C. Hopkinson, K. W. M. Siu, *J. Am. Soc. Mass Spectrom.* **2002**, *13*, 408.

[73] F. Rogalewicz, Y. Hoppilliard, G. Ohanessian, *Int. J. Mass Spectrom.* **2003**, *227*, 439.

[74] C. L. Gatlin, F. Turecek, T. Vaisar, *J. Mass Spectrom.* **1995**, *30*, 1605.

[75] C. L. Gatlin, F. Turecek, T. Vaisar, *J. Am. Chem. Soc.* **1995**, *117*, 3637.

[76] T. Shoeib, K. W. M. Siu, A. C. Hopkinson, *J. Phys. Chem. A* **2002**, *106*, 6121.

[77] R. M. Moision, P. B. Armentrout, *Phys. Chem. Chem. Phys.* **2004**, *6*, 2588.

[78] R. M. Moision, P. B. Armentrout, *J. Phys. Chem. A* **2002**, *106*, 10350.

[79] W. Y. Feng, S. Gronert, C. Lebrilla, *J. Phys. Chem. A* **2003**, *107*, 405.

[80] M. T. Rodgers, P. B. Armentrout, *Acc. Chem. Res.* **2004**, *37*, 989.

[81] C. Ruan, M. T. Rodgers, *J. Am. Chem. Soc.* **2004**, *126*, 14600.

[82] M. M. Kish, G. Ohanessian, C. Wesdemiotis, *Int. J. Mass Spectrom.* **2003**, *227*, 509.

[83] V. Ryzhov, R. C. Dunbar, B. Cerda, C. Wesdemiotis, *J. Am. Soc. Mass Spectrom.* **2000**, *11*, 1037.

[84] A. Gapeev, R. C. Dunbar, *Int. J. Mass Spectrom.* **2003**, *228*, 825.

[85] A. Gapeev, R. C. Dunbar, *J. Am. Chem. Soc.* **2001**, *123*, 8360.

[86] W. Y. Feng, S. Gronert, C. B. Lebrilla, *J. Am. Chem. Soc.* **1999**, *121*, 1365.

[87] T. Wyttenbach, J. E. Bushnell, M. T. Bowers, *J. Am. Chem. Soc.* **1998**, *120*, 5098.

[88] M. M. Kish, C. Wesdemiotis, G. Ohanessian, *J. Phys. Chem. B* **2004**, *108*, 3086.

[89] B. A. Cerda, C. Wesdemiotis, *J. Am. Chem. Soc.* **1995**, *117*, 9734.

[90] B. A. Cerda, C. Wesdemiotis, *Int. J. Mass Spectrom.* **1999**, *187*, 107.

[91] S. A. McLuckey, D. Cameron, R. G. Cooks, *J. Am. Chem. Soc.* **1981**, *103*, 1313.

[92] P. B. Armentrout, *Int. J. Mass Spectrom.* **2000**, *200*, 219.

[93] S. Hoyau, G. Ohanessian, *J. Am. Chem. Soc.* **1997**, *119*, 2016.

[94] M. T. Rodgers, P. B. Armentrout, *Mass Spectrom. Rev.* **2000**, *19*, 215.

[95] R. Amunugama, M. T. Rodgers, *J. Phys. Chem. A* **2002**, *106*, 5529.

[96] R. Amunugama, M. T. Rodgers, *J. Phys. Chem. A* **2002**, *106*, 9092.

[97] R. Amunugama, M. T. Rodgers, *Int. J. Mass Spectrom.* **2003**, *227*, 339.

[98] R. Amunugama, M. T. Rodgers, *J. Phys. Chem. A* **2002**, *106*, 9718.

[99] R. Amunugama, M. T. Rodgers, *Int. J. Mass Spectrom.* **2003**, *222*, 431.

[100] R. Amunugama, M. T. Rodgers, *Int. J. Mass Spectrom.* **2003**, *227*, 1.

[101] B. S. Freiser, Editor, *Organometallic Ion Chemistry. [In: Understanding Chem. React.; Vol. 15]*, Kluwer Academic Publishers, Dordrecht, **1996**.

[102] F. Jensen, *J. Am. Chem. Soc.* **1992**, *114*, 9533.

[103] S. Hoyau, J.-P. Pelicier, F. Rogalewicz, Y. Hoppilliard, G. Ohanessian, *Eur. J. Mass Spectrom.* **2001**, *7*, 303.

[104] S. Hoyau, G. Ohanessian, *Chem. Eur. J.* **1998**, *4*, 1561.

[105] R. C. Dunbar, *J. Phys. Chem. A* **2000**, *104*, 8067.

[106] F. M. Siu, N. L. Ma, C. W. Tsang, *J. Am. Chem. Soc.* **2001**, *123*, 3397.

[107] F. M. Siu, N. L. Ma, C. W. Tsang, *Chem. Eur. J.* **2004**, *10*, 1966.

[108] J. M. Mercero, J. E. Fowler, J. M. Ugalde, *J. Phys. Chem. A* **1998**, *102*, 7006.

[109] J. M. Mercero, J. E. Fowler, J. M. Ugalde, *J. Phys. Chem. A* **2000**, *104*, 7053.

[110] J. M. Mercero, A. Irigoras, X. López, J. E. Fowler, J. M. Ugalde, *J. Phys. Chem. A* **2001**, *105*, 7446.

[111] J. M. Mercero, J. M. Matxain, X. López, J. E. Fowler, J. M. Ugalde, *Int. J. Quant. Chem.* **2002**, *90*, 859.

[112] J. Bertrán, L. Rodríguez-Santiago, M. Sodupe, *J. Phys. Chem. B* **1999**, *103*, 2310.

[113] E. Constantino, L. Rodríguez-Santiago, M. Sodupe, J. Tortajada, *J. Phys. Chem. A* **2005**, *109*, 224.

[114] C. Kapota, G. Ohanessian, *Phys. Chem. Chem. Phys.* **2005**, *7*, 3744.

[115] T. Shoeib, C. F. Rodriquez, K. W. Michael Siu, A. C. Hopkinson, *Phys. Chem. Chem. Phys.* **2001**, *3*, 853.

[116] C. H. S. Wong, N. L. Ma, C. W. Tsang, *Chem.-Eur. J.* **2002**, *8*, 4909.

[117] E. Constantino, A. Rimola, L. Rodríguez-Santiago, M. Sodupe, *New J. Chem.* **2005**, *29*, 1585.

[118] B. S. Freiser, J. L. Beauchamp, *Chem. Phys. Lett.* **1975**, *35*, 35.

[119] L. R. Thorne, J. L. Beauchamp, *Infrared photochemistry of gas phase ions [In: Gas Phase Ion Chem.; Vol. 3]*, Academic Press, New York, **1984**.

[120] J. Oomens, D. T. Moore, G. von Helden, G. Meijer, R. C. Dunbar, *J. Am. Chem. Soc.* **2004**, *126*, 724.

[121] D. T. Moore, J. Oomens, J. R. Eyler, G. von Helden, G. Meijer, R. C. Dunbar, *J. Am. Chem. Soc.* **2005**, *127*, 7243.

[122] R. C. Dunbar, D. T. Moore, J. Oomens, *J. Phys. Chem. A* **2006**, *110*, 8316.

[123] N. C. Polfer, J. Oomens, R. C. Dunbar, *Phys. Chem. Chem. Phys.* **2006**, *8*, 2744.

[124] N. C. Polfer, J. Oomens, D. T. Moore, G. Von Helden, G. Meijer, R. C. Dunbar, *J. Am. Chem. Soc.* **2006**, *128*, 517.

[125] D. Wen, T. Yalcin, A. G. Harrison, *Rap. Comm. Mass Spectrom.* **1995**, *9*, 1155.

[126] T. Yalcin, J. Wang, D. Wen, A. G. Harrison, *J. Am. Soc.Mass Spectrom.* **1997**, *8*, 749.

[127] Q. P. Lei, I. J. Amster, *J. Am. Soc. Mass Spectrom.* **1996**, *7*, 722.

[128] S. Bouchonnet, Y. Hoppilliard, G. Ohanessian, *J. Mass Spectrom.* **1995**, *30*, 172.

[129] H. Lavanant, Y. Hoppilliard, *J. Mass Spectrom.* **1997**, *32*, 1037.

[130] H. Lavanant, E. Hecquet, Y. Hoppilliard, *Int. J. Mass Spectrom.* **1999**, *185/186/187*, 11.

[131] P. Hu, J. A. Loo, *J. Am. Chem. Soc.* **1995**, *117*, 11314.

[132] H. Lavanant, Y. Hoppilliard, *Eur. Mass Spectrom.* **1999**, *5*, 41.

[133] H. Li, K. W. M. Siu, R. Guevremont, J. C. Y. Le Blanc, *J. Am. Soc. Mass Spectrom.* **1997**, *8*, 781.

[134] A. Reiter, J. Adams, H. Zhao, *J. Am. Chem. Soc.* **1994**, *116*, 7827.

[135] Y. D. Xu, X. Zhang, A. L. Yergey, *J. Am. Soc. Mass Spectrom.* **1996**, *7*, 25.

[136] M. J. Polce, S. Beranova, M. J. Nold, C. Wesdemiotis, *J. Mass Spectrom.* **1996**, *31*, 1073.

[137] M. Massaouti, M. Velegrakis, *Int. J. Mass Spectrom.* **2003**, *225*, 89.

[138] Y. Hoppilliard, G. Ohanessian, S. Bourcier, *J. Phys. Chem. A* **2004**, *108*, 9687.

[139] A. Rimola, M. Sodupe, J. Tortajada, L. Rodríguez-Santiago, *Int. J. Mass Spectrom.* **2006**, *255*, 60.

[140] I. K. Chu, C. F. Rodriquez, A. C. Hopkinson, K. W. M. Siu, T. C. Lau, *J. Am. Chem. Soc.* **2001**, *12*, 1114.

[141] I. K. Chu, S. O. Siu, C. N. W. Lam, J. C. Y. Chan, C. F. Rodriquez, *Rap. Comm. Mass Spectrom.* **2004**, *18*, 1798.

[142] C. L. Gatlin, F. Turecek, T. Vaisar, *J. Mass Spectrom.* **1995**, *30*, 1617.

[143] E. Bagheri-Majdi, Y. Ke, G. Orlova, I. K. Chu, A. C. Hopkinson, K. W. M. Siu, *J. Phys. Chem. B* **2004**, *108*, 11170.

[144] C. K. Barlow, S. Wee, W. D. McFadyen, R. A. J. O'Hair, *Dalton Trans.* **2004**, 3199.

[145] C. Seto, J. A. Stone, *Int. J. Mass Spectrom.* **1999**, *192*, 289.

[146] H. Wincel, R. H. Fokkens, N. M. M. Nibbering, *Rapid Commun. Mass Spectrom.* **2000**, *14*, 135.

[147] A. J. Dempster, *Phys. Rev.* **1918**, *11*, 316.

[148] W. Bleakney, *Phys. Rev.* **1929**, *34*, 157.

[149] A. O. Nier, *Rev. Sci. Instrum.* **1947**, *18*, 415.

[150] M. S. B. Munson, F. H. Field, *J. Am. Chem. Soc.* **1966**, *88*, 2681.

[151] A. G. Harrison, *Chemical Ionization*, CRC Press, Boca Raton, FL, **1983**.

[152] R. E. Ferguson, K. E. McCulloh, H. M. Rosenstock, *J. Chem. Phys.* **1965**, *42*, 100.

[153] W. Stephens, *Phys. Rev.* **1946**, *69*, 691.

[154] W. C. Wiley, J. B. McLaren, *Rev. Sci. Instrum.* **1955**, *16*, 1150.

[155] R. A. Yost, *Anal. Chem.* **1979**, *51*, 1251A.

[156] L. Operti, R. Rabezzana, *Mass Spectrom. Rev.* **2003**, *22*, 407.

[157] V. H. Wysocki, K. A. Resing, Q. Zhang, G. Cheng, *Methods* **2005**, *35*, 211.

[158] M. L. Gross, R. Caprioli, Editors., *Biological Applications, Parts A and B. [In: The Encyclopedia Mass Spectrom.; Vol. 2 and 3]*, Elsevier, Oxford, **2004**.

[159] D. P. Little, J. P. Speir, M. W. Senko, P. B. O'Connor, F. W. McLafferty, *Anal. Chem.* **1994**, *66*, 2809.

[160] M. Rosi, C. W. Bauschlicher, Jr., *Chem. Phys. Lett.* **1990**, *166*, 189.

[161] C. W. Bauschlicher, Jr., S. R. Langhoff, *J. Phys. Chem.* **1991**, *95*, 2278.

[162] M. Sodupe, C. W. Bauschlicher, Jr., *J. Phys. Chem.* **1991**, *95*, 8640.

[163] Y. D. Hill, B. S. Freiser, C. W. Bauschlicher, Jr., *J. Am. Chem. Soc.* **1991**, *113*, 1507.

[164] C. W. Bauschlicher, Jr., H. Partridge, S. R. Langhoff, *J. Phys. Chem.* **1989**, *91*, 4733.

[165] H. Partridge, C. W. Bauschlicher, Jr., S. R. Langhoff, *J. Phys. Chem.* **1992**, *96*, 5350.

[166] H. Partridge, C. W. Bauschlicher, Jr., *J. Phys. Chem.* **1994**, *98*, 2301.

[167] M. Rosi, C. W. Bauschlicher, Jr., *J. Chem. Phys.* **1989**, *90*, 7264.

[168] M. Rosi, C. W. Bauschlicher, Jr., *J. Chem. Phys.* **1990**, *92*, 1876.

[169] N. L. Allinger, T. Clark, J. Gasteiger, P. A. Kollman, H. F. Schaefer III, P. R. Schreiner, Editors., *Encyclopedia of Computational Chemistry, Vol. 5*, John Wiley & Sons Ltd, Chichester, **1998**.

[170] T. Ziegler, J. Li, *Can. J. Chem.* **1994**, *73*, 743.

[171] V. Barone, C. Adamo, F. Mele, *Chem. Phys. Lett.* **1996**, *249*, 290.

[172] M. R. A. Blomberg, P. E. M. Siegbahn, M. Svensson, *J. Chem. Phys.* **1996**, *104*, 9546.

[173] M. C. Holthausen, C. Heinemann, H. H. Cornehl, W. Koch, H. Scwarz, *J. Chem. Phys.* **1995**, *102*, 4931.

[174] M. C. Holthausen, M. Mohr, W. Koch, *Chem. Phys. Lett.* **1995**, *240*, 245.

[175] A. Ricca, C. W. Bauschlicher, Jr., *Chem. Phys. Lett.* **1995**, *245*, 150.

[176] W. Koch, M. C. Holthausen, *A Chemists's Guide to Density Functional Theory*, Second ed., WILEY-VCH Verlag, Weinheim, Federal Republic of Germany, **2001**.

[177] A. Luna, M. Alcamí, O. Mó, M. Yáñez, *Chem. Phys. Lett.* **2000**, *320*, 129.

[178] A. Irigoras, O. Elizalde, I. Silanes, J. E. Fowler, J. M. Ugalde, *J. Am. Chem. Soc.* **2000**, *122*, 114.

[179] P. Jayaweera, A. T. Blades, M. G. Ikonomou, P. Kebarle, *J. Am. Chem. Soc.* **1990**, *112*, 2452.

[180] D. Schroeder, H. Schwarz, *J. Phys. Chem. A* **1999**, *103*, 7385.

[181] A. A. Shvartsburg, K. W. Siu, *J. Am. Chem. Soc.* **2001**, *123*, 10071.

[182] A. J. Stace, *J. Phys. Chem. A* **2002**, *106*, 7993.

[183] I. Corral, O. Mó, M. Yáñez, A. P. Scott, L. Radom, *J. Phys. Chem. A* **2003**, *107*, 10456.

[184] I. Corral, O. Mó, M. Yáñez, J.-Y. Salpin, J. Tortajada, L. Radom, *J. Phys. Chem. A* **2004**, *108*, 10080.

[185] I. Corral, O. Mó, M. Yáñez, J.-Y. Salpin, J. Tortajada, D. Moran, L. Radom, *Chem. Eur. J.* **2006**, *12*, 6787.

[186] M. Trachtman, G. D. Markham, J. P. Glusker, P. George, C. W. Bock, *Inorg. Chem.* **1998**, *37*, 4421.

[187] D. Schröder, M. Engeser, H. Schwarz, J. N. Harvey, *ChemPhysChem* **2002**, *3*, 584.

[188] A. M. El-Nahas, N. Tajima, K. Hirao, *Chem. Phys. Lett.* **2000**, *318*, 333.

[189] A. M. El-Nahas, *Chem. Phys. Lett.* **2001**, *345*, 325.

[190] A. J. Stace, N. R. Walker, S. Firth, *J. Am. Chem. Soc.* **1997**, *119*, 10239.

[191] D. Schröder, H. Schwarz, J. Wu, C. Wesdemiotis, *Chem. Phys. Lett.* **2001**, *343*, 258.

[192] J. A. Stone, D. Vukomanovic, *Chem. Phys. Lett.* **2001**, *346*, 419.

[193] A. Palacios, I. Corral, O. Mó, F. Martin, M. Yáñez, *J. Chem. Phys.* **2005**, *123*, 014315.

[194] P. M. W. Gill, *Mol. Phys.* **1996**, *89*, 433.

[195] C. Lee, W. Yang, R. G. Parr, *Phys. Rev. B* **1988**, *37*, 785.

[196] A. D. Becke, *Phys. Rev. A* **1988**, *38*, 3098.

[197] A. D. Becke, *J. Chem. Phys.* **1993**, *98*, 5648.

[198] C. Adamo, V. Barone, *J. Chem. Phys.* **1998**, *108*, 664.

[199] J. P. Perdew, J. A. Chevary, S. H. Vosko, K. A. Jackson, M. R. Pederson, D. J. Singh, C. Fiolhais, *Phys. Rev. B* **1992**, *46*, 6671.

[200] J. P. Perdew, Y. Wang, *Phys. Rev. B* **1992**, *45*, 13244.

[201] A. D. Becke, *J. Chem. Phys.* **1993**, *98*, 1372.

[202] J. Cizek, *J. Chem. Phys.* **1966**, *45*, 4256.

[203] A. J. H. Wachters, *J. Chem. Phys.* **1970**, *52*, 1033.

[204] P. J. Hay, *J. Chem. Phys.* **1977**, *66*, 4377.

[205] K. Raghavachari, G. W. Trucks, *J. Chem. Phys.* **1989**, *91*, 1062.

[206] J. Poater, M. Solà, A. Rimola, L. Rodríguez-Santiago, M. Sodupe, *J. Phys. Chem. A* **2004**, *108*, 6072.

[207] B. Braïda, P. C. Hiberty, A. Savin, *J. Phys. Chem. A* **1998**, *102*, 7872.

[208] M. Sodupe, J. Bertrán, L. Rodríguez-Santiago, E. J. Baerends, *J. Phys. Chem. A* **1999**, *103*, 166.

[209] H. Chermette, I. Ciofini, F. Mariotti, C. Daul, *J. Chem. Phys.* **2001**, *115*, 11068.

[210] I. Georgieva, N. Trendafilova, L. Rodríguez-Santiago, M. Sodupe, *J. Phys. Chem. A* **2005**, *109*, 5668.

[211] H. Ai, Y. Bu, P. Li, Z. Li, X. Hu, Z. Chen, *J. Phys. Org. Chem.* **2005**, *18*, 26.

[212] M. Saunders, K. N. Houk, Y. D. Wu, W. C. Still, M. J. Lipton, *J. Am. Chem. Soc.* **1990**, *112*, 1419.

[213] F. Mohamadi, N. G. J. Richards, W. C. Guida, R. Liskamp, M. Lipton, C. Caufield, G. Chang, T. Hendrickson, W. C. Still, *J. Comput. Chem.* **1990**, *11*, 440.

[214] F. Maseras, K. Morokuma, *J. Comput. Chem.* **1995**, *16*, 1170.

[215] M. Svensson, S. Humbel, R. D. J. Froese, T. Matsubara, S. Sieber, K. Morokuma, *J. Phys. Chem.* **1996**, *100*, 19357.

[216] S. Dapprich, I. Komiromi, K. S. Byun, K. Morokuma, M. J. Frisch, *Theochem* **1999**, *461-462*, 1.

[217] T. Vreven, K. Morokuma, *J. Comput. Chem.* **2000**, *21*, 1419.

[218] I. Roggero, B. Civalleri, P. Ugliengo, *Chem. Phys. Lett.* **2001**, *341*, 625.

[219] X. Solans-Monfort, J. Bertrán, V. Branchadell, M. Sodupe, *J. Phys. Chem. B* **2002**, *106*, 10220.

[220] X. Solans-Monfort, V. Branchadell, M. Sodupe, C. M. Zicovich-Wilson, E. Gribov, G. Spoto, C. Busco, P. Ugliengo, *J. Phys. Chem. B* **2004**, *108*, 8278.

[221] X. Solans-Monfort, M. Sodupe, O. Mó, M. Yáñez, J. Elguero, *J. Phys. Chem. B* **2005**, *109*, 19301.

[222] X. Solans-Monfort, M. Sodupe, V. Branchadell, J. Sauer, R. Orlando, P. Ugliengo, *J. Phys. Chem. B* **2005**, *109*, 3539.

[223] U. Eichler, C. M. Kölmel, J. Sauer, *J. Comput. Chem.* **1996**, *18*, 463.

[224] M. Sierka, J. Sauer, *J. Chem. Phys.* **2000**, *112*, 6983.

[225] B. Kovacevic, M. Rozman, L. Klasinc, D. Srzic, Z. B. Maksic, M. Yañez, *J. Phys. Chem. A* **2005**, *109*, 8329.

[226] J. Sunner, K. Nishizawa, P. Kebarle, *J. Phys. Chem.* **1981**, *85*, 1814.

[227] D. A. Dougherty, *Science* **1996**, *271*, 163.

[228] J. C. Ma, D. A. Dougherty, *Chem. Rev.* **1997**, *97*, 1303.

[229] R. A. Kumpf, D. A. Dougherty, *Science* **1993**, *261*, 1708.

[230] W. Zhong, J. P. Gallivan, Y. Zhang, L. Li, H. A. Lester, D. A. Dougherty, *Proc. Natl. Acad. Sci. U.S.A.* **1998**, *95*, 12088.

[231] O. Donini, D. F. Weaver, *J. Comp. Chem.* **1998**, *19*, 1515.

[232] C. Miller, *Science* **1991**, *252*, 1092.

[233] L. Heginbotham, R. MacKinnon, *Neuron* **1992**, *8*, 483.

[234] S. L. de Wall, E. S. Meadows, L. J. Barbour, G. W. Gokel, *Proc. Natl. Acad. Sci. U.S.A.* **2000**, *97*, 6271.

[235] O. M. Cabarcos, C. J. Weinheimer, J. M. Lisy, *J. Chem. Phys.* **1999**, *110*, 8429.

[236] H. Minoux, C. Chipot, *J. Am. Chem. Soc.* **1999**, *121*, 10366.

[237] J. P. Gallivan, D. A. Dougherty, *Proc. Natl. Acad. Sci. U.S.A.* **1999**, *96*, 9459.

[238] V. A. Zakian, *Science* **1995**, *270*, 1601.

[239] M. Rooman, J. Lievin, E. Buisine, R. Wintjens, *J. Mol. Biol.* **2002**, *319*, 67.

[240] S. Mecozzi, A. P. West, Jr., D. A. Dougherty, *J. Am. Chem. Soc.* **1996**, *118*, 2307.

[241] S. Mecozzi, A. P. West, Jr., D. A. Dougherty, *Proc. Natl. Acad. Sci. U.S.A.* **1996**, *93*, 10566.

[242] J. W. Caldwell, P. A. Kollman, *J. Am. Chem. Soc.* **1995**, *117*, 4177.

[243] K. S. Kim, J. Y. Lee, S. J. Lee, T.-K. Ha, D. H. Kim, *J. Am. Chem. Soc.* **1994**, *116*, 7399.

[244] J. Y. Lee, S. J. Lee, H. S. Choi, S. J. Cho, K. S. Kim, T.-K. Ha, *Chem. Phys. Lett.* **1995**, *232*, 67.

[245] H. Basch, W. J. Stevens, *Theochem* **1995**, *338*, 303.

[246] N. C. Polfer, B. Paizs, L. C. Snoek, I. Compagnon, S. Suhai, G. Meijer, G. Von Helden, J. Oomens, *J. Am. Chem. Soc.* **2005**, *127*, 8571.

[247] S. J. Lippard, J. M. Berg, *Principles of Bioinorganic Chemistry*, University Science Books, Mill Valley, CA, **1994**.

[248] C. W. Bauschlicher, A. Ricca, H. Partridge, S. R. Langhoff, *Recent Advances in Density Functional Theory, Part II*, World Scientific Publishing Co, Singapore, **1997**.

[249] S. J. Weiner, P. A. Kollman, D. A. Case, U. C. Singh, C. Ghio, G. Alagona, S. Profeta Jr., P. Weiner, *J. Am. Chem. Soc.* **1984**, *106*, 765.

[250] S. J. Weiner, P. A. Kollman, D. T. Nguyen, D. A. Case, *J. Comput. Chem.* **1986**, *7*, 230.

[251] S. F. Boys, F. Bernardi, *Mol. Phys.* **1970**, *19*, 553.

[252] M. J. Frisch, G. W. Trucks, H. B. Schlegel, G. E. Scuseria, M. A. Robb, J. R. Cheesman, J. A. Montgomery, T. Vreven, K. N. Kudin, J. C. Burant, J. M. Millam, S. S. Iyengar, J. Tomasi, V. Barone, B. Mennucci, M. Cossi, G. Scalmanu, N. Rega, G. A. Petersson, H. Nakatsuji, M. Hada, M. Ehara, K. Toyota, R. Fukuda, J. Hasegawa, M. Ishida, T. Nakajima, Y. Honda, O. Kitao, H. Nakai, M. Klene, X. Li, J. E. Knox, H. P. Hratchian, J. B. Cross, C. Adamo, J. Jaramillo, R. Gomperts, R. E. Stratmann, O. Yazyev, A. J. Austin, R. Cammi, C. Pomelli, J. W. Ochterski, P. Y. Ayala, K. Morokuma, G. A. Voth, P. Salvador, J. J. Dannenberg, V. G. Zakrzewski, S. Dapprich, A. D. Daniels, M. C. Strain, O. Farkas, D. K. Malick, A. D. Rabuck, K. Raghavachari, J. B. Foresman, J. V. Ortiz, Q. Cui, A. G. Baboul, S. Clifford, J. Cioslowski, B. B. Stefanov, G. Liu, A. Liashenko, P. Piskorz, I. Komaromi, R. L. Martin, D. J. Fox, T. Keith, M. A. Al-Laham, C. Y. Peng, A. Nanayakkara, M. Challacombe, P. M. W. Gill, B. Johnson, W. Chen, M. W. Wong, C. Gonzalez, J. A. Pople, Gaussian 03; Wallingford CT, 2004

[253] D. McQuarrie, *Statistical Mechanics*, Harper and Row, New York, **1986**.

[254] F. Weinhold, C. Landis, R., *Valency and Bonding. A Natural Bond Orbital Donor-Acceptor Perspective*, Cambridge University Press, Cambridge, **2005**.

[255] J. H. Jensen, M. S. Gordon, *J. Am. Chem. Soc.* **1995**, *117*, 8159.

[256] E. F. Strittmatter, A. S. Lemoff, E. R. Williams, *J. Phys. Chem. A* **2000**, *104*, 9793.

[257] P. Deschamps, P. P. Kulkarni, M. Gautam-Basak, B. Sarkar, *Coord. Chem. Rev.* **2005**, *249*, 895.

[258] J. G. Mesu, T. Visser, F. Soulimani, E. E. Van Faassen, P. de Peinder, A. M. Beale, B. M. Weckhuysen, *Inorg. Chem.* **2006**, *45*, 1960.

[259] A. P. Scott, L. Radom, *J. Phys. Chem.* **1996**, *100*, 16502.

[260] A. Rimola, M. Sodupe, S. Tosoni, B. Civalleri, P. Ugliengo, *Langmuir* **2006**, *22*, 6593.

[261] A. E. Finefrock, A. I. Bush, P. M. Doraiswamy, *J. Am. Geriatrics Soc.* **2003**, *51*, 1143.

[262] A. Gil, J. Bertrán, M. Sodupe, *J. Am. Chem. Soc.* **2003**, *125*, 7461.

[263] A. Gil, J. Bertrán, M. Sodupe, *J. Chem. Phys.* **2006**, *124*, 154306/1.

[264] X. Huang, M. P. Cuajungco, C. S. Atwood, M. A. Hartshorn, J. D. Tyndall, G. R. Hanson, K. C. Stokes, M. Leopold, G. Multhaup, L. E. Goldstein, R. C. Scarpa, A. J. Saunders, J. Lim, R. D. Moir, C. Glabe, E. F. Bowden, C. L. Masters, D. P. Fairlie, R. E. Tanzi, A. I. Bush, *J. Biol. Chem.* **1999**, *274*, 37111.

[265] S. Varadarajan, J. Kanski, M. Aksenova, C. Lauderback, D. A. Butterfield, *J. Am. Chem. Soc.* **2001**, *123*, 5625.

[266] W. R. Markesbery, *Free Radical Biol. Med.* **1997**, *23*, 134.

[267] C. S. Atwood, X. Huang, R. D. Moir, R. E. Tanzi, A. I. Bush, *Met. Ions Biol. Syst.* **1999**, *36*, 309.

[268] A. I. Bush, W. H. Pettingell, G. Multhaup, M. d Paradis, J. P. Vonsattel, J. F. Gusella, K. Beyreuther, C. L. Masters, R. E. Tanzi, *Science* **1994**, *265*, 1464.

[269] X. Huang, C. S. Atwood, R. D. Moir, M. A. Hartshorn, J. P. Vonsattel, R. E. Tanzi, A. I. Bush, *J. Biol. Chem.* **1997**, *272*, 26464.

[270] C. S. Atwood, R. D. Moir, X. Huang, R. C. Scarpa, N. M. Bacarra, D. M. Romano, M. A. Hartshorn, R. E. Tanzi, A. I. Bush, *J. Biol. Chem.* **1998**, *273*, 12817.

[271] C. S. Atwood, R. C. Scarpa, X. Huang, R. D. Moir, W. D. Jones, D. P. Fairlie, R. E. Tanzi, A. I. Bush, *J. Neurochem.* **2000**, *75*, 1219.

[272] C. D. Syme, R. C. Nadal, S. E. J. Rigby, J. H. Viles, *J. Biol. Chem.* **2004**, *279*, 18169.

[273] W. Garzón-Rodríguez, M. Sepulveda-Becerra, S. Milton, C. G. Glabe, *J. Biol. Chem.* **1997**, *272*, 21037.

[274] R. P. Grese, R. L. Cerny, M. L. Gross, *J. Am. Chem. Soc.* **1989**, *111*, 2835.

[275] R. P. Grese, M. L. Gross, *J. Am. Chem. Soc.* **1990**, *112*, 5098.

[276] B. A. Cerda, S. Hoyau, G. Ohanessian, C. Wesdemiotis, *J. Am. Chem. Soc.* **1998**, *120*, 2437.

[277] S. W. Lee, H. S. Kim, J. L. Beauchamp, *J. Am. Chem. Soc.* **1998**, *120*, 3188.

[278] P. Hu, M. L. Gross, *J. Am. Chem. Soc.* **1992**, *114*, 9153.

[279] R. Gómez-Balderas, D. F. Raffa, G. A. Rickard, P. Brunelle, A. Rauk, *J. Phys. Chem. A* **2005**, *109*, 5498.

[280] M. J. Pushie, A. Rauk, *J. Biol. Inorg. Chem.* **2003**, *8*, 53.

[281] L. Shen, H.-Y. Zhang, H.-F. Ji, *Theochem* **2005**, *757*, 199.

[282] T. Miura, K. Suzuki, N. Kohata, H. Takeuchi, *Biochemistry* **2000**, *39*, 7024.

[283] N. V. Nagy, T. Szabo-Planka, A. Rockenbauer, G. Peintler, I. Nagypal, L. Korecz, *J. Am. Chem. Soc.* **2003**, *125*, 5227.

[284] M. Noguera, J. Bertrán, M. Sodupe, *J. Phys. Chem. A* **2004**, *108*, 333.

[285] S. L. Miller, *Science* **1953**, *117*, 528.

[286] D. Ring, Y. Wolman, N. Friedmann, S. L. Miller, *Proc. Natl. Acad. Sci. U.S.A* **1972**, *69*, 765.

[287] J. Oró, *Nature* **1961**, *191*, 1193.

[288] J. Oró, S. S. Kamat, *Nature* **1961**, *190*, 442.

[289] J. P. Ferris, R. A. Sanchez, L. E. Orgel, *J. Mol. Biol.* **1968**, *33*, 693.

[290] S. Pizzarello, *Acc. Chem. Res.* **2006**, *39*, 231.

[291] L. J. Allamandola, D. M. Hudgins, *NATO Science Series, II: Mathematics, Physics and Chemistry* **2003**, *120*, 251.

[292] G. Wächtershäuser, *Micr. Rev.* **1988**, *52*, 452.

[293] G. Wächtershäuser, *Mol. Orig. Life* **1998**, 206.

[294] J. D. Bernal, *The Physical Basis of Life*, Routledge and Kegan Paul, London, **1951**.

[295] L. E. Orgel, *Origins Life Evol. Biosphere* **1998**, *28*, 227.

[296] M. Rao, D. G. Odom, J. Oró, *J. Mol. Evol.* **1980**, *15*, 317.

[297] J. R. Collins, G. H. Loew, B. T. Luke, D. H. White, *Origins Life Evol. Biosphere.* **1988**, *18*, 107.

[298] N. Lahav, D. White, S. Chang, *Science* **1978**, *201*, 67.

[299] R. M. Hazen, *Scientific Am.* **2001**, *284*, 76.

[300] J. Bujdàk, B. M. Rode, *J. Mol. Evol.* **1997**, *45*, 457.

[301] A. J. A. Aquino, D. Tunega, M. H. Gerzabek, H. Lischka, *J. Phys. Chem. B* **2004**, *108*, 10120.

[302] V. A. Basiuk, T. Gromovoy, V. G. Golovaty, A. M. Glukhoy, *Origins Life Evol. Biosphere.* **1990-1991**, *20*, 483.

[303] P. Boulet, H. C. Greenwell, S. Stackhouse, P. V. Coveney, *Theochem* **2006**, *762*, 33.

[304] T. L. Porter, M. P. Eastman, E. Bain, S. Begay, *Biophys. Chem.* **2001**, *91*, 115.

[305] T. Oie, G. H. Loew, S. K. Burt, R. D. MacElroy, *J. Am. Chem. Soc.* **1984**, *106*, 8007.

[306] Y. Yamagata, K. Inomata, *Origins Life Evol. Biosphere* **1997**, *27*, 339.

[307] B. M. Rode, *Peptides* **1999**, *20*, 773.

[308] B. M. Rode, Y. Suwannachot, *Coord. Chem. Rev.* **1999**, *190-192*, 1085.

[309] T. Matsubara, K. Hirao, *Organometallics* **2001**, *20*, 5056.

[310] H. L. Son, Y. Suwannachot, J. Bujdàk, B. M. Rode, *Inorg. Chim. Acta* **1998**, *272*, 89.

[311] Y. Suwannachot, B. M. Rode, *Orig. Life Evol. Biosph.* **1998**, *28*, 79.

[312] Y. Suwannachot, B. M. Rode, *Orig. Life Evol. Biosph.* **1999**, *29*, 463.

[313] K. Plankensteiner, A. Righi, M. Rode Bernd, *Orig. Life Evol. Biosph.* **2002**, *32*, 225.

[314] M. Cossi, N. Rega, G. Scalmani, V. Barone, *J. Comput. Chem.* **2003**, *24*, 669.

[315] A. Klamt, G. Schueuermann, *J. Chem. Soc., Perkin Trans. 2* **1993**, 799.

[316] A. Rimola, S. Tosoni, M. Sodupe, P. Ugliengo, *Chem. Phys. Lett.* **2005**, *408*, 295.

[317] M. J. S. Dewar, W. Thiel, *J. Am. Chem. Soc.* **1977**, *99*, 4899.

[318] A. Rimola, S. Tosoni, M. Sodupe, P. Ugliengo, *ChemPhysChem* **2006**, *7*, 157.

[319] S. Grimme, *J. Comp. Chem.* **2006**, *27*, 1787.

[320] J. Antony, S. Grimme, *Phys. Chem. Chem. Phys.* **2006**, *8*, 5287.

[321] P. Ugliengo, http://www.moldraw.unito.it: MOLDRAW: a molecular graphics program to display and manipulate molecular structures; H1 (32-bit) ed. Torino, 2005

[322] M. Remko, B. M. Rode, *J. Phys. Chem. A* **2006**, *110*, 1960.

[323] A. M. Lamsabhi, M. Alcami, O. Mó, M. Yáñez, J. Tortajada, *ChemPhysChem* **2004**, *5*, 1871.

[324] A. M. Lamsabhi, M. Alcami, O. Mó, M. Yáñez, J. Tortajada, *J. Phys. Chem. A* **2006**, *110*, 1943.

[325] P. D'Angelo, E. Bottari, M. R. Festa, H. F. Nolting, N. V. Pavel, *J. Phys. Chem. B* **1998**, *102*, 3114.

[326] J. W. Gauld, H. Audier, J. Fossey, L. Radom, *J. Am. Chem. Soc.* **1996**, *118*, 6299.

[327] A. J. Chalk, L. Radom, *J. Am. Chem. Soc.* **1997**, *119*, 7573.

[328] J. W. Gauld, L. Radom, *J. Am. Chem. Soc.* **1997**, *119*, 9831.

[329] S. Yamabe, T. Minato, K. Hirao, *J. Chem. Phys.* **1984**, *80*, 1576.

[330] J. Sauer, J. Hill, *Chem. Phys. Lett.* **1994**, *218*, 333.

[331] B. Civalleri, E. Garrone, P. Ugliengo, *Langmuir* **1999**, *15*, 5829.

[332] J. V. Smith, *Proc. Natl. Acad. Sci. U.S.A.* **1998**, *95*, 3370–3375.

APPENDIX

A DEEPER INSIGHTS ON THE EXPERIMENTAL DETERMINATION OF THERMODYNAMIC PROPERTIES AND STRUCTURAL INFORMATION

In chapter 2 it was commented that chemistry in the gas phase offers the unique possibility to study the intrinsic properties and reactivity of transition metal-ligand species. It means that there is a wide variety of mass spectrometry methods that are capable of giving quantitative thermochemical information (such as metal ion-ligand binding energies) or that provide valuable information related with the structure of the ions generated. Since the comparison between theoretical and experimental data constitutes a crosscheck, in which sometimes calculations are used to gain complementary information from experimental results, an in other cases experimental data help to assess the reliability of theoretical results, consequently it has been considered convenient to address Appendix A to give a deeper insight on the experimental techniques exposed in chapter 2.

On the other hand, it is worth to note that the following techniques are based on guided ion beam tandem mass spectrometers. In ion beam experiments, reactant ions are created in the source region, mass selected by a mass spectrometer, and accelerated to a desired kinetic energy. Reactions then take place with a neutral reagent in a collision cell. In order to measure absolute reaction probabilities, this cell should have a well-defined length and the pressure of the neutral should be low enough that multiple collisions between the ion and neutral reagents are unlikely. Overall, as a resulting of the collisions, dissociations and/or fragmentations take place, the intensities and the m/z of the ions being used for structural elucidation or determining binding energies.

A.1 THE KINETIC METHOD

There are a great number of papers that use the kinetic method to determine relative metal affinities between different ligands. According to this technique developed by Cooks and coworkers, the relative metal (M^+) affinities of two ligands (L1 and L2) can be obtained by comparing the dissociation rates of the metal-bound heterodimer $[L1 + L2]M^+$ to each of the individual M^+-attached monomers:

$$[L1+L2]M^+ \xrightarrow{k_1} [L1]M^+ + L2$$ **Reaction A.1**

$$[L1+L2]M^+ \xrightarrow{k_2} L1+[L2]M^+$$ **Reaction A.2**

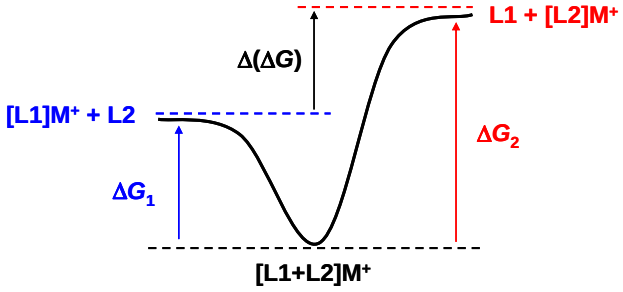

Figure A.1 Top: competitive dissociation reactions involved in the kinetic method. Below: energy diagram of the dissociation reactions above-described.

Applying the thermodynamic formulation of transition state theory to the competing reactions

$$k_i = \frac{k_B T}{h} \exp\left(\frac{-\Delta G_i^{\neq}}{RT}\right)$$ **Equation A.1**

leads to

$$\ln\left(\frac{k_1}{k_2}\right) = -\frac{\left[\Delta G_1^{\neq} - \Delta G_2^{\neq}\right]}{RT_{eff}} = \frac{\left[\Delta S_1^{\neq} - \Delta S_2^{\neq}\right]}{R} - \frac{\left[\Delta H_1^{\neq} - \Delta H_2^{\neq}\right]}{RT_{eff}}$$ **Equation A.2**

which relates the natural algorithm of k_1/k_2 with the relative free energy of activation of the two competing dissociations of the heterodimer, and consequently with the enthalpy and entropy components. R is the ideal gas constant and T_{eff} is a kinetic parameter called effective temperature of the activated dimer. T_{eff} may be taken as the temperature of a Boltzmann distribution of the activated dimer ions that fragment to give the same fragment ion abundance ratio for the non-Boltzmann population sampled in the experiment.

The unimolecular Reaction A.1 and Reaction A.2 involve simple bond cleavages from the loosely bound complex, which usually proceed without appreciable reverse activation energy. In such cases, the relative enthalpy of activation can be approximate to the difference in binding enthalpies of M^+ to L1 and L2 (in these studies so-called relative metal affinitiy, which is defined as the enthalpy change of the reaction $[L1]M^+ \xrightarrow{\Delta H_1} L1 + M^+$). Further, if L1 and L2 are chemically similar species, then

negligible differences in the entropy requirements for the competitive channels can be assumed ($\Delta S_1^{\neq} \approx \Delta S_2^{\neq}$) so that the entropic term in Equation A.2 should be close to 0. Thus, the final expression is

$$\ln\left(\frac{I_{[L1]M^+}}{I_{[L2]M^+}}\right) = \ln\left(\frac{k_1}{k_2}\right) \approx \frac{\Delta(\Delta H)_{M^+L}}{RT_{eff}} \qquad \textbf{Equation A.3}$$

now directly relating the difference in metal ion affinities between ligands L1 and L2 ($\Delta(\Delta H)_{M^+L}$) to the ratio of the rate constants of the competitive reactions. The abundance ratio of the $[L1]M^+$ and $[L2]M^+$ peaks in a given spectrum represents an approximate measure of the rate constant ratio k_1/k_2.

Because of the assumptions made, the kinetic method is best applied to ionic heterodimers of chemically related species that undergo simple dissociations. Although it has successfully been used for the determination of some thermochemical data that are in very close agreement with values measured by more accurate techniques, discrepancies have however been documented, specially when entropy effects do not cancel (using heterodimers composed by molecules of different chemical classes) and/or when reverse activation energies cannot be neglected. Recognizing such problems, the results sometimes should be considered as a qualitative ordering of metal affinities to a set of ligands.

The kinetic method has been widely used for thermochemical determination of gas-phase proton affinities, electron affinities, ionization energies and metal affinities, the type of reactions and relative affinities expressions being summarized as follows:

$$B1H^+ + B2 \xleftarrow{k_1} B1 - H^+ - B2 \xrightarrow{k_2} B1 + B2H^+$$

Reaction A.3

$$\ln\left(\frac{I[B1H^+]}{I[B2H^+]}\right) \approx \frac{\Delta(PA)B}{RT_{eff}}$$

Equation A.4

$$R1^{-\bullet} + R2 \xleftarrow{k_1} R1 - e^- - R2 \xrightarrow{k_2} R1 + R2^{-\bullet}$$

Reaction A.4

$$\ln\left(\frac{I[R1^{-\bullet}]}{I[R2^{-\bullet}]}\right) \approx \frac{\Delta(EA)R}{RT_{eff}}$$

Equation A.5

$$R1^{+\bullet} + R2 \xleftarrow{k_1} R1R2^{+\bullet} \xrightarrow{k_2} R1 + R2^{+\bullet}$$

Reaction A.5

$$\ln\left(\frac{I[R1^{+\bullet}]}{I[R2^{+\bullet}]}\right) \approx \frac{-\Delta(EI)R}{RT_{eff}}$$

Equation A.6

$$[L1]M^+ + M2 \xleftarrow{k_1} [L1 - M^+ - L2] \xrightarrow{k_2} L1 + [L2]M^+$$

Reaction A.6

$$\ln\left(\frac{I[L1M^+]}{I[L2M^+]}\right) \approx \frac{-\Delta(M^+)L}{RT_{eff}}$$

Equation A.7

Interesting results were obtained when comparing metal ion affinities of amino acids to the corresponding proton affinities, since significant differences were observed as a consequence of the modes of binding and the binding sites for protons and metal cations.

The representation of the $ln(k_1/k_2)$ values measured are usually used for the construction of the M^+ affinity ladder, which is represented in stair-step form. As example, partial results found by Cerda et al. for the relative Cu^+ ion affinities of amino acids (AA) in the gas phase will be used (see Figure A.2).

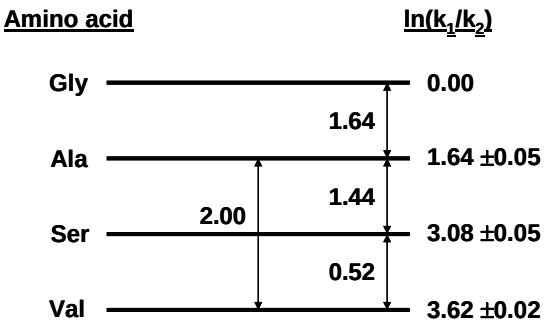

Figure A.2 Measured $ln(k_1/k_2)$ values for Cu^+-bound dimers of Glycine (Gly), Alanine (Ala), Serine (Ser) and Valine (Val).

The values at the right-hand part of the ladder correspond to $ln(k_{AA}/k_{Gly})$ so that the ladder is the sequence of the relative Cu^+ affinities of the amino acids studied (Gly < Ala < Ser < Val). The AA1/AA2 pairs of the dimers investigated are connected by arrows and they enable us to examine the validity of the assumptions made in the kinetic approach. Using these arrow-values one can realize that the results are internally consistent. For example $ln(k_{Val}/k_{Gly})$ is 3.62; very similar value is obtained by summing the $ln(k_1/k_2)$ values for the three intermediate steps, viz. 3.60=1.64+1.44+0.52. The same happens summing the $ln(k_{Ala}/k_{Gly})$ and $ln(k_{Val}/k_{Ala})$ values (3.64=1.64+2.00). This accord confirms that entropic effects are indeed negligible for these amino acids coordinating to Cu^+ cation.

A.2 EQUILIBRIUM MEASUREMENTS

There are two types of equilibrium measurements according to the experimental conditions: high-pressure and low-pressure.

A.2.1 HIGH PRESSURE ION-MOLECULE EQUILIBRIUM

In high-pressure experiments, direct clustering equilibria may be examined, and hence absolute binding energies derived. The interest remains in knowing the binding energy between a metal cation M^+ and a neutral ligand A. In order to form the MA^+ complex M^+ reacts with the substrate A, both possessing a perfectly known initial pressure. Reaction A.7 is usually referred as direct association and the equilibrium constant K_{MA^+} is expressed as Equation A.8.

$$M^+ + A \Leftrightarrow MA^+; \quad \mathrm{K}_{MA^+} \qquad \textbf{Reaction A.7}$$

$$\mathrm{K}_{MA^+} = \frac{p_{MA^+}}{p_{M^+} p_A} \qquad \textbf{Equation A.8}$$

At equilibrium conditions, the equilibrium constant K_{MA^+} is related with the mass spectrometer intensities of the ions, which are are assumed to be equal to the partial pressure ratio of these ions in the reaction chamber. The partial pressure of the neutral reagent will be taken as the initial partial pressure of A. This is justified because the concentrations of the ions are always many orders of magnitude smaller than the concentration of the neutral reagent. Accordingly, the expression of the equilibrium constant follows

$$\mathrm{K}_{MA^+} = \frac{I_{MA^+}}{I_{M^+} p_{A_0}} \qquad \textbf{Equation A.9}$$

where I_{MA^+} and I_{M^+} are the intensities of cluster MA^+ and of monomer M^+, respectively, and p_{A_0} is the initial pressure of neutral A. Therefore, the value of K_{MA^+} can be easily calculated.

According to the Van't Hoff equation (Equation A.10), plots of $\ln(\mathrm{K}_{MA^+})$ versus 1/T obtained by different experiments varying temperature yield ΔS and ΔH values of the reaction under examination, and hence absolute binding energies are derived.

$$\ln(\mathrm{K}_{MA^+}) = \frac{\Delta S}{R} - \frac{\Delta H}{RT} \qquad \textbf{Equation A.10}$$

Inspection of the procedure reveals key experimental requirements such as methods for preparation the required precursor M^+, methods for supplying known partial

pressures of the neutral reagents A, or devices to control and measure the temperature. Additionally, to obtain K_{MA^+} the ratio of the ion concentration must be known. However this is experimentally difficult. Indeed, the ion ratio may be distorted in the scape through the sampling orifice or later as a consequence of collision-induced decomposition processes caused by the high-pressure conditions.

A.2.2 LOW-PRESSURE ION-MOLECULE EQUILIBRIUM

When trying to obtain binding energies from Reaction A.7 in low-pressure experiments (such as those in FT-ICR) there is a problem given rise by the fact of working in low-pressure regime (working with isolated reactants and products). This lies on that exothermic direct association reactions in which bonds are formed, the energy released resides in the product and is sufficient to break the nascent bond. This contrasts with the situation at higher pressures, where collisions are frequent enough to dissipate rapidly the binding energy so that products are easily stabilized. In the absence of these dissipative processes, the lifetime of the "energized" product ion depends on the strength of the bond formed and on the number of degrees of freedom into which the energy can be distributed. According to the theory of unimolecular reactions, stronger bonds and more degrees of freedom lead to longer lifetimes. Therefore, direct association is only observed if the interaction between the reactants is strong and the product has many internal degrees of freedom into which energy can be partitioned. At the same time, the interaction must not be too strong because then dissociation back to reactants will not be observed at accessible temperatures, preventing measurement of the equilibrium constant. As a result, only a few cases of direct association equilibrium have been characterized at low pressures.

The most typical low-pressure ion-molecule equilibrium method is the ligand exchange equilibrium approach. In this procedure the reaction under study is a bimolecular transfer reaction

$$XM^+ + Y \Leftrightarrow X + MY^+; \quad K_{eq} \qquad \textbf{Reaction A.8}$$

in which the species are M^+ the metal cation and X/Y the exchanged ligands. Unfortunately, since only the energetics associated with M^+ transfer can be obtained, measurements of exchange equilibrium do not directly yield absolute binding thermochemistry, but rather a relative scale of binding enthalpies may be derived.

Under these conditions the equilibrium constant is expressed as

$$\mathrm{K}_{eq} = \frac{p_X p_{MY^+}}{p_{XM^+} p_Y} = \frac{I_{MY^+} p_X}{I_{XM^+} p_Y} \quad \textbf{Equation A.11}$$

where p_X and p_Y are the partial pressures of species X and Y at equilibrium, respectively. As exposed previously, measures of K_{eq} as a function of temperature allows the determination of the Δ(ΔS) and Δ(ΔH) reaction values, in which the latter term corresponds to the relative M^+ affinity between X and Y.

A.3 THRESHOLD COLLISION-INDUCED DISSOCIATION

In this technique a dissociation process of the metal complex MA^+ is induced by a collision partner (identified as an inert rare gas Rg) in the collision cell, as is represented by the Reaction A.9

$$MA^+ + Rg \rightarrow M^+ + A + Rg \quad \textbf{Reaction A.9}$$

It is worth to note that this CID-reaction is intrinsically endothermic. Rare gases are the mostly-used collision gases because they guarantee an efficient kinetic energy → internal energy transfer, since they are heavy and polarisable. As a general rule, the loss of one intact ligand molecule is the most frequent path.

The idea for obtaining BDEs is to study the Reaction A.9 as a function of the reactants in such a way that the energy threshold for the process is determined. If there is no activation energy in excess of the reaction endothermicity then the energy threshold measured for this reaction (E_T) can be converted to the bond energy (D_T) of M^+-A: $D_T(M^+\text{-}A)=E_T$.

The raw data of a reaction threshold measurement are the reactant and product ion intensities as a function of the ion kinetic energy. However, to analyze these data for thermochemical information, the raw data must be converted to a form that is independent of the instrument used to acquire the data; i. e., cross-sections as a function of the energy in the centre-of-mass frame.

Cross-section σ_{tot} is the intrinsic property in collision/reaction theory that describes the probability that two particles collide and evolve to products. Calculation of the total cross-section from the ion intensities uses a Beer-Lambert law

$$I_{MA^+} = \left(I_{MA^+} + \sum I_P\right)\exp\left(-\sigma_{tot}\rho l\right) \quad \textbf{Equation A.12}$$

where I_{MA^+} and I_P are the measured transmitted intensities of the reactant and product ions, respectively, ρ is the gas density, and l is the effective path length.

The reactant kinetic energy is approximated to reactant centre-of-mass (E_{CM}), which is related to the laboratory ion energies (E_{lab}) using Equation A.13

$$E_{CM} = E_{lab}\left(\frac{m_{Rg}}{M_{MA^+} + m_{Rg}}\right) \quad \textbf{Equation A.13}$$

where m_{Rg} and M_{MA^+} are the masses of the neutral and ion reactant, respectively. It comes from removing the energy involved in motion of the reaction system so that E_{CM} corresponds to the relative kinetic energy of the centre-of-mass available to induce chemical processes.

Typical plot of a threshold dissociation reaction is performed by representing the cross-section versus the E_{CM} (see Figure A.3). In this case the dissociation is between K^+ cation and Trp amino acid induced by Xe as the rare gas.

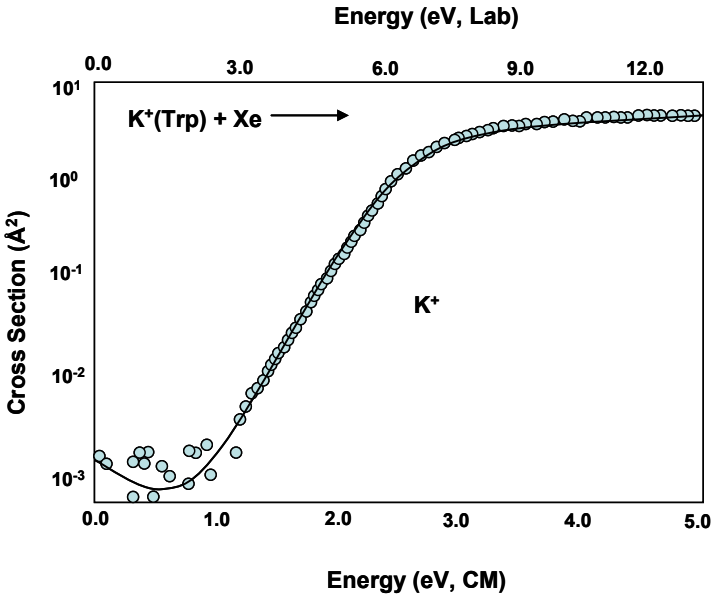

Figure A.3 Cross section for the collision-induced dissociation of the K^+-(Trp) complex with Xe as a function of collision energy in the centre-of-mass frame (lower *x*-axis) and laboratory frame (upper *x*-axis).

The energy dependence of cross-sections can be analyzed using Equation A.14

$$\sigma(E) = \sigma_0 \sum gi \frac{(E_{CM} + E_i - E_0)^n}{E_{CM}} \quad \textbf{Equation A.14}$$

where σ_0 is an energy-independent scaling factor, E_{CM} is the centre-of-mass relative kinetic energy, and n an adjustable parameter that controls the shape of the energy dependence plot. This equation involves an explicit sum of the contributions of individual reactant states (vibrational, rotational and/or electronic), denoted by *i*, with energies E_i and populations g_i. E_0 is the reaction threshold. The use of Equation A.14 requires molecular parameters (electronic, vibrational and rotational constants) of both reactants along with information regarding the population of these states. These parameters can be experimental values when available or obtained from *ab-inito* calculations.

The threshold regions of the CID cross-sections are modelled using Equation A.14 and nonlinear least-squares analysis of the data is performed to give optimized values for the parameters σ_0, E_0 and *n*. Thus, through threshold CID measurements accurate absolute 0 K binding energies can be obtained.

A.4 COLLISION-ACTIVATED OR COLLISION-INDUCED DECOMPOSITION

Tandem mass spectrometry is often addressed to the fragmentation of precursor ions selected by the first analyzer in order to allow the second analyzer to analyze the product ions.

Collision-activated and collision-induced decompostions (CAD and CID, respectively) refer to the same principal process, i. e. fragmentation of an ionic species accelerated to a certain kinetic energy upon collision with a quasi-stationary neutral target gas, CAD usually describe experiments with ions having large kinetic energies (typically keV) whereas CID is mostly used for collisions at lower kinetic energies (0 – 200 eV). In order to appreciate the differences between CAD and CID let us consider a hypothetical cation $[ABC]^+$ having bond dissociation energies

$$[ABC]^+ \rightarrow [AB]^+ + C \quad D(AB^+ - C) = 1.0 \text{ eV} \qquad \textbf{Reaction A.10}$$

$$[ABC]^+ \rightarrow A + [BC]^+ \quad D(A - BC^+) = 2.0 \text{ eV} \qquad \textbf{Reaction A.11}$$

At low collision energies, $[AB]^+$ predominates because its formation is thermochemically favoured. At an effective collision energy of 1.5 eV $[ABC]^+$ can only yield $[AB]^+$ as an ionic fragment because the route to $[BC]^+$ is energetically inaccessible (Figure A.4.a). Upon gradual increase of the collision energy $[BC]^+$ is also formed but $[AB]^+$

still prevails on thermochemical grounds. At collision energies of several keV $[AB]^+$ and $[BC]^+$ are likely to be formed in comparable quantities (see Figure A.4.b)

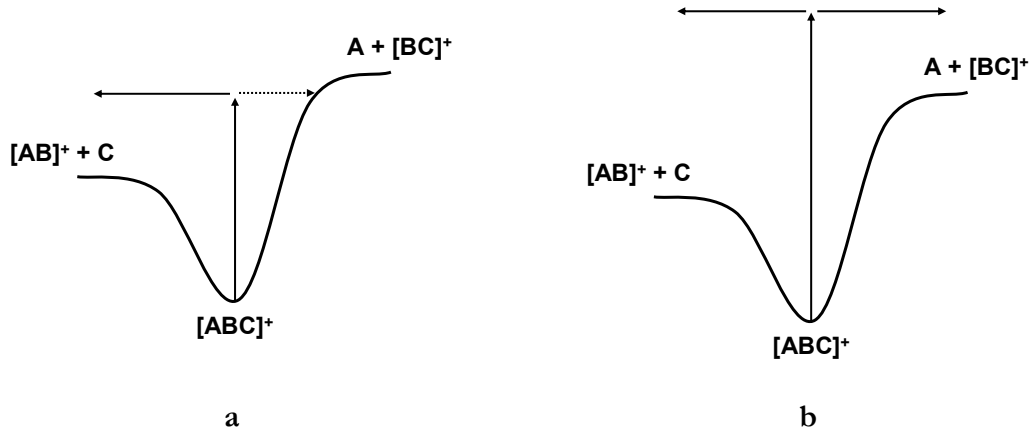

Figure A.4 Scehematic representation of the $[ABC]^+$ fragmentations: low collision energies lead to $[AB]^+$ as the major ion fragment (a) whereas high collision energies lead to the formation of both $[AB]^+$ and $[BC]^+$ ion fragments (b).

The fragmentation takes place when the precursor ion is excited via an energetic collision with neutral gaseous targets as describes the

$$m_p^+ + N \xrightarrow{1} \left[m_p^+\right]^* + N' \xrightarrow{2} m_f^+ + m_n + N' \qquad \textbf{Reaction A.12}$$

where $\left[m_p^+\right]$ and *N'* represent the post-collision states of the precursor ion m_p^+ and the target N, respectively, and m_f^+ and m_n are the ionic and neutral products of the unimolecular decomposition. That is, under commonly used conditions CAD and CID are regarded as a two-step processes involving activation of the m_p^+ ion via one or more collisions (step 1) and a discrete unimolecular decomposition process (step 2).

CAD and CID applications are plentiful in elucidation of structure such, especially when treating with metal-containing biological systems. Indeed, it is well known that the interaction of transition metal cations with biological macromolecules depends strongly on the metal cation, especially on its electronic configuration. Consequently, when treating the metal-cationized system under collisional activation conditions metal-specific fragmentations occur in such a way that from the fragment ions one can indirectly obtain structural information. Figure A.5 shows an invented case just to exemplify the procedure of structure elucidation (the intensities have been drawn in a random way). The ESI mass spectrum of an isolated peptide (P) is obtained in presence of the silver monocation (Ag^+). One ion at m/z 399 is selected and fragmented using the CID technique. The clear-cut

fragmentation at the peptide bonds allows straightforward sequence assignment, as shown by the fragmentation scheme. Therefore, from the fragment ions one can elucidate the peptide sequence by means of the well-known corresponding features for this class of compounds.

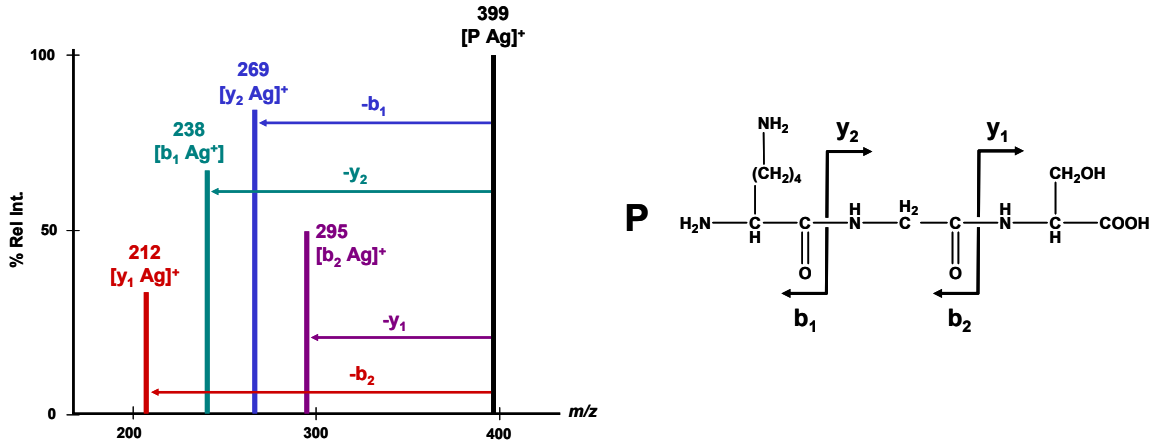

Figure A.5 Hypothetical CID spectrum of the [P Ag]$^+$ complex. Through the ion fragments observed one can elucidate the structure of P.

Following with the same line, the study of small complexes that can be used as models of bigger systems can provide important structural clues by analyzing the fragments obtained in CID experiments. For example, the CID spectrum of Cu^+-His reveals that the major fragment-channel is the consecutive loss of CO_2 and NH_3 and that is specific for this aminoacid. Accordingly, when trying to elucidate the sequence of an unknown peptide via Cu^+ cationization CID experiments, if the major loss of the Cu^+-peptide corresponds to CO_2+NH_3 then one can suspect that the peptide must contain His.

Finally it is possible to suggest structures of the ions formed in the source using the fragmentations observed. From any structure one can try to establish the mechanisms that yield the fragments observed in such a way that if the structure proposed is consistent with the experimental data then it could be the right structure of the ion. In order to avoid rude speculations, theoretical calculations are useful techniques that can help us to determine the structure of the ion generated, both by computing the relative energy of the isomers that the ion can have as well as by calculating the potential energy surface of the decomposition mechanisms suggested.

A.5 INFRARED MULTIPLE-PHOTON DISSOCIATION

The aforementioned techniques provide information about absolute and relative binding energies as well as reactivity. However, they only offer inconclusive (sometimes

uninformative) probes of the geometric and electronic structures of the ion complexes. To investigate such species it would be attractive the use of spectroscopic approaches that characterize the ionic complexes in situ, giving more direct and definitive structural probes than indirect reactivity and fragmentation exams.

IR spectroscopy has long been employed as a tool in condensed phases to study structure and bonding of transition metal complexes. However, direct IR absorption spectroscopy on ions under mass-spectrometric control is still challenging because of the low-density of mass-selected gas-phase ions as a consequence of the Coulombic repulsion between ions. Thus, in order to obtain similar information about the optical absorption spectrum the strategy of "action spectroscopy" needs to be employed. "Action spectroscopy" techniques are based on observation of a secondary change in the system, in mass spectroscopy experiments the fragmentations. For systems in which the binding energy is greater than that of a single IR photon (such as metal ion-molecule) infrared multi-photon dissociation (IRMPD) spectroscopy can be used to fragment the parent ion, that is, the resulting change in mass of the ions is the basis for the "action spectroscopy" in this case.

Therefore, while in collisional activated techniques the mechanisms involve a collision of the parent ion to a neutral target gas, in IRMPD the fragmentation arises from the absorption of multiple infrared by the ions. The parent ion becomes excited into more energetic vibrational states until the bonds are broken resulting in gas phase fragments. In fact, the fragmentation of the ions via IRMPD is based on the principle of resonant photofragmentation, which states that he energy resulting from the absorption of a photon by an ion is rapidly relaxed to the other vibration modes via intramolecular vibrational redistribution (IVR). This redistribution does not appreciably shift the original optical transition and so it remains in resonant with the laser allowing absorption of another photon. In this way, many photons can be rapidly absorbed in a non-coherent fashion, until the ion is "heated" sufficiently to induce fragmentation or threshold dissociation, and hence a change in the mass of the species.

Using IRMPD as a spectroscopic tool requires high photon fluxes produced by intensive and continuously tuneable laser sources in order to keep the process of multiphoton absorption. Free electron lasers for infrared experiments (FELIX) have been proven to be very adequate for this task because they are capable of delivering high-energy macropulses over a wide wavelength region, thus enabling many structurally relevant vibrational regions to be explored.

The photodissociation products and any remaining parent ion are then measured normally using standard analyzers. IRMPD spectra are generated by plotting the fragmentation yield as a function of the wavelength of the FELIX laser. For example, for K^+ tagged biomolecules such as amino acids or small peptides, the lowest barrier dissociation channel is the desorption of K^+ so that monitoring the appearance of K^+ as a function of the wavelength and normalizing it respect to the total ion population yields a background-free infrared spectrum of species. Therefore, IRMPD is a plenty useful technique that gives an infrared spectrum of the ionic specie fragmented, it means, direct structural information, which by comparing with those theoretically simulated for various candidate isomers allows to determine the structure of metal ion complexes.

However, the interpretation of the spectra needs some special attention. First of all, although the IRMPD spectra are not identical to linear absorption spectra, the assumption that the IRMPD yield is linearly proportional to the IR absorption intensity is accepted as a useful approximation, allowing the IRMPD spectra to be a reflection of the true IR absorption spectra. Despite that, it is important no to forget that multiple photon absorption occurs in an incoherent fashion, so that highly nonlinear power dependencies are largely avoided. In addition, there are some caveats when interpreting IRMPD spectra by comparison with calculated linear absorption spectra, such as a general redshifting and broadening of bands, as well as possible changes in the relative intensities of bands due to the presence of nearby bands. Such effects can be ascribed to anharmonicities of the vibrational modes in combination with the large number of photons that are absorbed in the IRMPD process. Although models have been developed to investigate these effects the precise imprint of the IRMPD process on the spectrum of a particular ion remains difficult to estimate, especially since anharmonicity parameters are generally unknown.

To sum up, IRMPD is a promising alternative technique that, similarly to the collisional-activated experiments, fragments parent ions but in a softer way. Aside from that, its potential applicability arises from obtaining successfully the IRMPD spectra of such ions in such a way that direct characterisation of ionic complexes in the gas phase, usually supported by theoretical calculations, can be carried out.

B INTRODUCTION TO DENSITY FUNCTIONAL THEORY

The energy of a system calculated by the Hartree-Fock method (HF) is not properly described because the electron correlation is not introduced. Such a problem is solved with more or less degree by the post-HF methods, which introduce the electron correlation expanding the wave function Ψ in a function basis of N-particles using an exact $\hat{H}$. However, the density functional methods allow to compute the energy of a given systems introducing the correlation energy by means of an alternative procedure that modifies the molecular $\hat{H}$. These methods are based on the Density Functional Theory (DFT).

B.1 THE HOHENBERG-KOHN THEOREMS

The DFT is based on the Hohenberg-Kohn theorems, which can be summarized in two statements.

1. *Any observable of a non-degenerate stationary state can be exactly calculated by means of the electron density of its ground state.*

That is, the ground state energy, the wave function and the rest of the properties of a non-degenerate system can be determined by the electron density $\rho(r)$. Thus, every property is a density functional.

The N-electrons of a non-degenerate system that are moving under the influence of an external potential field generated by the fix nucleus, the expression of the electronic Hamiltonian $\hat{H}$ is

$$\hat{H} = \hat{T}_e + \hat{V}_{ee} + \hat{V}_{ext} \quad \textbf{Equation B.1}$$

the $\hat{T}_e = \sum_i -\frac{1}{2}\nabla_i^2$ term being the kinetic energy of the electrons, the $\hat{V}_{ee} = \sum_{i<j}\frac{1}{r_{ij}}$ term being the electron-electron interaction energy, and the $\hat{V}_{ext} = \sum_{i,A}\frac{-Z_A}{R_{iA}} = \sum_i \hat{V}(r_i)$ term being the energy of interaction between the electrons and an external potential, which in a molecular system is created by the nucleus so that it corresponds to the electron-nucleus

interaction energy. Since the energy is a density functional, the Equation B.1 can be rewritten as

$$E[\rho] = T[\rho] + E_{ee}[\rho] + V_{ext}[\rho] \qquad \textbf{Equation B.2}$$

It is worth to note that the $E_{ee}[\rho]$ term can be decomposed by a coulombic component $J[\rho]$, which is the classic coulombic electron-electron repulsion, and by an exchange-correlation component $\widetilde{E}_{xc}[\rho]$, which includes the non-classical bielectronic repulsion.

2. *The electron density of a non-degenerate ground-state can in principle be exactly calculated by determining the density that minimizes the ground state energy.*

This theorem is the application of the variational theorem to $E[\rho]$. Given a trial density $\tilde{\rho}$, which satisfies $\tilde{\rho}(r) \geq 0$ and $\int \tilde{\rho}(r) d\vec{r} = N$, then the energy obtained $E[\tilde{\rho}]$ will be higher or equal than the energy obtained by using the exact electron density of the system $E[\rho_{exact}]$.

$$E[\tilde{\rho}] = T[\tilde{\rho}] + V_{ee}[\tilde{\rho}] + V_{ext}[\tilde{\rho}] \geq E[\rho_{exact}] \qquad \textbf{Equation B.3}$$

B.2 THE KOHN-SHAM APPROACH

The application of the DFT methods arises from the Kohn-Sham approximation.

Let us first consider that the wave-function of an independent N-electron reference system is described by a Slater determinant (Equation B.4).

$$\Psi_s = \frac{1}{\sqrt{N!}} \left| \phi_1(1)\phi_2(2)...\phi_N(N) \right| \qquad \textbf{Equation B.4}$$

Since this reference system is under the influence of an external potential $V_s(r)$, the approximation consists in assuming that this external potential $V_s(r)$ is associated to an electron density equal to the real system (non-independent electrons) interacting with a $V(r)$ potential. Thus, for the non-interacting reference system exists a potential $V_s(r)$ for which its electron density $\rho_s(r)$ is equal to the electron density of the real system $\rho(r)_{exact}$

$$\rho_s(r) = \sum_i |\phi_1(r)|^2 = \rho(r)_{exact}$$ **Equation B.5**

Thus, the Hamiltonian of the real system can be expressed as a sum of monoelectronic Hamiltonians

$$\hat{H} = \sum_i \hat{h}_s(i) = \sum_i \left(-\frac{1}{2}\nabla_i^2 + \hat{V}_s(i) \right)$$ **Equation B.6**

where $\hat{V}_s(i)$ is the potential that allows the electron density of the non-interacting reference system to be equal as the electron density of the real system. However the problem is to find such a potential $\hat{V}_s(i)$.

B.3 ENERGY FUNCTIONALS

As mentioned, the energy is a density functional and it can be decomposed in several terms, which are also density functionals (see Equation B.2).

The electronic kinetic term $T[\rho]$ can be decomposed by exact the kinetic energy of the non-interacting electron system $T_s[\rho]$ and by a term called correlation correction $T_c[\rho]$, which is the residual electronic kinetic energy not included in $T_s[\rho]$ for assuming a non-interacting electron system.

$$T[\rho] = T_s[\rho] + T_c[\rho]$$ **Equation B.7**

On the other hand, it was mentioned that the electron-electron interaction term $E_{ee}[\rho]$ can be detached by the coulombic component $J[\rho]$, which corresponds to the classic repulsion between two electrons and by the bielectronic exchange-correlation component $\widetilde{E}_{xc}[\rho]$, which includes the non-classic bielectronic repulsion of the $E_{ee}[\rho]$ term

$$E_{ee}[\rho] = J[\rho] + \widetilde{E}_{xc}[\rho]$$ **Equation B.8**

The terms of $\widetilde{E}_{xc}[\rho]$ and $T_c[\rho]$ constitute an important term called global exchange-correlation energy functional $E_{xc}[\rho]$

$$E_{xc}[\rho] = \widetilde{E}_{xc}[\rho] + T_c[\rho] \qquad \textbf{Equation B.9}$$

and it is the functional which contains everything that is unknown.

Introducing all these new energy functionals to Equation B.2 and considering that the external potential is caused by the fix nucleus, the expression of the total electronic energy $E[\rho]$ is

$$E[\rho] = T_s[\rho] + V_{en}[\rho] + J[\rho] + E_{xc}[\rho] \qquad \textbf{Equation B.10}$$

The target is now to know $E_{xc}[\rho]$. The different functionals developed have been addressed to find the expression of $E_{xc}[\rho]$.

B.4 KOHN-SHAM EQUATIONS

Let us, now, assume that the expression of $E_{xc}[\rho]$ is known. Then the global electronic energy of a system $E[\rho]$ can be obtained by solving the orthogonal functions set ϕ_i that minimizes the energy, as the second Hohenberg-Kohn theorem states.

The energy minimization via variational theorem leads to the Kohn-Sham equations

$$\hat{h}_{KS}(1)\phi_i = \left[-\frac{1}{2}\nabla^2(1) + \hat{V}_{ef}(1)\right]\phi_i = \varepsilon_i\phi_i \qquad \textbf{Equation B.11}$$

where $\hat{V}_{ef}(1) = \hat{V}_{en}(1) + 2\sum_{i=1}^{N}\hat{J}_i(1) + \hat{V}_{xc}(1)$ is an effective potential operator that includes the electron-nucleus attraction $\hat{V}_{en}$, the classical bielectronic repulsion $\hat{J}$, and the exchange-correlation potential $\hat{V}_{xc} = \frac{\delta E_{xc}[\rho]}{\delta\rho(\vec{r})}$. This last term is how the $E_{xc}[\rho]$ is included in the Kohn-Sham operator $\hat{h}_{KS}$. Since $\hat{V}_{ef}$ depends on the electron density, the search of the orbitals ϕ_i that minimize the energy from the Kohn-Sham equation requires an iterative procedure.

Introducing the expression of $\hat{V}_{ef}(1)$ in Equation B.11, now the Kohn-Sham operator can be expressed as

$$\hat{h}_{KS}(1) = \hat{h}(1) + 2\sum_{i=1}^{N} \hat{J}_i(1) + \hat{V}_{xc}(1)$$ **Equation B.12**

If $\hat{V}_{xc} = -\sum_{i=1}^{N} \hat{K}_i$, the $\hat{K}_i$ term being the exchange operator, then the Kohn-Sham operator is the Fock operator $\hat{f}$

$$\hat{f}(1) = \hat{h}(1) + 2\sum_{i=1}^{N} \hat{J}_i(1) - \sum_{i=1}^{N} \hat{K}_i(1)$$ **Equation B.13**

It is worth noting that the Fock operator $\hat{f}$ only includes the exchange operator $\hat{K}_i$, while the Kohn-Sham operator $\hat{h}_{KS}$ involves the exchange-correlation operator $\hat{V}_{xc}$. Therefore, in Kohn-Sham expressions the lack of electron correlation given in the HF method is corrected. That is, density functional methods include the electron correlation from $\hat{h}_{KS}$ through the $\hat{V}_{xc}$ operator. However $\hat{V}_{xc}$ gives us the exchange-correlation energy $E_{xc}[\rho]$ in an approximate way. In case that the exact $E_{xc}[\rho]$ functional was perfectly known then the resolution of the Kohn-Sham equations would give the exact energy of a system in its ground state.

B.5 THE LOCAL DENSITY APPROXIMATION (LDA)

This approximation assumes that the exchange-correlation functional $E_{xc}[\rho]$ depends on the electron density ρ of an uniform electron gas and follows the expression of

$$E_{xc}^{LDA} = \int \rho(r)\varepsilon_{xc}[\rho]dr$$ **Equation B.14**

where $\varepsilon_{xc}[\rho]$ is the exchange-correlation energy per electron in the uniform electron gas.

The $E_{xc}^{LDA}[\rho]$ term can be detached from the sum of the exchange and correlation components

$$E_{xc}^{LDA}[\rho] = E_x^{LDA}[\rho] + E_c^{LDA}[\rho]$$ **Equation B.15**

For the uniform electron gas model system the exchange component $E_x^{LDA}[\rho]$ is an exact functional that follows the Dirac formulae

$$E_x^{LDA}[\rho] = -\frac{9}{4}\alpha\left(\frac{3}{8\pi}\right)^{1/3}\int \rho^{4/3} dr \qquad \textbf{Equation B.16}$$

while the correlation component $E_c^{LDA}[\rho]$ is obtained by means Monte-Carlo calculations as were proposed by Vosko, Wilk and Nusair. This functional is often referred as $E_c^{VWN}[\rho]$.

A particular case is when the correlation term is omitted so that $E_{xc}^{LDA}[\rho] = E_x^{LDA}[\rho]$. This approximation leads to the $X\alpha$ mehod proposed by Slater in which $\alpha = 2/3$ for the exchange functional.

B.6 THE GENERALIZED GRADIENT APPROXIMATION (GGA)

In the LDA methods the excange-correlation energy depends exclusively on the electronic density; i. e. $E_{xc}[\rho] = f(\rho)$. In contrats, in the Generalized Gradient Approximation (GGA) methods, the exchange-correlation functional depends also on the density gradient. Thus, the density variations around every point of a system is accounted for so the density charge does not behave as an homogeneous electron gas because of the presence of the nucleus. Therefore, the exchange-correlation energy is a functional that depends on both the electronic density ρ and the electronic density gradient $\nabla\rho$

$$E_{xc}^{GGA}[\rho] = \int f(\rho, \nabla\rho) dr = E_x^{GGA}[\rho] + E_c^{GGA}[\rho] \qquad \textbf{Equation B.17}$$

The GGA functionals derive from the LDA ones (E_{xc}^{LDA}), for which gradient corrections have been included (ΔE_{xc}^{GGA}). Some of them are:

- B88, which modifies the LDA exchange functional; $E_x^{B88} = E_x^{LDA} + \Delta E_x^{B88}$
- PW91, which modifies the LDA correlation functional; $E_c^{PW91} = E_c^{LDA} + \Delta E_c^{PW91}$
- LYP, which is a correlation functional but not-derived from the E_c^{LDA} one.

The combination of the different exchange and correlation functionals lead to the different GGA methods: BLYP, BPW91, etc…

B.7 HYBRID FUNCTIONALS

Hybrid functionals are of particular interest because part of the HF exact exchange is included in the exchange functional. Thus, the correlation energy from the exchange-correlation functional is composed by i) LDA-exchange energy E_x^{LDA}; ii) the gradient corrections included in the of the LDA-exchange energy ΔE_x^{GGA}, and iii) a percentage of the exact HF exchange energy E_x^{HF}. The energy of this third term is obtained by solving the exact integral of the HF method

$$E_x^{HF} = -\sum_{i=1}^{N}\sum_{j>i}^{N} K_{ij} \qquad \textbf{Equation B.18}$$

The first hybrid functional was the so-called *half-and-half* and it includes a 50% of the HF exact exchange energy

$$E_x^{BH} = 0.5E_x^{LDA} + 0.5E_x^{HF} + 0.5\Delta E_x^{B} \qquad \textbf{Equation B.19}$$

Nowadays, one of the most used hybrid functionals is that proposed by Becke (B3), in which the exchange-correlation functional is expressed by

$$E_{xc}^{B3} = E_x^{LDA} + a_0\left(E_x^{HF} - E_x^{LDA}\right) + a_x\Delta E_x^{B} + E_c^{LDA} + a_c\Delta E_c^{GGA} \qquad \textbf{Equation B.20}$$

were a_0, a_x and a_c are parameters obtained by linear least-square of experimental spectroscopic data. It is worth to note that the *half-and-half* exchange functional is a particular case of the B3 exchange one where $a_0 = a_x = 0.5$.

When the B3 exchange functional is combined by the correlation functionals of LYP or PW91 the methods are called B3LYP or B3PW91, respectively. Particularly, B3LYP functional follows Equation B.21

$$E_{xc}^{B3LYP} = E_x^{LDA} + a_0\left(E_x^{HF} - E_x^{LDA}\right) + a_x\Delta E_x^{B88} + E_c^{VWN} + a_c(\Delta E_c^{LYP} - E_C^{VWN}) \qquad \textbf{Equation B.21}$$

The E_x^{HF}, E_x^{LDA}, ΔE_x^{B88} and ΔE_c^{LYP} terms are the HF exchange energy based on Kohn-Sham orbitals, the uniform electron gas exchange-correlation energy, Becke's 1998

gradient correction for exchange, and the LYP gradient correction to correlation, respectively. Since the LYP functional already contains a local part and a gradient correction, one has to remove the local part to obtain a coherent implementation. This can be done in an approximate way by substracting E_c^{VWN} from ΔE_c^{LYP}. Note that in Gaussian 98 the VWN functional is the one derived by Vosko et al. from fit to the random phase approximation results. The parameters a_0, a_x and a_c were determined by linear least-squares fit to 56 experimental ionization energies, 42 ionization potentials, and 8 proton affinities. The values thus obtained were a_0=0.20, a_x=0.72 and a_c=0.81.

B.8 THE SELF-INTERACTION ERROR

In the HF approximation, the energy is given by

$$E_{HF} = \sum_{i=1}^{N} h_{ii} + \frac{1}{2}\sum_{i=1}^{N}\sum_{j=1}^{N}\left(J_{ij} - K_{ij}\right) \qquad \textbf{Equation B.22}$$

where h_{ii} defines the contribution of the electron *i* due to the kinetic energy and the electron-nucleus attraction and J_{ij} and K_{ij} are the so-called coulomb and exchange integrals, respectively

$$J_{ij} = \left\langle \chi_i(\vec{x}_1)\chi_j(\vec{x}_2)\left|\frac{1}{r_{12}}\right|\chi_i(\vec{x}_1)\chi_j(\vec{x}_2)\right\rangle = \iint \chi_i^*(\vec{x}_1)\chi_j(\vec{x}_2)\frac{1}{r_{12}}\chi_i^*(\vec{x}_1)\chi_j(\vec{x}_2)d\vec{x}_1 d\vec{x}_2 \qquad \textbf{Equation B.23}$$

$$K_{ij} = \left\langle \chi_i(\vec{x}_1)\chi_j(\vec{x}_2)\left|\frac{1}{r_{12}}\right|\chi_j(\vec{x}_1)\chi_i(\vec{x}_2)\right\rangle = \iint \chi_i^*(\vec{x}_1)\chi_j(\vec{x}_2)\frac{1}{r_{12}}\chi_j^*(\vec{x}_1)\chi_i(\vec{x}_2)d\vec{x}_1 d\vec{x}_2 \qquad \textbf{Equation B.24}$$

The term $J_{ij} - K_{ij}$ represents the average repulsion between the electrons *i* and *j*. K_{ij} has no classical interpretation whereas J_{ij} represents the classical coulomb repulsion that the electron *i* at position $\vec{x}_1$ experiences due to the average charge distribution of the electron *j* in spin orbital $\chi_j(\vec{x}_2)$. Consequently J_{ii} describes the coulomb repulsion of the charge distribution of one electron with itself and is called as self-interaction (SI). J_{ii} gives a non-zero results so that since there is definitely no electron *i* - electron *i* repulsion the SI is physical nonsense. However, the exchange term takes care for this. For $i = j$, the coulomb and exchange integrals are identical and both reduce to

$$J_{ij} = K_{ij} = \iint |\chi_i(\vec{x}_1)|^2 \frac{1}{r_{12}} |\chi_i(\vec{x}_2)|^2 d\vec{x}_1 d\vec{x}_2 \qquad \textbf{Equation B.25}$$

Since in Equation B.22 the coulomb and exchange integrals enter with opposite signs, the SI is exactly cancelled and such a problem is elegantly solved in the HF scheme.

However, in DFT methods the SI becomes a problem caused by using approximate exchange-correlation functionals. Consider the energy expression for a one electron system in the Kohn-Sham scheme

$$E[\rho] = T_s[\rho] + V_{en}[\rho] + J[\rho] + E_{xc}[\rho] \qquad \textbf{Equation B.26}$$

the classical electrostatic term $J[\rho]$ being

$$J[\rho] = \frac{1}{2} \iint \frac{\rho(\vec{r}_1)\rho(\vec{r}_2)}{r_{12}} d\vec{r}_1 d\vec{r}_2 \qquad \textbf{Equation B.27}$$

This term does not exactly vanish for a one electron system since it contains the spurious interaction of the density with itself. Thus, to cancel the SI in Equation B.26 we must demand that $J[\rho]$ exactly equals $-E_{xc}[\rho]$

$$\frac{1}{2} \iint \frac{\rho(\vec{r}_1)\rho(\vec{r}_2)}{r_{12}} d\vec{r}_1 d\vec{r}_2 = -E_{xc}[\rho] \qquad \textbf{Equation B.28}$$

Nevertheless, as mentioned, in any realization of the Kohn-Sham density functional scheme we have to employ approximations to the exchange-correlation energy which are independent of $J[\rho]$. Consequently, for multiple-electron systems none of the currently used exchange-correlation functional is self-interaction free, giving rise to the SI error, which is expressed as

$$SI_{error} = J[\rho] + E_{xc}[\rho] \qquad \textbf{Equation B.29}$$

SI error is of great importance when the approximate exchange-correlation functional tries to describe the dissociation of radicals. For example, it was shown that the dissociation curve for the one-electron hydrogen molecular ion H_2^+ is significantly in error leading to excessively small binding energies. Another intriguing case was found for the dimer of water in its radical cation state. In fact the Kohn-Sham calculations predicted a

wrong order of stability for the two low-lying structural isomers of the $(H_2O)_2^+$ dimer, overestimating the stability of the hemibonded $(H_2O\cdots OH_2)^+$ structure in detriment of the proton transferred $(H_2OH\cdots OH)^+$ isomer (see Figure B.1), the latter one being 7.7 kcal/mol more stable at the CCSD(T) level.

hemibonded structure proton transferred structure

Figure B.1 The two low-lying structural isomers of the $(H_2O)_2^+$ dimer. The hemibonded structure was found to be the ground-state isomer for LDA, GGA and hybrid functionals with low percentatge of exact exchange. The proton transferred structure was found as the most stable isomer for the BHLYP hybrid functional as well as at the MP2 and CCSD(T) levels of theory.

C COMPLEMENTARY RESULTS OF THE Cu^{2+}-H_2O SYSTEM

C.1 PARAMATER SETS EMPLOYED FOR B3LYP CALCULATIONS

Parameter set	a_0	a_x	a_c
0	0.000	1.000	1.000
1	0.100	0.900	0.900
2	0.200	0.800	0.800
3	0.300	0.700	0.700
4	0.400	0.600	0.600
5	0.500	0.500	0.500
6	0.600	0.400	0.400
7	0.700	0.300	0.300
8	0.800	0.200	0.200
9	0.900	0.100	0.100

C.2 RELATIVE ENERGIES (in kcal/mol) OF THE GROUND AND LOW-LYING ELECTRONIC STATES COMPUTED WITH THE B3LYP METHOD USING DIFFERENT PARAMETER SETS

	parameter									
state	1	2	3	4	5	6	7	8	9	HF
$^2A_1$	0.0	0.0	0.0	0.0	0.0	0.0	0.0	0.0	0.0	0.0
$^2B_1$	-6.6	-2.3	1.9	5.1	6.8	7.4	7.6	7.6	7.5	6.7
$^2B_2$	20.8	18.1	16.0	14.4	13.2	12.2	11.6	11.0	10.6	9.4
$^2A_2$	24.0	20.9	18.7	17.0	15.8	14.9	14.3	13.8	13.3	12.1

C.3 SPIN DENSITY (au) AT THE Cu ATOM FOR THE C_{2v} Cu^{2+}-H_2O SPECIES IN THE DIFFERENT ELECTRONIC STATES COMPUTED WITH THE B3LYP METHOD USING DIFFERENT PARAMETER SETS (SEE C.1)

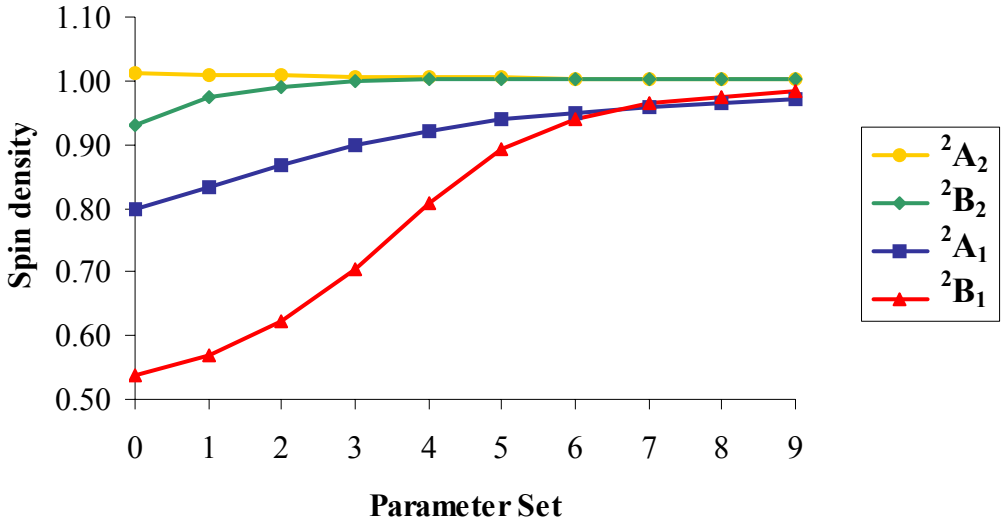

D CONFORMATIONAL EXPLORATION OF THE $Cu^{+}/^{2+}$-AA_{arom} SYSTEMS

D.1 Cu^{+}-Phe

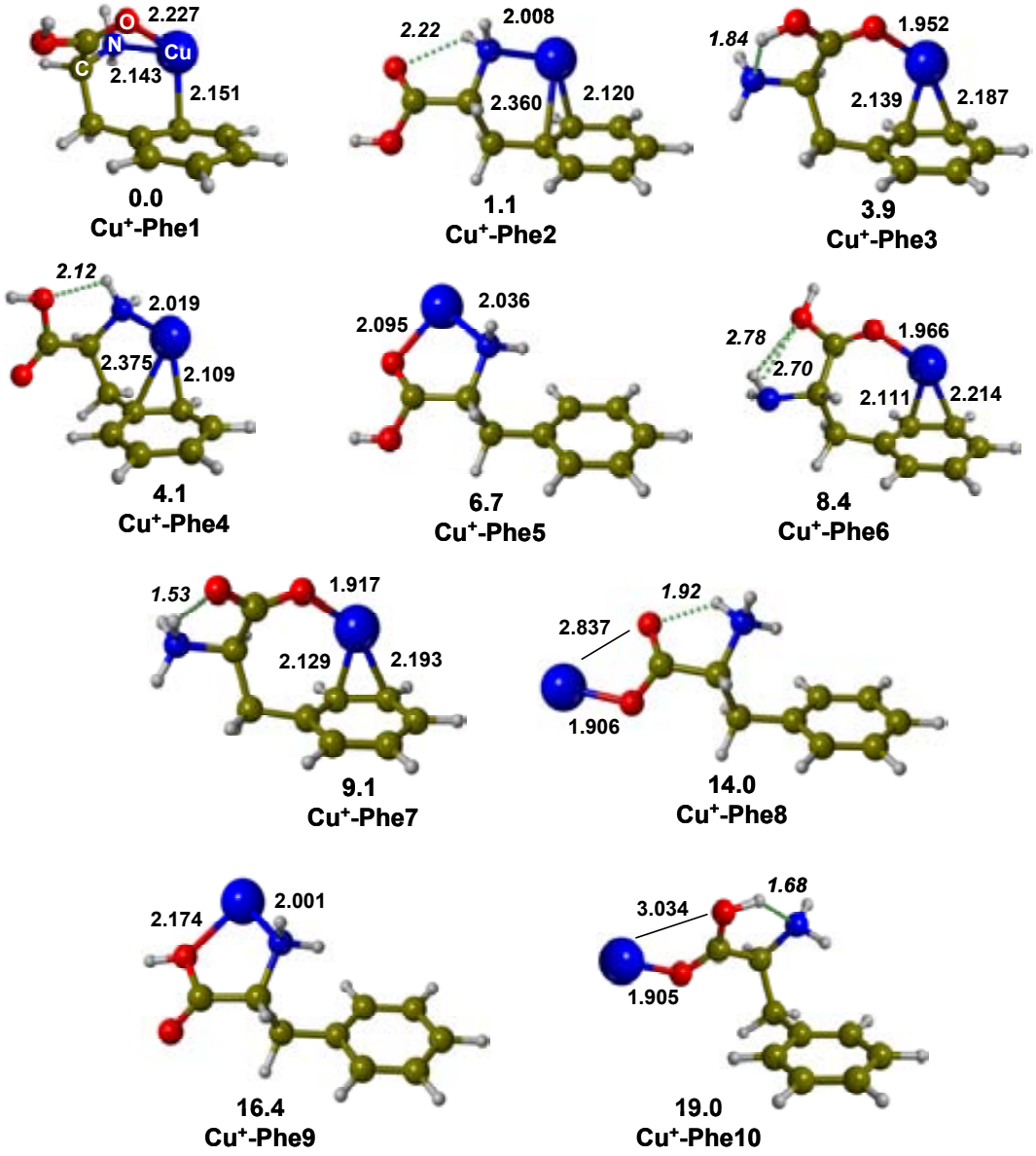

Figure D.1 B3LYP-conformational exploration of the Cu^{+}-Phe system. Electronic energies including ZPE corrections in kcal/mol. Bond lengths in Å.

D.2 Cu^+-Tyr

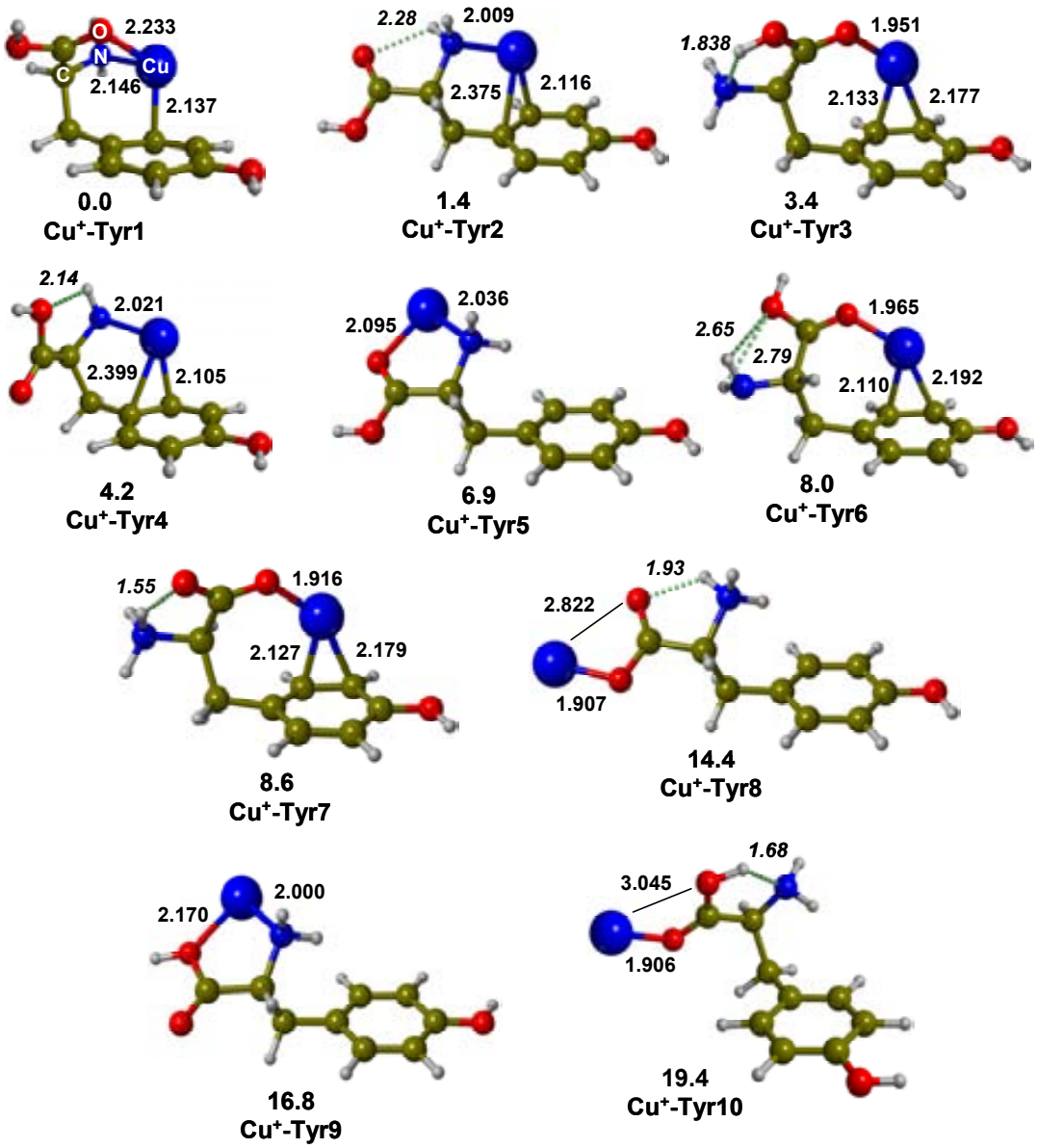

Figure D.2 B3LYP-conformational exploration of the Cu^+-Tyr system. Electronic energies including ZPE corrections in kcal/mol. Bond lengths in Å.

D.3 Cu^{+}-Trp

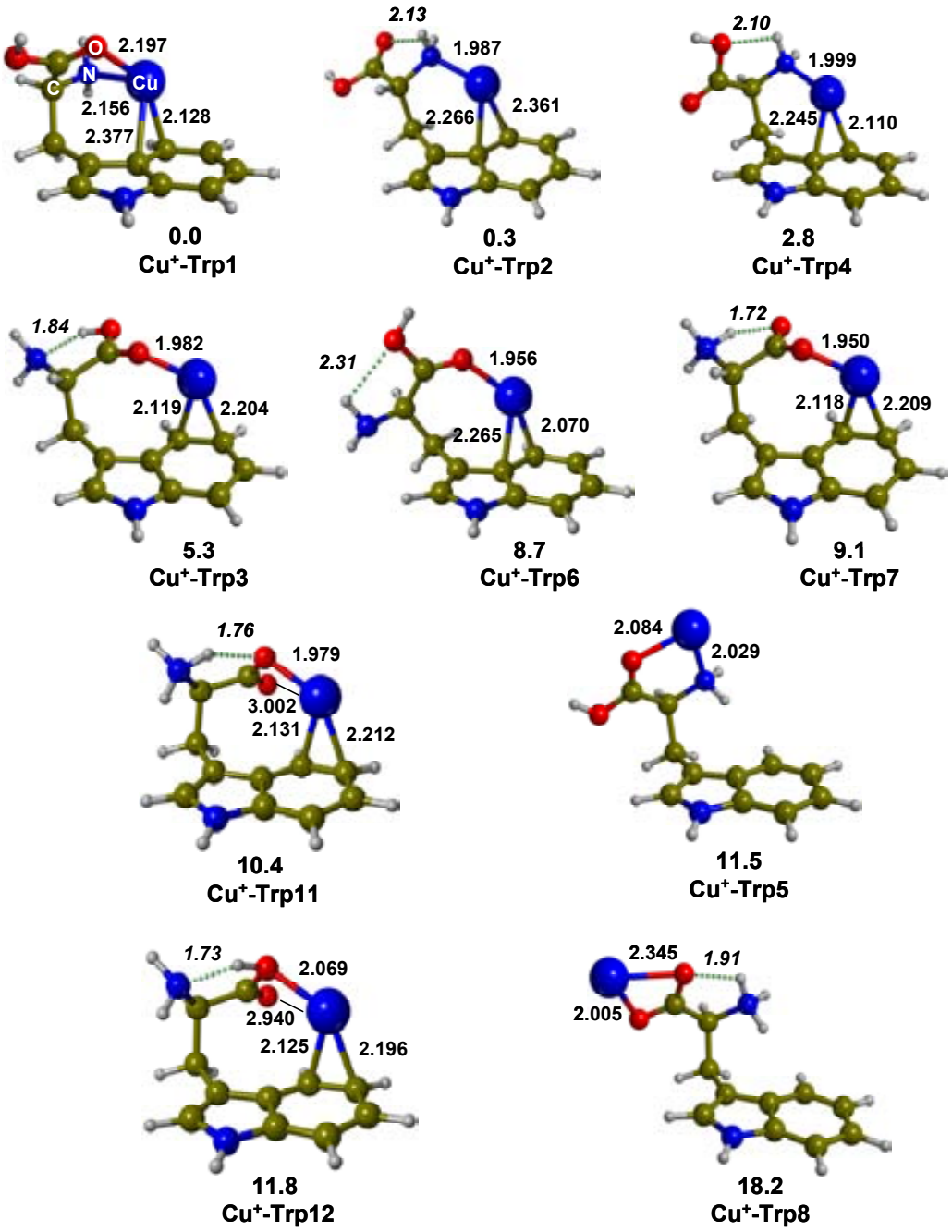

Figure D.3 B3LYP-conformational exploration of the Cu^{+}-Trp system. Electronic energies including ZPE corrections in kcal/mol. Bond lengths in Å.

D.4 Cu^{+}-His

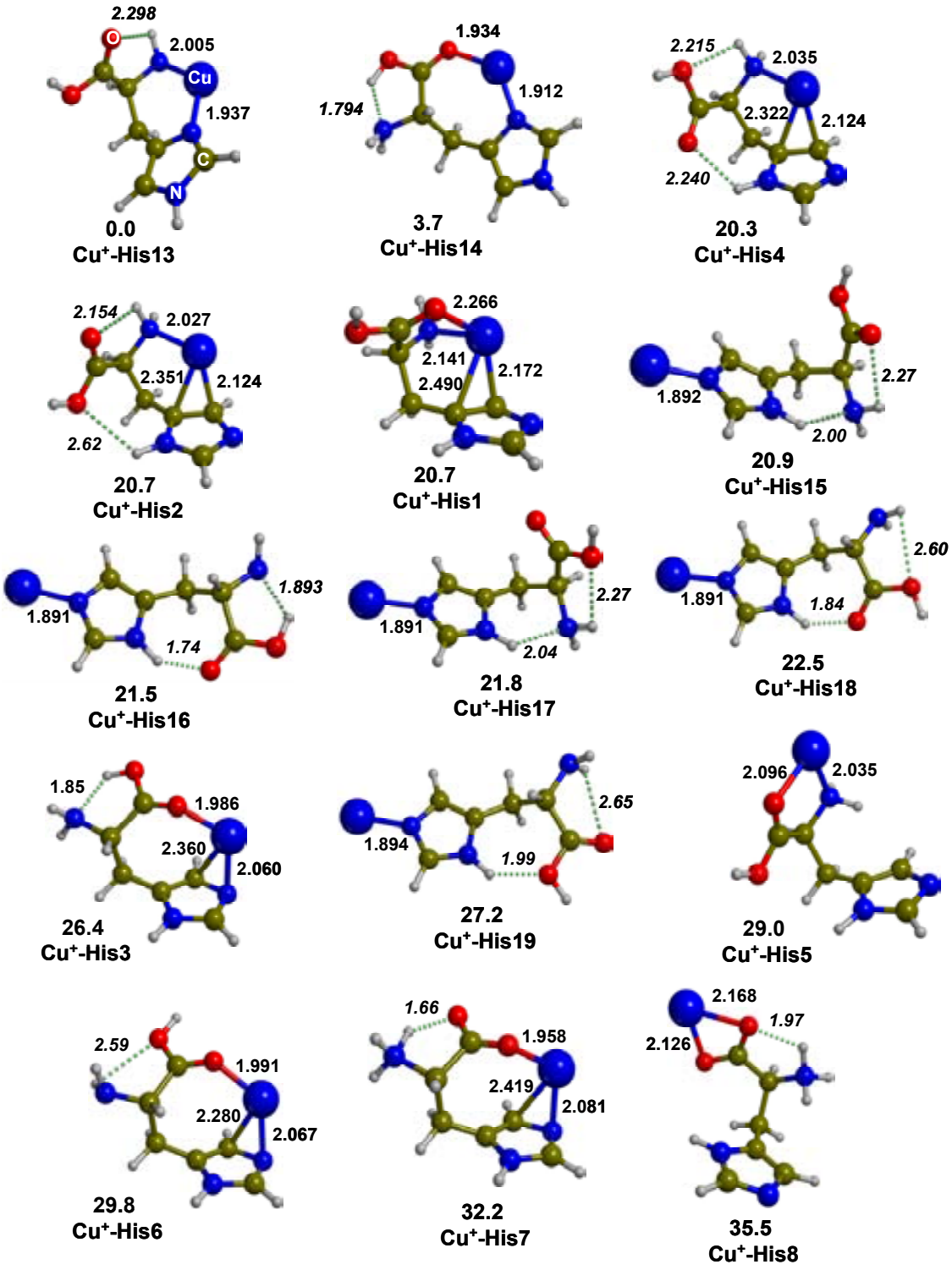

Figure D.4 B3LYP-conformational exploration of the Cu^{+}-His system. Electronic energies including ZPE corrections in kcal/mol. Bond lengths in Å.

D.5 Cu^{2+}-Phe

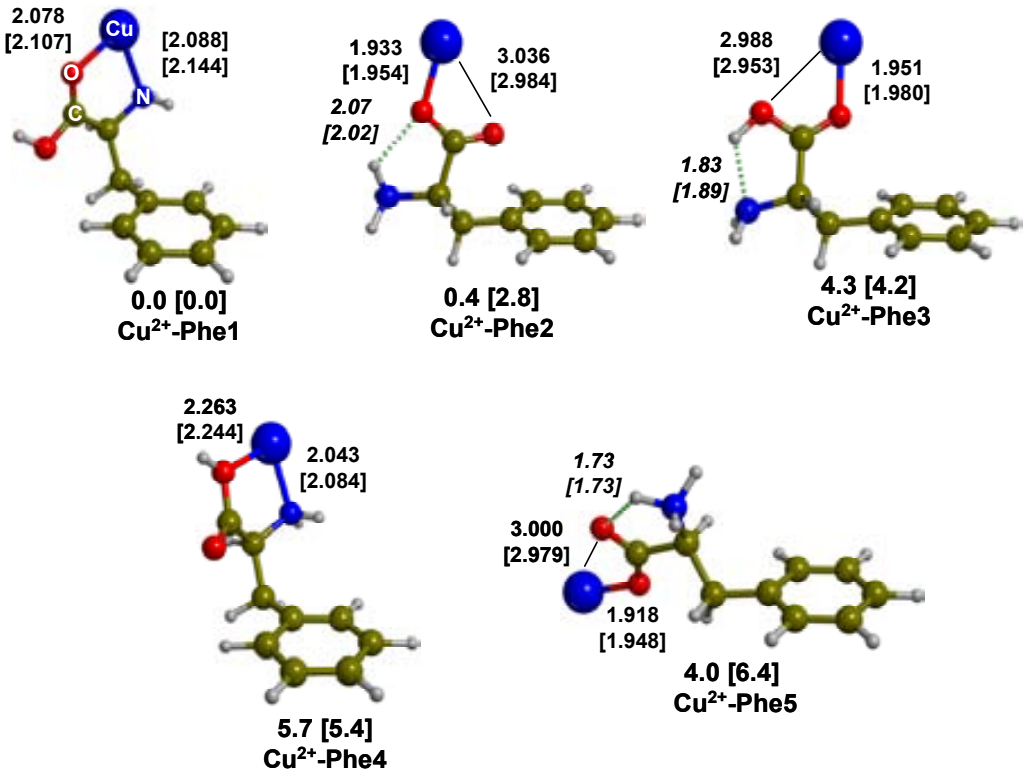

Figure D.5 B3LYP [BHLYP]-conformational exploration of the Cu^{2+}-Phe system. Electronic energies including ZPE corrections in kcal/mol. Bond lengths in Å.

D.6 Cu^{2+}-Tyr

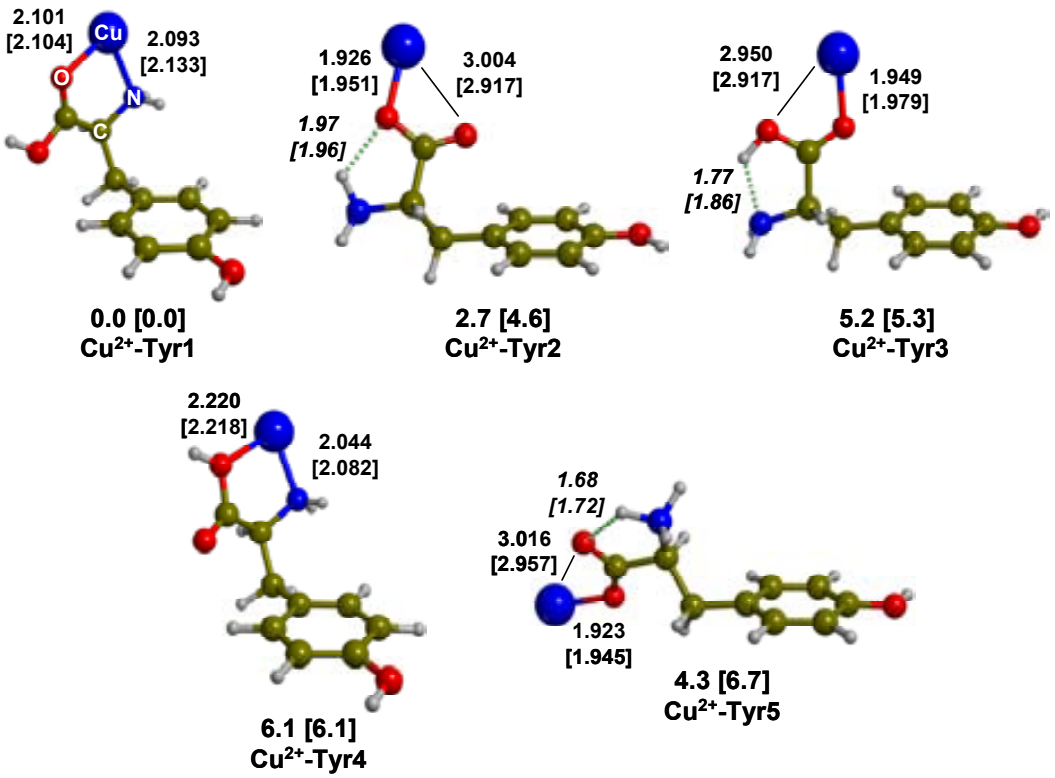

Figure D.6 B3LYP [BHLYP]-conformational exploration of the Cu^{2+}-Tyr system. Electronic energies including ZPE corrections in kcal/mol. Bond lengths in Å.

D.7 Cu^{2+}-Trp

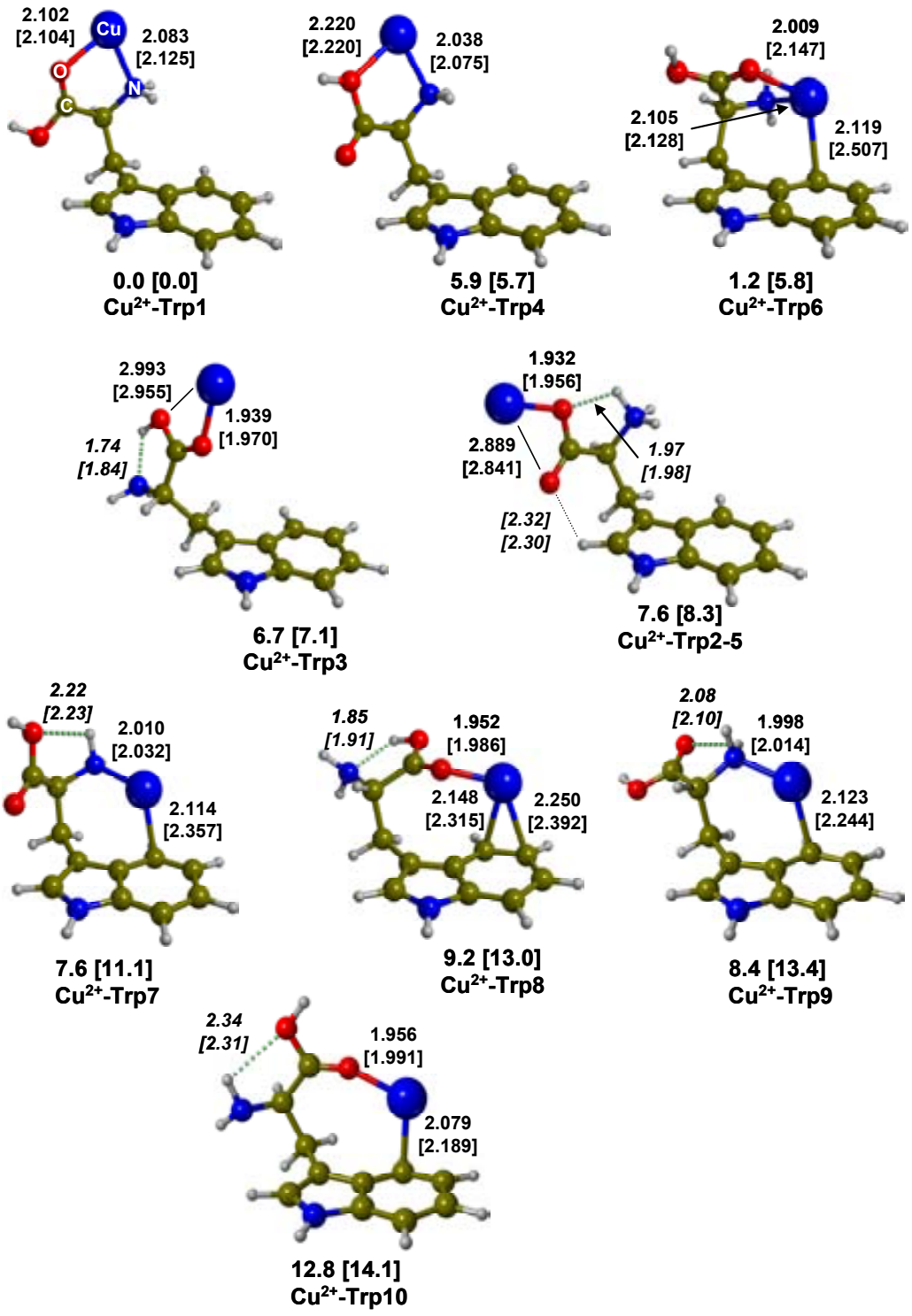

Figure D.7 B3LYP [BHLYP]-conformational exploration of the Cu^{2+}-Trp system. Electronic energies including ZPE corrections in kcal/mol. Bond lengths in Å.

D.8 Cu^{2+}-His

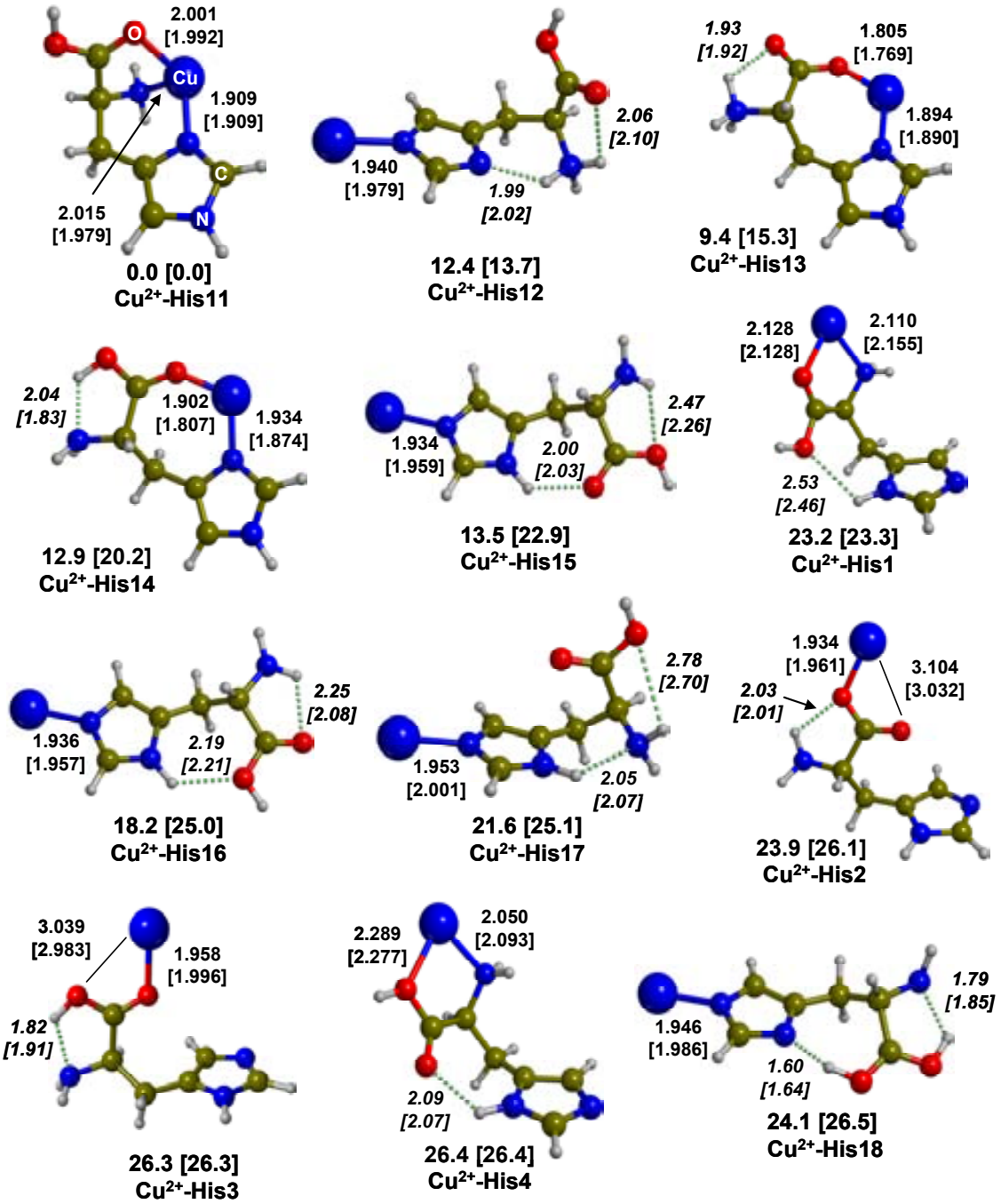

Figure D.8 B3LYP [BHLYP]-conformational exploration of the Cu^{2+}-His system. Electronic energies including ZPE corrections in kcal/mol. Bond lengths in Å.